

BIOACTIVE AGENTS CARRYING QUANTUM DOT LABELED LIPOSOMES

A THESIS SUBMITTED TO
THE GRADUATE SCHOOL OF NATURAL AND APPLIED SCIENCES
OF
MIDDLE EAST TECHNICAL UNIVERSITY

BY

ARDA BÜYÜKSUNGUR

IN PARTIAL FULFILLMENT OF THE REQUIREMENTS
FOR
THE DEGREE OF DOCTOR OF PHILOSOPHY
IN
BIOTECHNOLOGY

SEPTEMBER 2013

Approval of the thesis:

**BIOACTIVE AGENT LOADED, QUANTUM DOT-LABELED LIPOSOMES FOR
SIMULTANEOUS CANCER THERAPY AND IMAGING *IN VITRO***

submitted by **ARDA BÜYÜKSUNGUR** in partial fulfillment of the requirements for the degree of **Doctor of Philosophy in Department of Biotechnology, Middle East Technical University** by,

Prof. Dr. Canan Özgen
Dean, Graduate School of **Natural and Applied Sciences** _____

Prof. Dr. Nesrin Hasırcı
Head of Department, **Biotechnology** _____

Prof. Dr. Vasıf Hasırcı
Supervisor, **Biological Sciences Dept., METU** _____

Dr. Celestino Padeste
Co-Supervisor, **Paul Scherrer Institut,
Laboratory for Micro- and Nanotechnology** _____

Examining Committee Members:

Prof. Dr. Menemşe Gümüşderelioğlu
Chemical Engineering Dept., Hacettepe Univ _____

Prof. Dr. Vasıf Hasırcı
Biological Sciences Dept., METU _____

Assoc. Prof. Dr. Elif Erson Bensan
Biological Sciences Dept., METU _____

Assoc. Prof. Dr. Can Özen
Biotechnology Dept., METU _____

Asist. Prof. Dr. İrem Erel Göktepe
Chemistry Dept., METU _____

Date: 27.09.2013

I hereby declare that all information in this document has been obtained and presented in accordance with academic rules and ethical conduct. I also declare that, as required by these rules and conduct, I have fully cited and referenced all material and results that are not original to this work.

Name, Last name: Arda Büyüksungur

Signature:

ABSTRACT

BIOACTIVE AGENTS CARRYING QUANTUM DOT LABELED LIPOSOMES

Büyüksungur, Arda

Ph.D., Department of Biotechnology

Supervisor : Prof. Dr. Vasif Hasircı

Co-Supervisor: Dr. Celestino Padeste

September 2013, 105 pages

Among the many possible applications of nanotechnology in medicine, the use of various nanomaterials as delivery systems for pharmacologically active agents, drugs and nucleic acids (DNA, siRNA), and imaging agents is gaining increased attention. Liposomes are particularly important for these drug delivery systems because of their advantages such as their ability to carry hydrophilic and hydrophobic drugs, their being of biological origin and short life spans. Quantum Dots (QDs) are nano-scale, semiconductive, fluorophore crystals of inorganic origin. QDs are highly resistant against photobleaching unlike organic, fluorescent dyes and are very suitable for use as tracking agents. Cancer tissues produce angiogenesis agents such as VEGF, and angiopoietin that lead to the production of new blood vessels. These vessels of cancer tissue have a chaotic structure. Abnormal and dysfunctional blood vessels are a hallmark of solid tumors and they prevent medication from reaching and killing cancer cells. In the recent years, however, drug release systems were developed to use these highly porous blood vessels for cancer drug delivery.

In this study liposomes were tested for their ability to attach to charged surfaces and were shown to perform this function especially on oppositely charged surfaces. Polystyrene sulfonate and poly(allylamine) were used to coated onto glass surfaces and were found successful by binding oppositely charged liposomes; cationic liposomes were attached preferably an anionic regions coated onto glass surfaces and anionic liposomes were attached preferably an cationic regions coated onto glass surfaces. Polymer brush surfaces were used to investigate the liposomal preference towards the surfaces. Cationic multilamellar liposomes and cationic extruded SUV liposomes were attached preferably on

negatively charged PMA polymer brushes. Cationic extruded liposomes found to be more stable than the multilamellar liposomes on the surfaces.

Doxorubicin, an anticancer drug, is used in cancer therapy due to its cytotoxic effect towards the cells. Liposomes decreased the cytotoxic effect of the doxorubicin and released doxorubicin for more extended periods.

Quantum Dots with CdTe core were used as the imaging or tracking agent to observe the route of liposomes. Liposomes masked the cytotoxic effect of CdTe quantum dots arising from the inorganic core by 30%. The fluorescent quantum dots were entrapped in liposomes and observed under a confocal microscope and the interactions of the liposomes and Saos2 cells were studied. Real time observation studies showed both cationic and neutral liposomes bound to the Saos2 cells but cationic liposomes shown to be faster in binding to Saos2 cells.

Bevacizumab, anti-angiogenesis agent, was tested for its ability to prevent HUVEC from proliferation was shown to be ineffective in tested conditions but it was found that the drug decreased proliferation of HITAEC.

Keywords: Liposome, Quantum Dots, Anti-angiogenesis, Anti-cancer, Polymer Brush, Drug delivery.

ÖZ

BİYOAKTİF AJANLAR TAŞIYAN KUANTUM NOKTACIK İŞARETLİ LİPOZOMLAR

Büyüksungur, Arda

Doktora, Biyoteknoloji Bölümü

Tez Yöneticisi : Prof. Dr. Vasıf Hasırcı

Ortak Tez Yöneticisi : Dr. Celestino Padeste

Eylül 2013, 105 sayfa

Nanoteknolojinin tıptaki birçok olası uygulamaları arasında, biyoaktif ajanlar için ilaç dağıtım sistemleri, ilaçlar ve nükleik asitler (DNA, siRNA) ve görüntüleme ajanları gibi çeşitli nanomalzemelerin kullanımı giderek artan bir ilgi kazanmaktadır. Lipozomlar hidrofilik ve hidrofobik ilaçları taşıyabilme yetenekleri, biyolojik orijinli olmaları ve kısa ömürlü olmaları gibi avantajları nedeniyle ilaç dağıtım için özellikle önemlidir. Kuantum Noktacıkları (QDs) inorganik orijinli nano-ölçekte, yarı iletken fluorofor kristalleridir. Kuantum Noktacıkları organik floresan boyalar aksine florışıldama bozunmasına karşı yüksek dirence sahiptirler ve izleme aracı olarak kullanılmaya çok uygundur. Kanser dokuları VEGF gibi anjiyogenez ajanları ve yeni kan damarlarının üretimine yol açan anjiopoyetin üretirler. Bu kanser dokusunun damarları karmaşık bir yapıya sahiptir. Anormal ve işlevsiz kan damarları solid tümörlerin bir işaretidir ve ilaçların ulaşmasını ve kanser hücrelerini öldürmesini engellerler. Son yıllarda bununla birlikte kanser ilaç dağıtımında bu yüksek porlu kan damarlarını kullanan ilaç salım sistemleri geliştirildi.

Bu çalışmada lipozomlar yüklü yüzeylere bağlanma yetenekleri açısından test edildi ve bu fonksiyonu özellikle zıt yüklü yüzeylerde yerine getirdiği gösterildi. Polistren sulfonat ve poli(alilamin) cam yüzeyleri kaplamak için kullanıldı ve zıt yüklü lipozomlara bağlanmasıyla başarılı bulundu; katyonik lipozomlar cam yüzeyler üzerinde tercihen anyonik bölgelere bağlandılar, anyonik lipozomlar ise cam yüzey üzerine kaplanmış katyonik bölgelere bağlandıkları bulundu. Polimer fırça yüzeyler lipozomların yüzeylerle etkileşimini araştırmak için kullanıldı. Katyonik çok katmanlı lipozomlar ve katyonik tek katmanlı lipozomlar tercihen negatif yüklü PMA polimer fırçalara bağlandı. Katyonik tek

katmanlı lipozomların yüzeyler üzerinde çok katmanlı lipozomlardan daha kararlı olduğu bulundu.

Antikanser ilaç olan Doxorubicin hücelere karşı gösterdiği sitotoksik etkisinden dolayı kanser terapisinde kullanılır. Lipozomlar Doxorubicinin sitotoksik etkisini azalttı ve ilacı daha uzun süre boyunca saldı.

CdTe çekirdekli Kuantum Noktacıkları görüntüleme ve lipozomların rotalarını gözlemek için izleme ajanı olarak kullanıldılar. Lipozomlar CdTe kuantum noktalarının inorganik çekirdekten dolayı oluşan sitotoksik etkisini %30 engelledi. Floresan Kuantum noktaları lipozomların içinde tutuldu ve konfokal mikroskopu altında 16 saat süreyle gözlendi ve lipozomlar ile Saos2 hüceleri arasındaki etkileşimleri izlendi. Gerçek zamanlı gözlem çalışmaları hem katyonik hem de nötr lipozomların Saos2 hüceleri ile bağlandığını ancak katyonik lipozomların Saos2 hücelere bağlanmada daha hızlı olduğunu göstermektedir.

Endotel hücelerin çoğalmasını önlemesi açısından değerlendirilen Anti-anjiyogenez bir ajan olan Bevacizumab ise HUVEC hüceleri üzerinde değerlendirme koşullarında etkisiz olarak bulunmuştur ancak HITAEC hüceleri üzerinde çoğalmayı azalttıkları bulunmuştur.

Anahtar Kelimeler: Lipozom, Kuantum Tanecikleri, Anti-anjiyogenez, Anti-kanser, Polimer fırça, İlaç salımı.

Dedicated to Seher and H. İnan Büyüksungur

ACKNOWLEDGEMENTS

I would like to express my most sincere gratitude to my supervisor Prof. Dr. Vasif Hasircı for his continuous guidance, support and encouragement throughout my thesis.

I am also indebted to my co-supervisor Dr. Celestino Padeste for his support and guidance especially in Switzerland.

My sincere acknowledgements go to my thesis progress committee members, Prof. Dr. Menemşe Gümüşderelioğlu and Assoc. Prof. Dr. Ayşe Elif Erson Bensan for their useful comments and suggestions throughout this thesis.

I would like to express my sincere gratitude to Assoc Prof. Dr. Hilmi Volkan Demir and Dr. Evren Mutlugün (Bilkent University, Ankara, Turkey) for the provision of Quantum Dots.

I wish to thank to all members of METU BIOMAT Research Group who helped and influenced this study in many ways. I would like to thank to Senem Heper for her help and support. I also would like to thank Mr. Zeynel Akın for his support throughout my thesis and being an older brother for me.

I would like to thank Dr. Pınar Yılıgör Huri, Dr. Erkin Aydın, Gökhan Bahçecioglu and Dr. Aytaç Kocabaş for their invaluable friendship, support and help.

I am grateful to Melike Guzey for her kind friendship, suggestions and endless support throughout this thesis.

I enjoyed serving as BIOMED 2009 conference secretary and BDMD workshop secretary. I learned a lot about the computers and softwares by being computer coordinator and webmaster of www pages of BIOMAT, BIOMATEN, BDMD, BTEC and BIOMED 2009. Lastly supervising the BIOMATEN building renovation taught me a lot.

This thesis was supported by METU BAP, TUBITAK through project TBAG 105T508 and Ministry of Development via DPT 2011K120350. I would like to acknowledge TUBITAK for the 2211 PhD scholarship between 2006- 2011 and to the support from Ministry of Development via DPT 2011K120350 from 2011 September- 2013 September.

Finally, I would like to thank from the depth of my heart, my dear parents Seher Büyüksungur, who ironically got her diagnosis of breast cancer in July 2013, and Hamdi İnan Büyüksungur for their understanding, love, care and support during this study as well as all throughout my life.

TABLE OF CONTENTS

ABSTRACT	v
ÖZ	vii
ACKNOWLEDGEMENTS	x
TABLE OF CONTENTS	xii
LIST OF TABLES	xiv
LIST OF FIGURES.....	xv
LIST OF ABBREVIATIONS	xxi
CHAPTERS	
1 INTRODUCTION.....	1
1.1 Cancer.....	1
1.2 Cancer Therapy.....	2
1.2.1 Doxorubicin.....	3
1.3 Drug Delivery Systems.....	4
1.3.1 Nanoparticles in Drug Delivery.....	6
1.4 Liposomes.....	8
1.5 Anti-Angiogenesis Agents.....	13
1.5.1 Bevacizumab	19
1.6 Quantum Dots.....	19
1.7 Aim, Approach and Novelty of the Study	25
2 MATERIALS AND METHODS	27
2.1 Materials	27
2.2 Methods	28
2.2.1 Preparation of Liposomes.....	28
2.2.1.1 Active and Passive Loading of Doxorubicin into Liposomes.....	29
2.2.2 Preparation of Liposomes for Surface Interaction Studies	29
2.2.2.1 Preparation of Extruded Liposomes.....	29
2.2.2.1.1 Charged Liposome Production	29
2.2.3 Characterization of liposomes	30
2.2.3.1 Size distribution of liposomes.....	30
2.2.3.2 Encapsulation efficiency calculation	30
2.2.3.3 <i>In situ</i> release studies	30
2.2.4 QD Preparation.....	31

2.2.5 <i>In vitro</i> Studies	31
2.2.5.1 Cell Proliferation Assay	31
2.2.6 Microscopy.....	33
2.2.6.1 Live Cell Imaging.....	33
2.2.7 Characterization of Liposomes by Transmission Electron Microscopy (TEM)	34
2.2.8 Preparation of Surfaces with Modified Chemistry.....	34
2.2.9 Preparation of Surfaces with Polymer Brushes.....	35
2.2.10 Statistical Analysis	35
3 RESULTS AND DISCUSSION	37
3.1 Investigation of Liposome Surface Interaction	37
3.1.1 Selection of Compounds for Patterning Surfaces and Reacting with Liposomes ...	37
3.1.2 Liposome Behavior on Polymer Brushes	41
3.1.2.1 Liposome Behavior on Negative Polyelectrolyte Polymer Brush Surfaces	41
3.2 Preparation of Liposomes	44
3.3 Preparation of Quantum Dot Labeled Liposomes	45
3.4 Preparation of CdTe labeled liposomes	46
3.4.1 Separation of Free QDs from Liposome Loaded QDs	53
3.4.2 Determination of Liposome Size with Dynamic Light Scattering	55
3.4.3 Morphological Characterization of QD Loaded Liposomes by	
Transmission Electron Microscopy (TEM)	57
3.5 Cytotoxicity of Free QD and QD Loaded in Liposomes.....	58
3.6 Real Time Observation of Neutral and Positively Charged MLV Liposome- Cell Interactions	65
3.6.1 Real Time Observation of Anticancer Agent Doxorubicin	
Loaded Neutral MLV Liposomes	68
3.7 <i>In situ</i> and <i>In vitro</i> Studies with Doxorubicin	80
3.7.1 <i>In vitro</i> Testing of Toxicity of Free Doxorubicin on Saos2 Cells.....	82
3.8 <i>In Situ</i> and <i>In vitro</i> Studies with Bevacizumab	84
4 CONCLUSION.....	91
REFERENCES	93
APPENDICES	101
A. Saos2 MTS/PES Calibration Curve.....	101
B. HUVEC Alamar Blue Calibration Curve	102
CURRICULUM VITAE.....	103

LIST OF TABLES

TABLES

Table 1. Types of nanocarriers for drug delivery	7
Table 2. Liposomal drugs approved or under clinical evaluation	10
Table 3 Pro- and anti-angiogenesis factors.	15
Table 4. The fluorescence intensities of eluates 4, 5 and 6.	54
Table 5. DLS results of unloaded MLV.	55
Table 6. Average size and size distribution of QD-loaded MLV (DLS).....	56
Table 7. Mean diameter of unloaded SUV.....	56
Table 8. DLS results of QD-loaded SUV.....	57
Table 9. The test conditions for the influence of MLV on QD cytotoxicity	62

LIST OF FIGURES

FIGURES

Figure 1. Structure of Doxorubicin. A) Basic chemical structure, B) X-ray structure of a DNA–(doxorubicin) ₂ complex.....	3
Figure 2. Drug level in the plasma with conventional systemic drug dosing and with a DDS.....	5
Figure 3. Types of liposomes and basic structure.....	11
Figure 4. Capillary-to-cell relation in a healthy vascularized tissue.....	14
Figure 5. Schematic representation of endothelium coating in a blood vessel.....	15
Figure 6. Schematic representation of blood vessels. A) Healthy blood vessel, B) Tumor blood vessel.....	16
Figure 7. The problems related to tumor angiogenesis.....	17
Figure 8. Stages of vasculature organization.....	18
Figure 9. The size-dependent luminescence of quantum dots.....	20
Figure 10. Coated and targeted quantum dot.....	21
Figure 11. Spectrum with superimposed emission wavelengths of QD cores.....	22
Figure 12. Size dependence of the optical properties of CdSe quantum dots.....	23
Figure 13. Fluorescence of quantum dots and fluorescent organic molecules. Excitation with UV QD (A) CdTe, and (B) organic dye Calcein.....	23
Figure 14. Schematic representation of SUV liposome preparation.....	28
Figure 15. POC cell chamber system in the Confocal Scanning Light Microscope.....	33
Figure 16. Schematic representation of photolithography process.....	34
Figure 17. Schematic representation of polymer brush preparation through EUV exposure.....	35
Figure 18. Schematic representation of polymer coating on half photoresist coated glass slide. Polymer is applied onto the partially photoresist coated surfaces, the photoresist was then removed and the glass slide with one side with a polymer and the other just glass for treatment with the liposomes.....	38

Figure 19. Liposome attachment on FS (no charge) and APTMS (positive charge) surfaces treated with polystyrenesulfonate (PSS) solutions. A) FS treated with PSS (10 x), B) APTMS treated with PSS (10 x), C) APTMS treated with PSS (40 x) (Scale bar 5 μ m). ...	39
Figure 20. Scheme of the liposomal binding.....	39
Figure 21. Liposomal binding to fluorosilane deposited GTMS (3-glycidoxypropyltrimethoxysilane) and poly(allylamine) (PAA) covered surfaces with anionic liposomes. (Scale bar 5 μ m).	40
Figure 22. Scheme of the liposomal binding on fluorosilane deposited surface.....	40
Figure 23. Light micrograph of surface structures produced with the micro-/ nano-grafting technique (from Padeste et. al., 2004).	41
Figure 24. Cationic multilamellar liposome attachment on surfaces with PMA brush regions. A) Multilamellar liposomes (10x), B) Magnification of A (40x), C) Multilamellar liposomes with different lengths of brush polymer (10x). The light regions are where on surfaces with PMA brushes were formed.....	42
Figure 25. Cationic extruded liposome attachment on surfaces with PMA brush regions. A) Extruded liposomes (10x), B) Magnification of A (40x), C) extruded liposomes interacting with polymers of different length (10x). The light regions are where the PMA brushes were formed.	42
Figure 26. Presence of cationic MLV liposomes on polymer brush regions of the Teflon surface after 24 h incubation in the buffer solution. A) Multilamellar liposomes (10x), B) Magnification of A (40x).	43
Figure 27. Attachment of cationic extruded bilayer liposomes on polymer brush regions on the Teflon surface after 24 h incubation in the buffer solution. A) Extruded liposomes, B) and C).....	43
Figure 28. Cationic liposomes attached on polymer brush surfaces after 48 h in buffer solution. A) Multilamellar liposome (10 x), B) Extruded liposome (10 x).....	44
Figure 29. GPC of calcein loaded liposome.....	45
Figure 30. Absorption spectrum of CdTe Quantum Dots between 0-800 nm.....	46
Figure 31. Calibration curve for CdTe quantum dots at λ_{ex} 488 nm and λ_{em} 614 nm	47
Figure 32. GPC eluates of QD loaded SUV. A) Visible light, B) UV λ_{ex} : 352 nm.....	48
Figure 33. The effect of UV exposure on liposome, QDs and QD-loaded liposomes. A) QD-loaded liposomes, B) Free QDs, C) Empty liposomes.	48

Figure 34. CSLM and transmission microscopy of QD-loaded liposomes exposed to light source with different wavelengths. A) 458 nm laser, B) 543 nm laser, C) 633 nm laser. (x20).....	49
Figure 35. Micrographs of liposomes loaded with QD. A) Transmission, B) Confocal, C) Overlay (x40).....	50
Figure 36. Micrographs of Saos2 cells with QD-loaded liposome. a) Confocal at 488 nm, b) Transmission, c) Overlay. (x40). Arrow heads show the Saos2 cells.....	51
Figure 37. Control micrographs of Saos2 cells in the absence of liposomes. A) Transmission, B) Confocal at 488 nm, C) Overlay (x40).....	52
Figure 38. Control micrographs of Saos2 cells with empty liposomes. A) Transmission, B) Confocal at 488 nm, C) Overlay at 488 nm(x40).	53
Figure 39. GPC of loading of liposomes with QD. UV-Vis spectrophotometry (blue, 410 nm) and spectrofluorimetry (red, λ_{ex} : 497 nm, λ_{em} : 514 nm).	54
Figure 40. A representative DLS of size distribution for unloaded MLV.	55
Figure 41. TEM images of QD loaded MLV Liposomes. A) QD loaded MLV, B) Multilamellar lipid layer structure. Stained with uranyl acetate for the lipid membrane components.	57
Figure 42. TEM images of QD loaded SUV Liposomes (x 150,000). Stained with uranyl acetate for the lipid membrane components.	58
Figure 43. Light microscope images of Saos2 cells after 24 h of incubation. a) Saos2 cells, b) Saos2 cells with free Quantum Dots, c) Saos2 cells with Quantum Dot-loaded liposomes, d) Saos2 cells with unloaded liposomes (4x).....	59
Figure 44. Light microscopy images of Saos2 cells after 48 h of incubation. A) Saos2 cells, B) Saos2 cells with Quantum Dots, C) Saos2 cells with quantum Dot-loaded liposomes, D) Saos2 cells with unloaded liposomes (4x).	60
Figure 45. MTS results of unloaded liposomes with Saos2 cells.	61
Figure 46. Influence of Quantum Dots on the proliferation of Saos2 cells (MTS test) loaded into SUV liposomes or free. After 48 h incubation with the cells. (+) indicates the significant difference (p value lower than 0.05). (n=2)	61
Figure 47. MTS results of control (no QD, blue), free QDs (red) and QD loaded in MLV liposomes (QDL, black) allowed to interact with Saos2 cells for 24 h. The numbers are volumes of the test solutions added to the wells. (+) indicates the significant difference ...	63

Figure 48. Alamar Blue cell viability test for the exposure of Saos2 cells to free QDs and SUV encapsulated QDs. Exposure duration 24 h. Seeding density 30,000 cells/well. (+) indicates the significant difference (p value lower than 0.05). (n=2)..... 64

Figure 49. Confocal Micrograph of Saos2 cells treated with 100 nM QD loaded SUV liposomes. Test duration: 24 h. (x60)..... 65

Figure 50. CLSM micrographs of Saos2 cells in interaction with calcein loaded neutral MLV liposomes. Duration of interaction. A) 0 min, B) 60 min. (63x) 66

Figure 51. CLSM and transmission micrographs of Saos2 cells in the presence of calcein loaded cationic MLV liposomes. Interaction time: 0. A) Confocal micrograph, B) Transmission micrograph, C) Overlay micrograph. (60x) Arrow heads show the MLV. C denotes the Saos2 cell..... 67

Figure 52. CLSM and transmission micrographs of Saos2 cells in the presence of calcein loaded cationic MLV liposomes. Interaction time: 88 min. A) Confocal micrograph, B) Transmission micrograph, C) Overlay micrograph. (60x) Arrowhead shows the MLV and C denotes the Saos2 cells. 67

Figure 53. CLSM and transmission micrographs of Saos2 cells in the presence of calcein loaded cationic MLV liposomes. Interaction time: 180. A) Confocal micrograph, B) Transmission micrograph, C) Overlay micrograph. (60x) Arrowhead shows the MLV and C denotes the Saos2 cells. 68

Figure 54. Time zero for the real time observation a) Location map of the cells, b) CLSM overlay micrographs showing Saos2 and doxorubicin loaded neutral liposomes, 0 min. (40x) 69

Figure 55. Doxorubicin loaded liposome in contact with Saos2 cell (within red circle). (40x) 70

Figure 56. Doxorubicin loaded liposomes in contact with the Saos2 cells. (40x)..... 71

Figure 57. Three doxorubicin loaded liposomes in contact with three Saos2 cells. (40x) ... 72

Figure 58. Liposomes move on the cells. (40x) 73

Figure 59. Another liposome in contact with a cell. (40x) 74

Figure 60. Saos2 cells start to shrink time of exposure: 846 min. (40x) 75

Figure 61. Dead Saos2 cell. t: about 16 h. (40x) 76

Figure 62. End of the real time observation. Indicated region with a circle was scanned for 8.8 μm thickness..... 77

Figure 63. 3D scanning of Saos2 cell interacting with the Doxorubicin loaded liposomes z:- 4.8 μm . A) Confocal micrograph, B) Transmission micrograph, C) Overlay micrograph. . 77

Figure 64. 3D scanning of Saos2 cells with the Doxorubicin loaded liposomes z:-0 μm A) Confocal micrograph, B) Transmission micrograph, C) Overlay micrograph.	78
Figure 65. 3D scanning of Saos2 cells with the Doxorubicin loaded liposomes z= +4 μm . A) Confocal micrograph, B) Transmission micrograph, C) Overlay micrograph.	78
Figure 66. 3D projection of 3D scanning of the Saos2 and Doxorubicin interaction A) Confocal micrograph, B) Transmission micrograph, C) Overlay micrograph.	79
Figure 67. CLSM and transmission micrographs lateral 3D projection. A) Confocal micrograph, B) Transmission micrograph, C) Overlay micrograph.	80
Figure 68. Release of Doxorubicin from passive loaded neutral SUV liposomes, inlet Higuchi's release model prediction.....	81
Figure 69. Release of Doxorubicin from FAT SUV liposome vs. Time	82
Figure 70. Effect of concentration of Doxorubicin on viability of Saos2 as determined with Alamar Blue test after 24 and 48 h incubation. Cell seeding density 3×10^4 /well in RPMI medium. (n=2)	83
Figure 71. MTS results of Control cells, free Doxorubicin and FAT doxorubicin-loaded MLV liposomes with Saos2 cells. Time of exposure: 24 h. The numbers are concentrations in nM. Doxorubicin-loaded MLVs (Dox-L), Free Doxorubicin (Doxo).	84
Figure 72. Influence of Bevacizumab concentration on the proliferation of HUVEC (Alamar test). After 24 h incubation. Control contains only the cells, Control PB contains the phosphate buffer in the amount of Bevacizumab added. Cell seeding density:.....	85
Figure 73. Light micrographs of HUVEC and Saos2 in the co-culture system. 24 h after incubation in DMEM low glucose medium (x10). The round cells are HUVEC and spindle shaped cells are Saos2.....	86
Figure 74. Effect of Bevacizumab concentration on the proliferation of HUVEC and Saos2 cells in a co-culture system. Time of incubation 24 h. Medium: DMEM low glucose..	86
Figure 75. Influence of Bevacizumab concentration and encapsulation in liposomes on the viability of HUVEC (Alamar test). 0.5-20 indicate the dose for free Bevacizumab, and 0.5L-20L for liposome encapsulated Bevacizumab. VEGF was added into the control indicated with (+) and to all the other samples.	88
Figure 76. Influence of the concentration of Bevacizumab on HUVEC proliferation in the presence of ECGS. 0.5L- 20L are the dose in liposome encapsulated Bevacizumab samples. ECGS was added in control indicated with (+) and all the other samples except control ...	89

Figure 77. Influence of the concentration of Bevacizumab on HITAEC and Saos2 cells proliferation in a co-culture system. Time of incubation 24 h. Medium: 0.5- 50 are the dose used Bevacizumab samples. 90

Figure 78. Saos2 MTS/PES Calibration Curve 101

Figure 79. HUVEC Alamar Blue Calibration Curve..... 102

LIST OF ABBREVIATIONS

3-D	3 Dimensional
ALP	Alkaline Phosphatase
BSA	Bovine Serum Albumin
CALCEIN	(3, 3'-Bis [N, N-bis (carboxymethyl) aminomethyl] fluorescein)
CLSM	Confocal Laser Scanning Microscope
DDS	Drug Delivery System
DMEM	Dulbecco's Modified Eagle Medium
DMSO	Dimethyl Sulfoxide
DNA	Deoxyribonucleic Acid
ECGS	Endothelial Cell Growth Supplement
EDTA	Ethylene Diamine Tetraacetic Acid
EE	Encapsulation Efficiency
ELISA	Enzyme-Linked ImmunoSorbent Assay
EPC	Egg Yolk Phosphatidylcholine
FBS	Fetal Bovine Serum
FDA	Food and Drug Administration
FITC	Fluorescein Isothiocyanate
GPC	Gel Permeation Chromatography
HUVEC	Human Umbilical Vein Endothelial Cell
HITAEC	Human Internal Thoracic Artery Endothelial Cells
LECITHIN	1, 2-Diacyl-sn-glycero-3-phosphocholine
MLV	Multilamellar Vesicles
MTS	3-(4,5-Dimethylthiazol-2-yl)-5-(3-carboxymethoxyphenyl)-2-(4-sulfophenyl)-2H-tetrazolium
MTT	(3-(4,5-Dimethylthiazol-2-yl)-2,5-diphenyltetrazolium bromide
MW	Molecular Weight
MWC	Molecular Weight Cut-off
PB	Phosphate Buffer
PBS	Phosphate Buffer Saline
PC	Phosphatidylcholine
RPMI	Roswell Park Memorial Institute Medium
SUV	Small Unilamellar Vesicles
QD	Quantum Dot
TCPS	Tissue Culture Polystyrene
TEM	Transmission Electron Microscope
UV	Ultraviolet
VEGF	Vascular Endothelial Growth Factor

CHAPTER 1

INTRODUCTION

Aim:

The aim of this study was to develop a drug delivery system based on liposomes for use in the treatment of cancer. The approach involved the use of a Quantum Dot based fluorescent agent to track the liposomal carrier when used *in vitro* and *in vivo*, an anticancer agent to kill cancer cells and anti-angiogenesis drug to prevent new vasculature formation. In all the cancer tissue would be attacked by depriving the cells of nutrients and oxygen meanwhile killing them by DNA crosslinking anticancer drugs. In this scenario Saos2 and HUVEC were the cancer and endothelial cells, Bevacizumab; the antiangiogenesis drug, Doxorubicin; the anticancer drug, and CdTe the inorganic core of the quantum dots.

1.1 Cancer

Cancer is a term used for diseases in which cell division is uncontrolled and can also invade other tissues. Cancer cells stimulate disorganized growth of new vasculature where the blood flow is more dynamic than in healthy tissues. Some vessels of solid tumors are leaky and some others are unusually tight, leading to distribution of drugs in the surrounding tissue. This is called nonuniform porousness. Because of this, the cancer drugs sometimes do not even reach the cancer cells.

Cancer was the cause of 7.6 million deaths and 12.7 million cases in 2008 worldwide, accounting for 64% of the deaths in the developing countries (Jemal et al., 2011). In females the breast cancer and in males the lung cancer are the most diagnosed cancers (Jemal et al., 2011). These cancer types are the leading causes of cancer related deaths but in the developed countries in males lung cancer is preceded by prostate cancer (Jemal et al., 2011).

Transformation of a healthy cell into a cancer cell can be described as uncontrolled division of the cell. For unlimited division, the cancer cells should have undergone some alterations. According to Hanahan and Weinberg (2011), cancer cells should acquire some capabilities; these are eight essential alterations in the physiology of the cell that collectively direct the malignant growth. These alterations are:

- Self-sufficiency in growth signals → activates H-Ras oncogene
- Insensitivity to anti-growth signals → loses retinoblastoma suppressor
- Evading apoptosis → produces IGF survival factors
- Limitless replicative potential → turns on telomerase
- Sustained angiogenesis → produces VEGF inducer
- Tissue invasion and metastasis → inactivates E-cadherin
- Reprogramming of energy metabolism → alters energy metabolism
- Evading immune destruction → disables components of the immune system

The order of emergence of these alterations is dependent on the cancer type (Hanahan and Weinberg, 2011).

The transformation of the cell can be started by genetic factors or physical, chemical, biological and environmental factors (Baba and Cătoi, 2007). Surgery, immunotherapy, radiation therapy, and chemotherapy are the common treatments currently in use.

1.2 Cancer Therapy

Conventional chemotherapeutic agents are actually cytotoxic agents and they have some limitations such as narrow therapeutic index, which limits the administered amount of the drug to get the intended response. Drugs have very high interindividual variability of drug kinetics, which needs optimization of the drug dose for each patient (Nishiyama and Eguchi, 2009). Cytotoxicity of some chemotherapeutic agents are concentration dependent and these can not be administered via routes that have a risk to produce high local concentrations such as oral and transdermal administration (Aluri et. al., 2009). Therefore, the development of new chemotherapeutics having more specificity to cancer cells is an urgent matter.

Drugs with different mechanisms of action and non-overlapping side effects can be used together for combination chemotherapy. Different types of combinations have been reported in the recent years including different liposomal drugs.

Surgery is generally used as a treatment for almost all cancer patients to remove as much tumor as possible. But it is not effective when used alone, it should be combined with other therapies. Surgery is invasive and it has some side effects.

Radiation therapy is a common method used for the treatment tumors. In this application ionizing radiation is used to irradiate the cancer cells. Radiation therapy can be used externally or internally and it also damages the healthy tissue around the tumor.

Chemotherapy involves the use of cytotoxic drugs that target cells undergoing mitosis. There are some other therapies such as immunotherapy, and photodynamic therapy (PDT) but these are in their development stages.

1.2.1 Doxorubicin

Doxorubicin, a secondary metabolite of *Streptomyces peucetius* var. *Caesius*, is used as an anticancer agent that directly interacts with DNA or DNA topoisomerase (Figure 1). It is used in the treatment of a number of carcinomas and Doxil is the first liposomal drug containing doxorubicin approved by FDA. Doxorubicin causes toxicity to the body leading to hematopoietic suppression, nausea, vomiting, and alopecia and most importantly cardiotoxicity. Therefore, it is very important to reduce its systemic administration. To reduce its cardiotoxicity liposomal formulations of the drug was developed and it was found that the liposomal formulation had decreased random distribution in the body while maintaining its anti-cancer efficacy. Additionally liposomal formulation improved the therapeutic index of the drug.

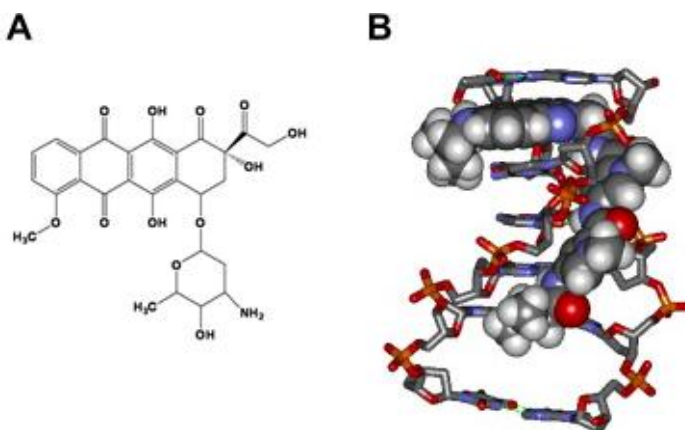


Figure 1. Structure of Doxorubicin. A) Basic chemical structure, B) X-ray structure of a DNA-(doxorubicin)₂ complex (adapted from Zhang et. al., 2010).

There are two different liposomal formulations of doxorubicin: Myocet, a non-PEGylated liposomal formulation, and Doxil, a PEGylated liposomal formulation of doxorubicin. Preclinical studies of non-PEGylated liposomal doxorubicin showed a significantly lower cardiac and gastrointestinal toxicity while having similar antitumor efficacy with equal dose of conventional doxorubicin (Visani and Isidori, 2011). PEGylated liposomal doxorubicin has reduced body distribution and extended circulation time, which shows the ability of using leaky vasculature to extravasate. However, the long circulation time leads to extended presence of the drug to the skin because of the delivery in the bloodstream (Soloman and Gabizon, 2008). Although the therapeutic index is increased with liposomal formulations, targeted liposomal doxorubicins are

being investigated to gain the advantage of increasing local concentrations and intracellular delivery.

1.3 Drug Delivery Systems

In conventional treatments, activity of most drugs in use against certain diseases or disease sites is not based on their ability to accumulate selectively in the pathological tissue or cell, but instead they are evenly distributed within the body (Torchilin, 2000). In the transport towards the site of action, the drug has to cross many biological barriers, such as membranes of organs, cells and intracellular compartments, where it can be inactivated or excreted, and therefore, rendered ineffective (Torchilin, 2000). In this systemic application it can cause damage to healthy tissues. To concentrate high concentrations of drug at the disease site, drug is administered systemically in large amounts, most of which just wasted by distribution in normal tissues; becoming the cause of many undesirable side effects. Drug delivery systems (DDS) are designed to overcome these problems.

A drug delivery system (DDS) can be defined as a system that aims to improve the efficacy and safety of the drug after administration to the patient (Demirbag et al., 2011). DDS attempts to control the released amount, rate, time, and localization of the drug in the body (Jain, 2008). The main purpose of targeted drug delivery systems is to deliver the drug efficiently and precisely to the targeted site in concentrations as high as possible and to healthy tissue as low as possible, in an appropriate period of time (Uekama et al., 1998).

Conventional chemotherapy against cancer is a systemic therapy and the dose is designed to not harm the healthy tissues. In these systems plasma drug level increases rapidly according to a first order kinetics after i.v. administration and then decreases with a similar order below the minimum effective level. Another dose should be administered to keep the concentration in the 'therapeutic window'. This administration protocol leads to rises and falls in the plasma drug level presenting a see-saw drug concentration. Figure 2 shows the drug level in the plasma with conventional drug administration and DDS.

The main aims for drug delivery system can be stated as (Torchilin, 2008);

- Extend bioavailability of the drug by protecting the drug from the host.
- Accumulate at the targeted site, avoid systemic distribution and protect the host from the drug.

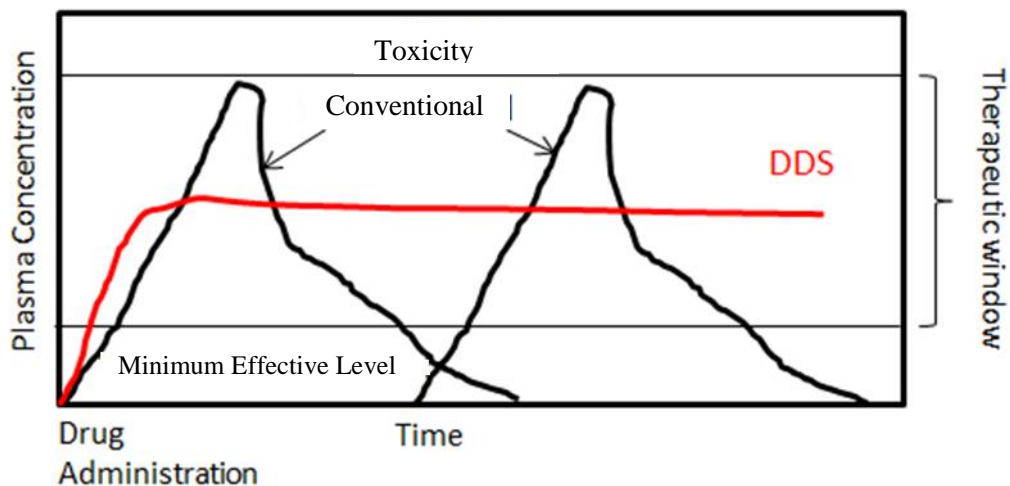


Figure 2. Drug level in the plasma with conventional systemic drug dosing and with a DDS.

For effective therapy and convenience of the patient the drug plasma concentration should be maintained in the therapeutic window. DDS are designed to release their content with zero order kinetics, constant drug level for a certain period of time. The rate equation for Zero Order kinetics $M_t = k_o \cdot t$: where M_t is the amount of drug released, it is time and k_o is a constant. According to this equation the rate or amount of delivery of the drug is independent of its concentration.

Generally, the chemotherapeutic agents interfere with the cell division cycle and any systemically administered chemotherapeutic drug (i.e. intravenous) affects healthy cells alongside the target cells such as: bone marrow cells and cells of follicles (Pankhurst et al., 2003).

Targeted DDS have been developed to solve these problems by increasing the concentration at the targeted side (Peer et al., 2007).

Targeting can be active or passive. In active targeting the drug is concentrated at a certain site because it is bound to a carrier or a moiety which specifically interacts with the cells or the tissue at this locality. In passive targeting the accumulation of drug is achieved by other means which do not involve such specific chemical interaction.

Specific surface antigens are generally selected for active targeting; ligands against these antigens can be conjugated to the carrier system or directly to the therapeutic agent. These antigens are selected depending on the expression levels in the particular cells. Some cancer cells produce these antigens more than the healthy cells and DDS can be targeted using these antigens to selectively accumulate in the cancer cells.

On the other hand, passive targeting uses the tumor's defective vasculature. The rapid vascularization process taking place at the tumor site leads to a chaotic structure of the tumor vasculature. These vessels have excessive loops and arterio-venous shunts, excessive branching, blind vascular endings, dilated microvessels, openings and a more leaky endothelium (Marcucci and Corti, 2012). These vessels have extra large pores on them and passive targeting takes advantage of this. Furthermore, solid tumors have fewer lymphatic vessels and the system cannot operate effectively leading to accumulation of extravasated macromolecules (Leu et al., 2000). These factors result in 'Enhanced Permeability and Retention' (EPR) effect (Matsamura and Maeda, 1986, Maeda et al., 2000). The EPR effect was realized more than 100 years ago by Goldmann who described tumor vasculature "The normal blood vessels of the organs in which the tumor is developing are disturbed by chaotic growth, there is a dilatation and spiraling of the affected vessels, marked capillary budding and new vessel formation, particularly at the advanced border". In 1971 Folkman showed the stimulation of vascularization by tumors. The EPR effect is quite significant when the drug carriers that are expected to extravasate at the target site are around 200 nm or smaller in diameter. When EPR is used for the targeting of the nanoparticles to the tumor site systemic toxicity can be avoided and high drug levels are achieved (Demirbag et al., 2011).

1.3.1 Nanoparticles in Drug Delivery

Nanomedicine is defined as the application of nanotechnology to disease treatment, diagnosis, monitoring and to the control of biological systems (National Institutes of Health, USA). Recent cancer therapies have significant toxicities, and side effects are common because in the process of treating cancer tissues, chemotherapeutic agents also damage healthy tissues (Liu et al., 2007). Nanocarriers can help overcome this problem because both the risk of killing the healthy tissues and the dosage of the drug used can be decreased if controlled delivery and targeting is achieved. Polymeric nanoparticles, quantum dots (QDs), silica nanoparticles, dendrimers, micelles, molecular conjugates, liposomes, and ultrasound microbubbles are examples of nanosystems that can be used for such purposes.

Solid, colloidal substances varying in size from 10 nm to 1000 nm are defined as nanoparticles (Brigger et al., 2002) even though nanotechnology calls particles nano if they are 100 nm or smaller. The properties of nanoparticles differ dramatically; these are high surface /volume ratio, improved solubility and multifunctionality (Gao and Xu, 2009). An active agent can be coupled with the nanoparticle through entrapment, adsorption, attachment, encapsulation or directly by dissolving the agent within the nanoparticle structure to create a nano-DDS (Sahoo et al., 2003). Nanoparticles are reported to improve the bioavailability, retention time and solubility of the bioactive agents associated with them (Kumari et al., 2010).

Most of the aims of targeting and controlled drug delivery can be achieved with conventional delivery systems (Sheridan et al., 2000; Yun et al., 2004); however, with

such micro systems, intracellular delivery and delivery across physiological barriers is not possible. With the usage of nanotechnology, drug delivery agents can deliver agents such as DNA (Kumar et al., 2004), antisense RNA and anticancer drugs (Park et al., 2005) and accumulation of agents at previously “unreachable” target sites such as blood-brain barrier (Olivier, 2005) is possible (Hasirci et. al., 2006). Nanoparticles of all sorts can permeate through capillary walls or gaps and their movement in the extracellular matrix and uptake by the cells is easier than the microparticles because of the size. The introduction of the nanoparticles through injection in close proximity to the disease site is sufficient to obtain high local concentration and minimal damage to healthy tissue can be achieved, this is another advantage of nanoparticles (Hasirci et. al., 2006). Moreover, enhanced targeting also decreases the total amount of drug used.

There are several types of carriers that can serve as drug carriers. Liposomes, polymeric nanoparticles, dendrimers are the mostly used controlled release systems. Their size can be scaled down to nanometers range (Table 1).

Table 1. Types of nanocarriers for drug delivery (adapted from Wang et al., 2005)

Form	Approach	Properties
Polymeric nanoparticles	<ul style="list-style-type: none"> • Drugs are conjugated to the side chain of a linear polymer with a (cleavable bond) linker, Surface modification (PEGylation) 	<ul style="list-style-type: none"> • Water soluble, non toxic biodegradable • Selective accumulation and retention in tumor tissue (EPR effect) • Specific targeting of cancer cells while sparing normal cells, cell-receptor mediated targeting with a ligand
Polymeric micelles	Amphiphilic block copolymers form a micelle with a hydrophobic core and hydrophilic shell	<ul style="list-style-type: none"> • Suitable carrier for water insoluble drug • Self assembled, biodegradable • Ease of modification • Targeting potential
Dendrimers	Radially emerging hyperbranched polymers with regular patterns and repeating units	<ul style="list-style-type: none"> • Biodistribution and pK can be tuned • High structural and chemical homogeneity • Ease of functionalization, high ligand density • Multifunctionality
Liposomes	Self assembly Structures composed of lipid bilayers	<ul style="list-style-type: none"> • Amphiphilic, biocompatible • Ease of modification • Targeting potential
Viral nanoparticles	Protein cages, which are multivalent, self assembled structures	<ul style="list-style-type: none"> • Surface modification by mutagenesis or bioconjugation multivalency • Specific tumor targeting, multifunctionality, biological compatibility • Defined geometry and uniformity
Carbon nanotubes	Carbon cylinders composed of benzene rings	<ul style="list-style-type: none"> • Water soluble and can be made biocompatible through chemical modifications • Multifunctionality

Properties required in nanoparticle DDS:

- **Release rate:** Nanoparticle should release its content in a way that it should not release its content while circulating. If the nanoparticle release its content to plasma then the release system become meaningless, its exposure, biodistribution and toxicity as if its free drug form.
-
- **Biocompatibility:** DDS should be biocompatible and hemocompatible. If not biocompatible it is dealt with as a foreign body. It will accumulate in the body and lead to induction of malignancy. If not hemocompatible it would lead to thrombogenicity.

Because of the EPR effect nanoparticles can reach the tumor site easily. In 1980s, Maeda et al., used the EPR effect to deliver the anticancer nanomedicine. Nanoparticles with a diameter under 7 nm are excreted by renal filtration; since most of the polymeric nanoparticles are larger this prolongs their circulation time (Taurin et. al., 2012). In the circulation particles larger than 100 nm are rapidly cleared by the reticulo-endothelial system (RES) (Taurin et. al., 2012). Therefore nanoparticles for chemotherapy have to be in this range to avoid the RES body and the renal clearance. FDA has approved 30 nanoparticles for clinical use, and liposomes were more successful compared to the others (Taurin et. al., 2012).

Multi-functionality is the major advantage of nanoparticles; they carry drugs, imaging agents and affinity ligands to achieve traceable targeted drug delivery (Probst et. al., 2013). With the help of this multi-functionality the distribution effect of the drug can be observed real time.

1.4 Liposomes

Liposomes are vesicles consisting of one or more phospholipid bilayers surrounding an aqueous cavity. Liposomes can be prepared using synthetic or natural phospholipids and safe to use because they are non-toxic. They can carry both hydrophilic and hydrophobic drugs and be targeted to a special cell type or site and they can be controlled by different parameters to deliver their ingredients at correct site and timing. Liposomes were first produced by Alec D. Bangham in 1965. Liposomes (also known as lipid bilayer vesicles) are cell-like spherical aggregates formed by self-assembling of amphiphilic molecules such as phospholipids. They can be prepared from synthetic or natural phospholipid sources. Until the 1970s liposomes were only used in the mimicking of the biological membranes and investigating their biophysical properties. Since then liposomes have also been used as drug delivery systems because of their high degree of biocompatibility and their ability to encapsulate large amounts of material inside the vesicle or in its membrane (Wang et al., 2005). Liposomes are important as models for biomembranes, for drug formulation, for gene delivery, and as vehicles for delivering various agents used in cancer therapy. Liposomes have been used to deliver anticancer drugs and antimicrobial agents, DNA and proteins, and the delivery

of drugs for diabetes and cardiovascular diseases (Wang et al., 2005). Liposomes have certain advantages over other drug carriers like biodegradability, relative toxicological and immunological safety (Banerjee, 2001). Liposomes meet the basic biocompatibility requirements of DDS by causing little or no antigenic, pyrogenic, allergic and toxic reactions. They protect both the drugs from the host and the host from the drug. The therapeutic index and bioavailability of liposome delivered drugs increase efficacy and reduce toxicity. Liposomes can carry both hydrophilic and hydrophobic molecules; hydrophilic molecules are encapsulated in the aqueous core and hydrophobic molecules embedded in the lipid bilayer.

Doxil was the first liposomal anticancer formulation approved by the Food and Drug Administration (FDA, USA) in 1995. Currently liposomes hold market leadership of the nanoparticles for cancer treatment (Bharali and Mousa, 2010). Table 2 shows the liposomal formulations that are currently approved or under clinical trials.

Table 2. Liposomal drugs approved or under clinical evaluation (from Elbayoumi and Torchilin, 2010)

Active Drug	Commercial Name	Indications
Daunorubicin	DaunoXome	Kaposi's sarcoma
Doxurubicin	Mycet	Combinational therapy of recurrent breast cancer
Doxorubicin in PEG-liposomes	Doxil, Caelyx	Refractory Kaposi's sarcoma; ovarian cancer; recurrent breast cancer
Annamycin	Annamycin	Doxorubicin-resistant tumors
Amphotericin B	AmBisome	Fungal infections
Cytarabine	DepoCyt	Lymphomatous meningitis
Vincristine	Marqibo	Metastatic malignant uveal melanoma
Lurtotecan	Lurtotecan liposome	Fallopian tube cancer, ovarian cancer, peritoneal cavity cancer
Irinotecan	LE-SN38	Advanced cancer
Camptothecin analogue	S-CDK602	Various tumors
Topotecan	INX-0076	Advanced cancer
Mitoxantrone	LEM-ETU	Leukemia, breast, stomach and ovarian cancers
Nystatin	Nyotran	Topical anti-fungal agent
All-trans retinoic acid	Altragen	Acute promyelocytic leukemia; non-Hodgkin's lymphoma; renal cell carcinoma; Kaposi's sarcoma
Platinum compounds	Platar	Solid tumors
Cisplatin	SPI-077	Head and neck cancer
Cisplatin	Lipoplatin	Various tumors
Paclitaxel	LEP-ETU	Ovarian, breast and lung cancers
E1A gene	E1A gene-cationic liposome	Various tumors
DNA plasmid encoding HLA-B7	Allovectin-7	Metastatic melanoma and b2 microglobulin
BLP 25 vaccine	Stimuvax®	Non-small cell lung cancer vaccine
DNA	HepaXen	Hepatitis B vaccine

Table 2 shows the liposomal formulations commercially available or are in clinical trial. However, the full therapeutic potential of liposomal drug delivery systems has not been tapped because there are several disadvantages of liposomes that have to be resolved such as stability, duration of release, high cost of preparation, short shelf life, and poor interaction with certain drugs (Wang et al., 2005).

Surface charge, size, lipid composition, dose and the route are the factors that affect the pharmacokinetic variables of the liposomes. There are a few types of liposomes that classified according to their lamellarity and their size. Figure 3 shows the types of liposomes and the basic membrane structure.

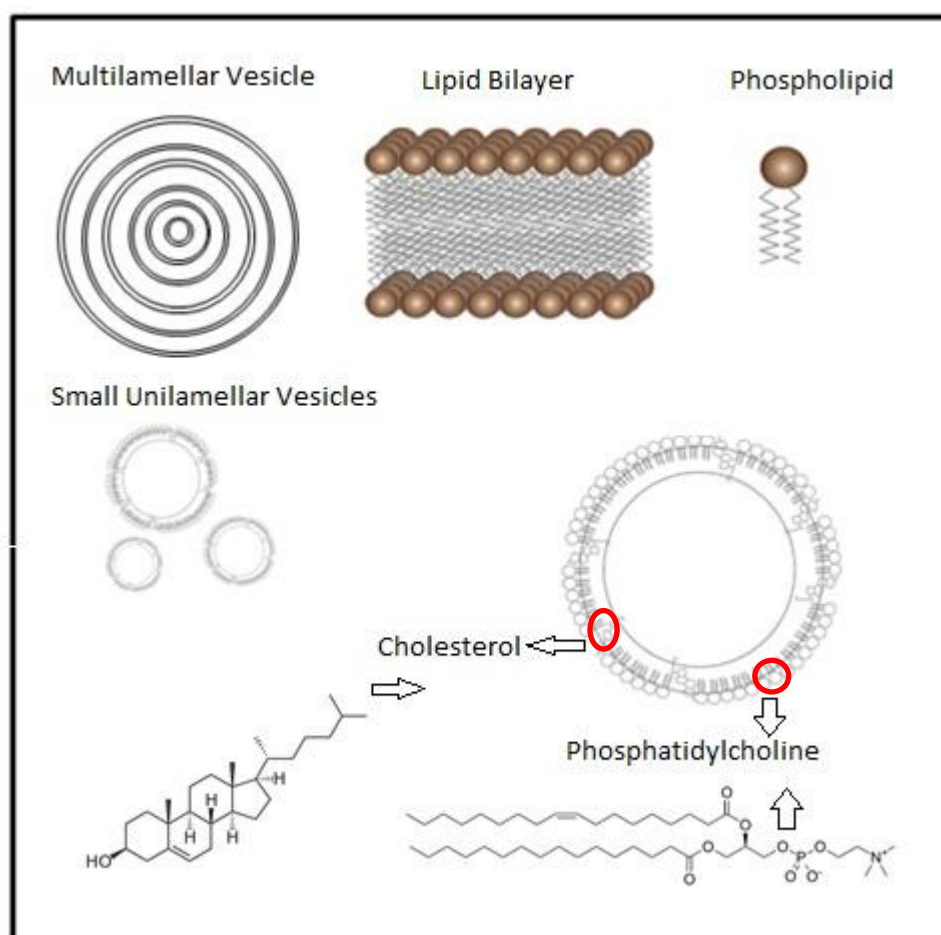


Figure 3. Types of liposomes and basic structure.

Figure 3 shows the basic structures of phosphatidylcholine (PC), cholesterol and the liposomes. Liposomes can be classified into 4 groups in terms of their lamellarities and size:

- Multilamellar vesicles (MLVs) have several concentric lipid bilayers like an onion and their diameter changes between 1 and 5 μm . They are very suitable for entrapping water insoluble drugs because of the high lamellarity.
- Small Unilamellar Vesicles (SUV) consist of one lipid bilayer. They are generally produced from MLVs and are 20-200 nm in diameter.
- Large Unilamellar Vesicles (LUV) have a single lipid bilayer like SUVs but the diameter is in the range 200-1000 nm.
- Multivesicular vesicles (MVV) consist of several vesicles (SUVs) encapsulated in one larger vesicle (LUV).

Liposomes can be classified according to their production method: (i) Thin lipid film hydration, (ii) Extrusion, (iii) Reverse phase evaporation, and (iv) Freeze-thaw.

Phosphatidylcholine is a mixture of phospholipids and is mainly used in the production of neutral liposomes because it does not have a net charge. Cholesterol is used in the liposome structure both to mimic the cell membrane and also because it increases the stability of the bilayer by increasing the packing of the phospholipids in the bilayer. The flat aliphatic rings of cholesterol are buried in the bilayer while the hydroxyl group is positioned towards the internal and external aqueous environments. It is reported that when the cholesterol concentration exceeds 30% the stability of the liposomes start to decrease (Cirli and Hasirci, 2004).

Reticuloendothelial system (RES) consists of liver, kidney and spleen and eliminates the liposomes from the circulation by accumulating them in these and liver, spleen, and the bone primary sites with the help of the macrophages (Elbayoumi and Torchilin, 2010). Mononuclear phagocytic system captures the liposome after i.v. administration mainly because of the opsonin molecules bound to surface of the liposomes (Storm et al., 1995). Changing the surface charge to neutral or to negative and decreasing the liposome size to 80-200 nm can reduce the uptake by the RES because the micron sized larger liposomes are phagocytosed more rapidly than the smaller ones. Therefore, SUVs have a longer life time than the MLVs *in vivo*.

Liposomes can be used to target drugs to certain sites or organs or tissues in the body. Certain proteins, peptides, antibodies and nucleic acids can be used for targeting the liposomes after their attachment to the liposome surface. Targeting leads to the accumulation of the liposomes in the target region but this does not automatically increase the efficacy because the interaction between cell and liposome is the main determinant in this process (Kirpotin et al., 2006). However, an increase of drug concentration in the microenvironment of a target site is very advantageous from the points of side effects, bioavailability and interaction with the cell membrane.

For systemic injection, the liposomes are coated with polyethylene glycol (PEG), which is a linear polyether diol that is inert, and biocompatible. PEG decreases the recognition of the liposomes by opsonins and clearance by macrophages by forming a

steric protective layer which is mainly a layer of highly hydrated molecules (Elbayoumi and Torchilin, 2010). PEG modified liposomes such as Doxil are also called 'stealth liposomes' by Papahadjopoulos who designed the PEGylated liposomes first. Most nanocarriers interact with the cells and trigger uptake regardless of surface coating but PEG coating prevents cell binding (Probst et al., 2013). Although PEG usage increases the accumulation of the liposomes in the tumor site, PEG affects the interaction with the tumor cell membrane and reduces the internalization of the liposome (Taurin et al., 2012). To improve the uptake, ligands are better molecules to cover the liposomes. These ligands (eg. folate) improve the endocytosis because these molecules are actively transported across cell membranes (Geidel, et al., 2012).

Generally drug delivery systems are designed to release their content at a certain region in the body and with zero order kinetics. In order to avoid continual fixed rate release drug delivery systems are designed to release their content in response to environmental stimuli such as changes in pH, temperature, magnetic field, etc. Responsive liposomes generally carry a stimuli sensitive component in their structure, upon the application of which destabilize the liposomal membrane.

1.5 Anti-Angiogenesis Agents

The development of the embryo, inflammation and wound repair processes lead to new blood vessel formation (Caterina and Libby, 2007). Formation of the vasculature in embryogenesis is defined as vasculogenesis, which involves the generation of new endothelial cells and their assembly (Hanahan and Folkman, 1996). Angiogenesis is the process of new branching (sprouting) of vessels from pre-existing vessels. Endothelial cells cover the inner surface of all vessels. Therefore, angiogenesis involves proliferation and migration of these cells. In the passage of tumors from dormant state to a malignant state angiogenesis is a fundamental step.

Homeostasis of tissue is dependent upon an adequate supply of nutrients delivered through blood vessels. Cells have to reside within 100 μm radius of a capillary, the diffusion limit for oxygen, to be supplied by oxygen and nutrients and for the removal of waste products and CO_2 from the tissue. Therefore, the maintenance of the vascular network is critical (Hanahan and Weinberg, 2000, Forough et al., 2006). Figure 4 shows a scheme of vascularized tissue.

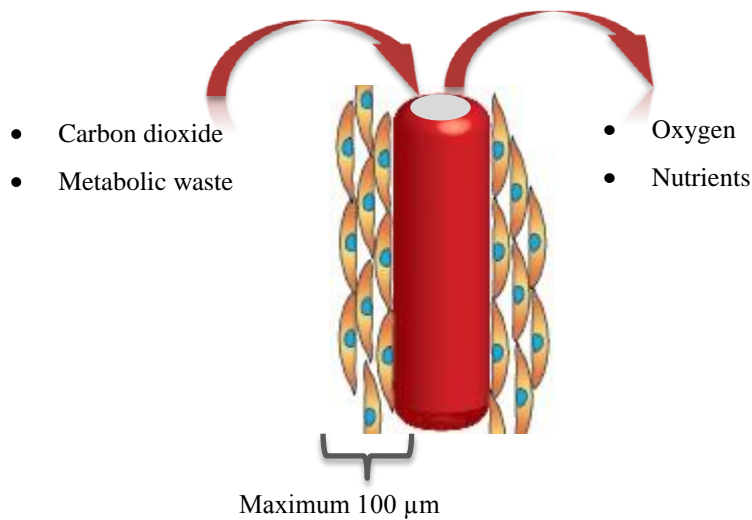


Figure 4. Capillary-to-cell relation in a healthy vascularized tissue.

Figure 4 represents the relation between the capillaries and the cells in a healthy, vascularized tissue where the distance between them has to be in the range of 100 μm . Otherwise, cells cannot be supplied with enough oxygen and nutrients and the waste cannot be removed.

In adults new blood vessels are produced mainly through angiogenesis. Angiogenesis is started with the signal from a cell and is activated by a lack of oxygen. Hypoxia-inducible transcription factors activate angiogenic genes. These angiogenic molecules activate endothelial cells to proliferate. Endothelial cells also secrete matrix metalloproteins, which degrade vessel walls. Then the cells migrate to the extracellular matrix and organize to form the capillary lumen. These normal processes lead to the formation of regular blood vessels. Angiogenesis process is controlled by pro- and anti-angiogenic signals. Stimulating and inhibiting signals are tightly regulated and balanced to produce healthy blood vessels. Counterbalancing of these signals induces or stops angiogenesis (Baeriswyl and Christofori, 2009). Table 3 presents the angiogenesis inhibitors and stimulators.

Table 3 Pro- and anti-angiogenesis factors (adapted from Forough, 2006).

Angiogenic Growth Factors	Angiogenesis Inhibitors
Angiogenin	Canstain
Vascular endothelial growth factor	Interferon
Fibroblast growth factor	Endostain
Platelet-derived endothelial cell	Canstain
Leptin	Tumstatin
Angiopoietins	Thrombospondin-1
Granulocyte colony-stimulating factor	Platelet factor-4
Interleukin-8	Prolactin 16 kD fragment
Hepatocyte growth factor	Interleukin-12
	Metalloproteinase inhibitors
	Proliferin-related protein
	Placental ribonuclease inhibitors
	Human chorionic gonadotropin

When these factors work in harmony the normal blood vessel formation occurs but an alteration of this equilibrium promotes dysregulated vessel growth with a consequent major impact on health (Forough, 2006).

Endothelial cells cover the inside of all blood vessels (Figure 5). Selective permeability, blood flow without clotting, angiogenesis and blood pressure regulation are the functions of these endothelial cells.

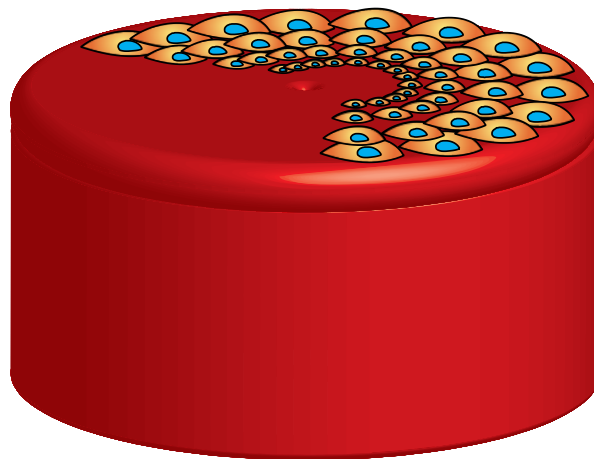


Figure 5. Schematic representation of endothelium coating in a blood vessel.

Tumors need blood vessels to obtain oxygen and nutrients and to discharge metabolic wastes and CO₂, and due to the diffusion limitation of oxygen without angiogenesis tumors cannot grow larger than 1-2 mm (Folkman, 1971). Angiogenesis which almost always continues leads to the sprouting of new vessels, which in turn helps sustain the expanding of neoplastic growths (Hanahan and Folkman, 1996).

Solid tumors disrupt the equilibrium by producing angiogenic growth factors and continually activating angiogenesis with the exception of prostate and pancreatic cancer (Maeda, 2012). The new blood vessels of the tumors have excessive branching, distorted and enlarged vessels, blind endings, excessive loops, precocious capillary sprouting, leakiness, irregular blood flow, abnormal endothelial cell proliferation and apoptosis (Hanahan and Weinberg, 2011). As such, tumor blood vessels are disorganized and highly abnormal in their structure and function. Figure 6 presents a tumor blood vessel. Blood flows fast in some vessels, while it is static in others (Jain, 2004). Blood may flow in one direction for a while and then reverse its direction. Flow problem is the major drawback for the conventional drug delivery. In some tumors, pore size can be as large as one or two microns wide in the blood vessels as compared with healthy blood vessels it is more than 100 times larger (Jain, 2008). As a result of this there is no normal pressure gradient in the walls. Therefore, the fluid inside the tumor blood vessels escapes through vessel walls. Tumor cells and various tumor-generated proteins can escape in the fluid from tumors and proteins activate the generation of new blood and lymphatic vessels in the surrounding normal tissue and lymph nodes; this is called the metastasis (Jain, 2008). This undesirable change in the fluid dynamics results in an increase in the retention of the nanoparticles and this is good when they carry drugs in them Figure 6.

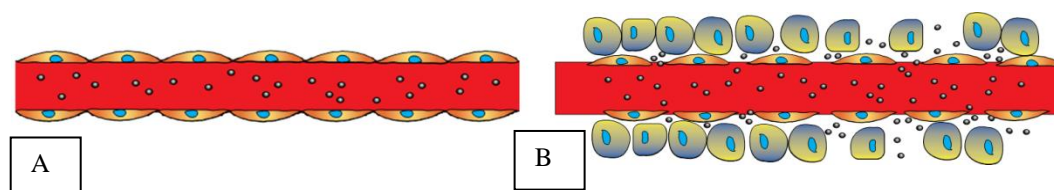


Figure 6. Schematic representation of blood vessels. A) Healthy blood vessel, B) Tumor blood vessel.

These abnormalities of tumor vessels lead to create unnatural microenvironment inside a tumor where insufficient oxygen delivery happens, a general state of hypoxia and low pH prevails in the tumor that makes the tumors more aggressive and prone to metastasis (Jain, 2008). Because of the acidity and low oxygen immune cells are blocked in the fighting the tumor. Figure 7 shows the problems related to tumor angiogenesis.

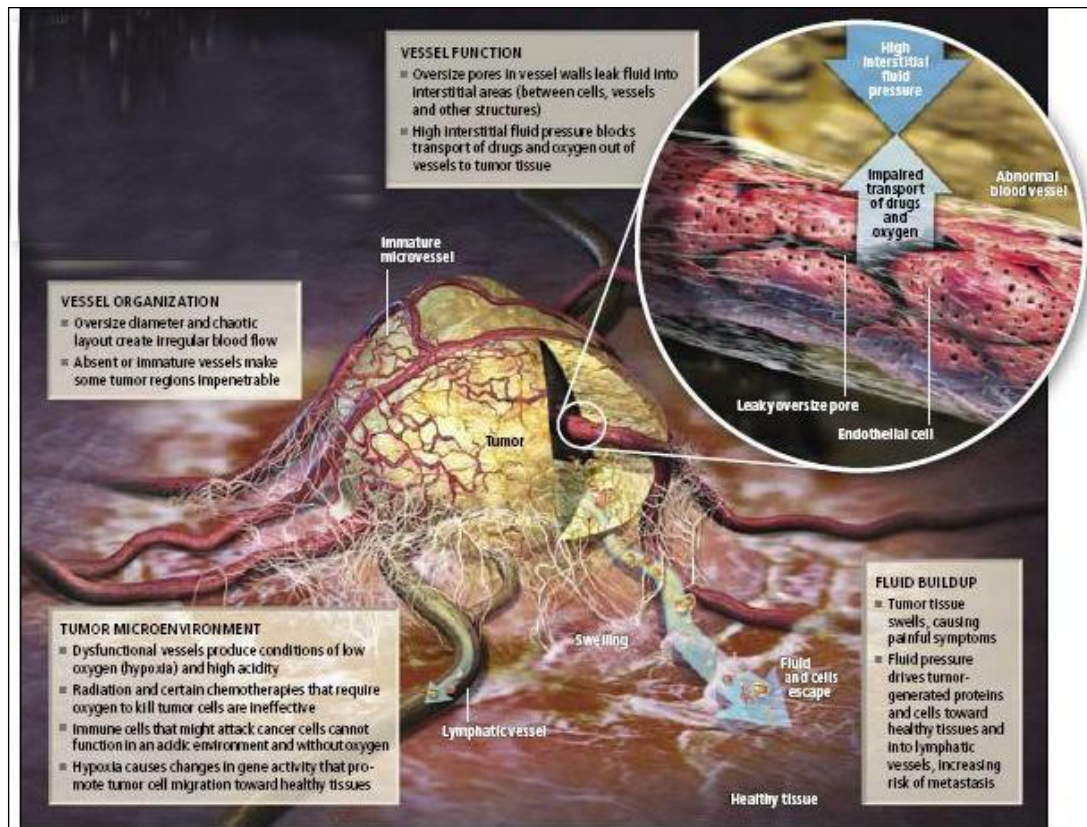


Figure 7. The problems related to tumor angiogenesis (From Jain, 2008).

In angiogenesis there are many factors that enhance new blood vessel formation. The most potent one is the Vascular Endothelial Growth Factor (VEGF) which promotes the survival and proliferation of the endothelial cells. In addition, it makes the vessels leaky. In tumor angiogenesis VEGF-A is the primary type of growth factor involved. There are three other types of VEGF (B, C and D). Isoforms of VEGF-A are 121, 165, 189. VEGF-A is a basic protein secreted into the blood. Endothelial cells are activated by VEGF through their receptors, VEGFR1, VEGFR2 and neuropilin (Kuesters and Campbell, 2010). In normal tissues, VEGF and other growth-stimulating molecules work in harmony with anti-angiogenesis molecules like thrombospondin to achieve a balance and a normal vascularization. However, in the solid tumors VEGF is abundant and it leads to the formation of disorganized and nonfunctional blood vessels. VEGF is one of the most potent angiogenesis agents that disrupt the equilibrium of vascularization. In order to normalize the tumor blood vessels, the activity of VEGF should be neutralized. The normalized blood vessels are less leaky, less dilated, less tortuous, and functionally improved such as; so that there is lower interstitial fluid pressure, higher oxygenation and improved of drug delivery (Jain, 2004). Figure 8 shows the schematic representation of different stages of blood vessel organization.

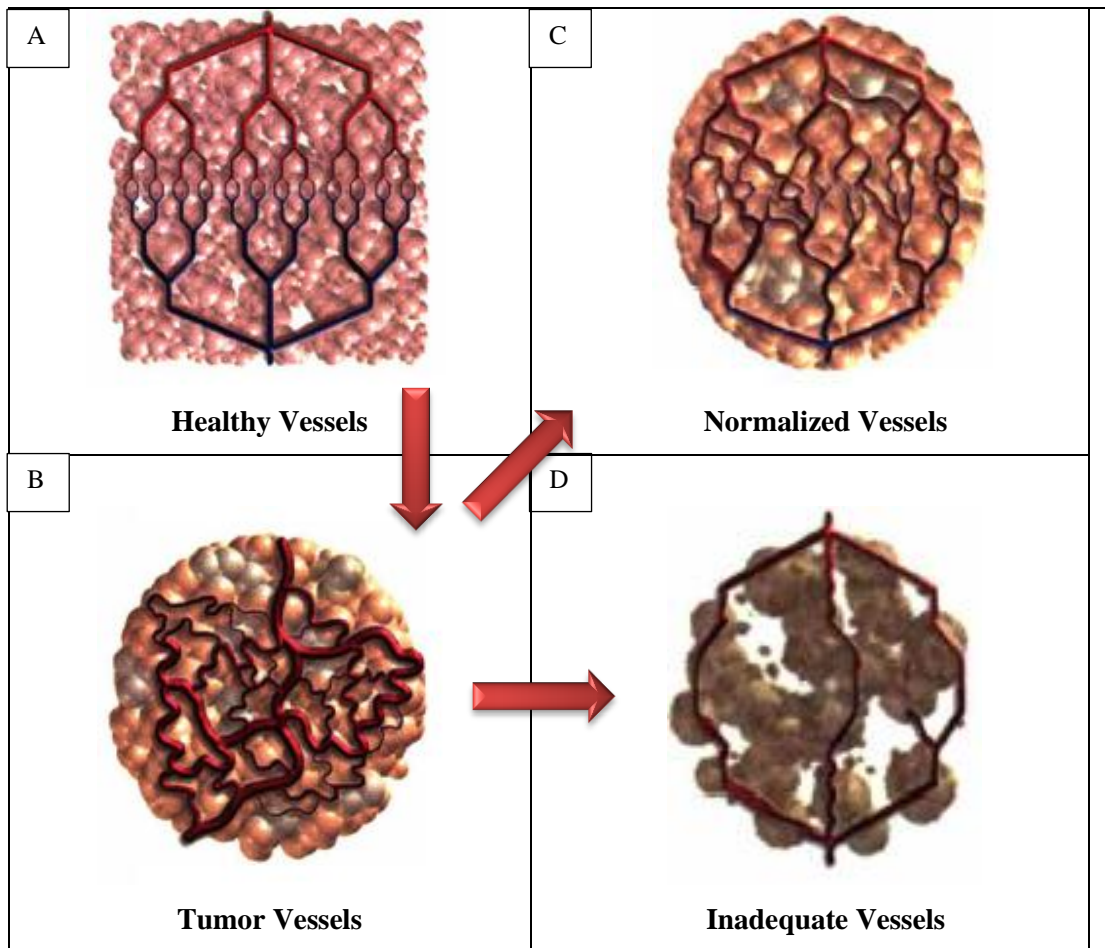


Figure 8. Stages of vasculature organization (Adapted from Duda et al., 2007).

Figure 8A shows that healthy blood vessels are organized very well and the blood flow feeds all the cells and remove the waste materials. The main reason for this is the balance between anti- and pro- angiogenesis agents. When the tumor starts to grow this equilibrium collapses and proangiogenesis agents are produced more than antiangiogenesis agents. The result is the leaky chaotic tumor vessel formation (Figure 8B). Anti-VEGF (antiangiogenesis agent) can regain the equilibrium by blocking the VEGF and as a result blocking the endothelial cell production. Thus normalization of the blood vessels can happen (Figure 8C). However, if the applied antiangiogenesis agents tilt the equilibrium towards the antiangiogenesis side, then the tissue blood vessel organization becomes inadequate and therefore the blood distribution is inadequate (Figure 8D). Neutralization of VEGF can lead to normalization of the tumor vessels but this treatment should establish a balance between the pro and anti-angiogenesis agents; otherwise the vessels can be inadequate and this leads to death of the healthy tissues.

There are two main routes to stop the action of VEGF; one of them is to make an antibody bind to VEGF and prevent it from serving as a growth signal molecule for

the endothelial cells by binding to receptors on the cell surface. The second route is to prepare an antibody that directly binds to the VEGF-receptors on the cell membrane.

Sengupta et al (2005) reported a drug delivery system they called 'nanocell' comprising a nuclear nanoparticle within an extracellular PEGylated-lipid envelope (liposome). They designed the nanocell so that it first released an anti-angiogenesis agent, and then released a chemotherapy agent. They found that the concentration of the anti-angiogenic agent, reached significant levels within 12 h while the release of the chemotherapy agent was extended to 15 days. With this system an increase in the lifespan of the nanocell treated animals were observed.

1.5.1 Bevacizumab

There are 8 different drugs that target the VEGF pathway approved or are pending approved by the FDA and Bevacizumab is the most prescribed drug among them (Carmeliet and Jain, 2011). It is a monoclonal antibody against VEGF, binds directly to VEGF and inhibits its activity instead of the receptors in the VEGF pathway. Bevacizumab is the first FDA approved biological agent designed to inhibit new blood vessel formation and it received FDA approval for metastatic colon cancer and non-small lung cancer in 2004 for a combination use with standard chemotherapy. In 2008, FDA approved it for in use metastatic breast cancer. Bevacizumab binds all these isoforms of VEGF-A but is ineffective against the other VEGFs (Ferrara et al., 2004). It was shown that the drug increases the survival times of patients when used in combination with chemotherapy. It was shown that Bevacizumab can benefit the patients only when combined with chemotherapy or immunotherapy.

When Bevacizumab inactivates VEGF some of the existing vessels are destroyed and others are remodeled. This leads to normalization of the vessels and in turn reduction in the hypoxia and increase in fluid pressure and these improve the efficacy of the chemotherapy against tumor. The concentration of an anti-angiogenesis agent like Bevacizumab in the plasma is very important because if the dose is too high then it causes excessive vessel pruning and this can result in decreased oxygen level (increased hypoxia) (Jain and Carmeliet, 2012).

1.6 Quantum Dots

When a photon is absorbed by a fluorescent material, the energy of the photon leads to the transition of an electron from the ground state to an excited state. Release of this energy induces photoluminescence and is a result of the relaxation of the electron. Excitation and relaxation of the electron are the main phenomena of the fluorescence. The radius of the electron hole pair of quantum dots is much smaller than the natural

radius of, therefore, when a quantum dot is excited, the required energy to confine excitation is higher and the result is emission at shorter wavelengths is the result (Ioannou and Griffin, 2010). Figure 9 shows the relation between the size and bandgap energy. This interaction leads to tunable emission of the quantum dots.

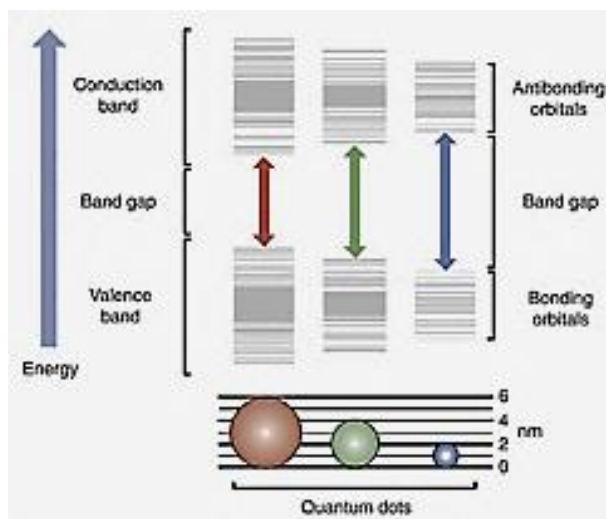


Figure 9. The size-dependent luminescence of quantum dots (Adapted from Ioannou and Griffin, 2010).

Quantum dots (QD) are a novel class of inorganic fluorophores. Conventional fluorescent dyes have narrow excitation spectra leading to excitation by a specific wavelength, but QDs have broad absorption spectra allowing excitation by a wide range of wavelengths and multiple different colored QDs can be excited using a single wavelength (Figure 10) (Jaimeson et. al., 2007). Also, a few minutes of excitation can lead to bleach of organic fluorophores but QDs are extremely stable and can fluoresce for hours with high level of brightness and can resist repeated cycles of excitation and emission and have high photobleaching threshold (Jaimeson et. al., 2007). Quantum dots, also known inorganic semiconductor nanocrystallites, have unique, size dependent optical properties (Murray et al. 1993). They have thousands of repeated unit cells. After their first introduction in the 1980s (Rossetti et el., 1983), they have gained a great deal of attention and a broad range of applications in different disciplines were introduced. In these applications, QDs have been used as optoelectronic components such as quantum dot lasers, IR photodetectors, display LEDs and as fluorescent labels in the life sciences (Bukowski and Simmons 2002). Quantum dots are composed of elements from the periodic table groups II–VI (eg. CdTe, CdSe) or III–V (eg. InAs, InP) elements (Chan et al., 2002). They are made of the same elements as the bulk semiconductors but quantum dots are very small, on the order of a few nanometers. The inorganic cores of quantum dots are generally covered with shells, which are also made of semiconductors. The core structures might have some imperfections and the shell structure covers these

imperfections and avoids the ‘blinking’ of the core structure (Raab and Stephanopoulos, 2004) and increases the stability of the quantum dots. Coating of inert polymers (e.g. PEG) onto the shell structure can increase the stability of quantum dots by decreasing their aggregation and also making them more biocompatible (Walling et al., 2009). Biomolecules can be added onto the surface of the polymeric coat for targeting of the QD in the body or in a cell but often decreases the fluorescence intensity and photostability (Al-Jamal et al., 2008). Figure 10 shows the basic structure of a quantum dot.

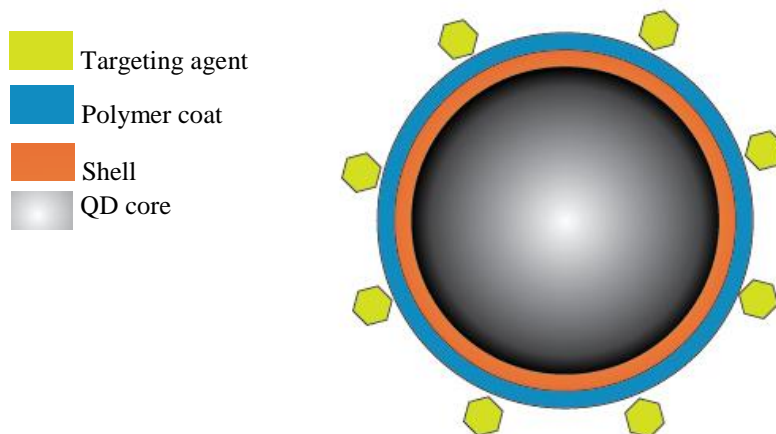


Figure 10. Coated and targeted quantum dot

Quantum dots are the most useful tools for researchers in biology especially when used as biomarkers because the photoluminescence from the quantum dots can be tuned to cover almost all the visible wavelength region (Xu, 2005), which is very important for visualizing the cells or tissues that being are investigated. Quantum dots have very different emission profiles and these profiles help choose the right quantum dot. Figure 11 shows emission wavelengths of different quantum dot cores.

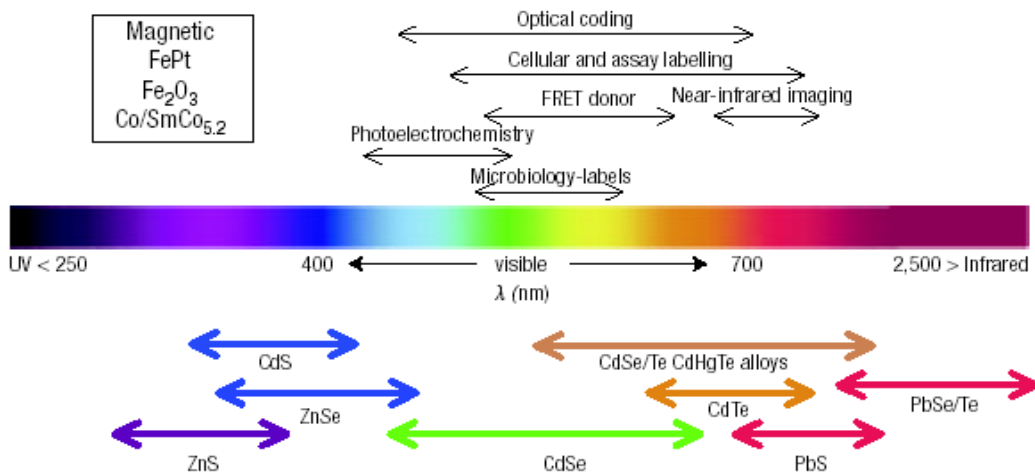


Figure 11. Spectrum with superimposed emission wavelengths of QD cores (Medintz et al., 2005).

Organic dyes have a narrow excitation spectra, and therefore, require excitation by light of a specific wavelength which is different for different dyes. But QDs have a broad absorption spectrum which allows them to be excited with different wavelengths (Smith et al., 2008). Organic dyes, however, have a broad emission spectra which leads to the overlap of emission from different organic dyes used in labeling one object. Thus, the use of a number of organic dyes together is very limited (Jamieson et al., 2007). QDs on the other hand have a narrow emission spectra that can be controlled by the core size, composition and surface coatings (Figure 12). Their size can be adjusted to emit light at a variety of precise wavelengths ranging from ultraviolet (UV) to infrared (Jamieson et al., 2007). Almost all quantum dots can be excited with UV so different colored quantum dots can be simultaneously excited by a single light source. The size dependent fluorescence properties of cadmium selenide QDs subjected to ultraviolet light, absorption and emission spectra are presented in Figure 12.

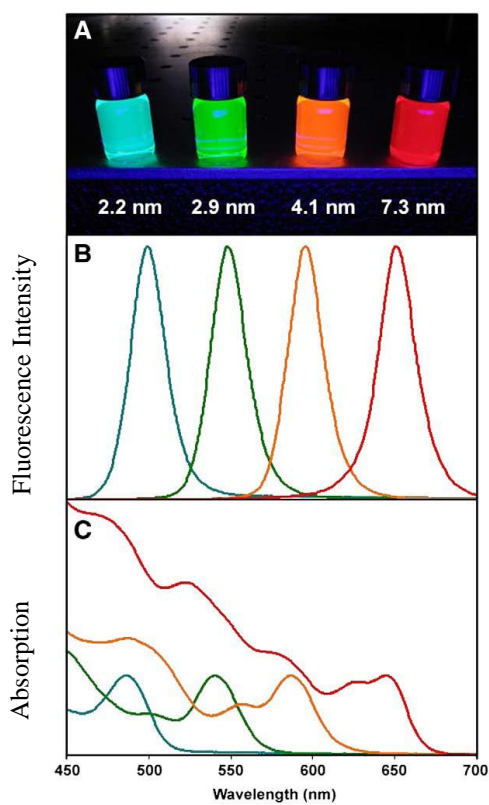


Figure 12. Size dependence of the optical properties of CdSe quantum dots (Smith et al., 2008).

Figure 13 shows the fluorescent emission by the CdTe quantum dot and organic dye Calcein after excitation with UV.

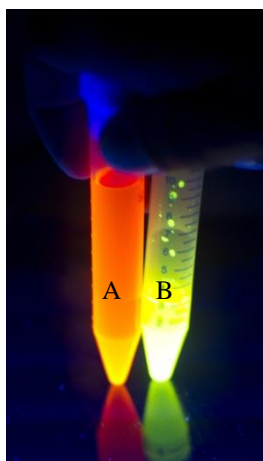


Figure 13. Fluorescence of quantum dots and fluorescent organic molecules. Excitation with UV QD (A) CdTe, and (B) organic dye Calcein.

Quantum dots are different from the organic dyes in their photostability. Organic fluorophores have very low photobleaching thresholds (bleaching very easily), in which irreversible light-induced photochemical reactions happen but QDs are extremely stable and can bear excitation and emission cycles for hours with a high level of brightness (Hang et al., 2001; Jamieson et al., 2007). For example, dihydrolipoic acid (DHLA)-capped cadmium selenide-zinc sulfide (CdSe-ZnS) QDs were nearly 100 times more stable, and 20 times brighter than, rhodamine 6G and showed no loss in intensity after 14 h (Chan et al., 2002; Jamieson et al., 2007). Quantum dots have a very high extinction coefficient, therefore, they absorb more photons than the organic dyes. They have unit cell structures, which increases their absorption of the photons intrinsically. Their light absorption rate is 10-50 times faster than the organic dyes, therefore, they are much brighter than organic dyes (Michalet et al., 2005). QDs also have a long fluorescent lifetime than the organic dyes after excitation. The emission by an organic dye upon excitation has a lifetime of about 5 ns (Jamieson et al., 2007). Conversely, QDs have 5-100 ns lifetime and the larger the quantum dot size the longer the fluorescent lifetime. These properties of QDs make them very suitable for long term monitoring of labeled substances. Autofluorescence from specimens decrease the sensitivity and common source of background. This decay of QDs leads to vanishing of the autofluorescence signal of the specimen while QDs emitting photons (Pinaud, et al., 2006).

In most applications bare core QDs are not used. There are three main reasons for that. First of all, QDs may have imperfections in their crystalline structure which leads to irregularities in emission (Jamieson et al., 2007). Secondly, since these cores possess high surface area to volume ratio they are highly reactive and unstable, and therefore, may easily be subject to photochemical degradation. This highly reactive nature could be very undesirable in biological applications in terms of cytotoxicity and carcinogenicity (Probst et al., 2013+). Thirdly, depending on the type of application, QDs may require certain modifications in their surface chemistry, and such modifications are not made on the bare cores. Considering all these, the bare cores are generally surrounded with a shell structure or a coating. The shell is another semiconductor which possesses a larger bandgap which provides a protection to the core against oxidation and fluorescence quenching by entrapping the hole-electron pairs inside the core (Jamieson et al., 2007).

In 2006, Chen et al., tried encapsulation of quantum dots in liposomes. They encapsulated commercially available quantum dots within the liposomes which were prepared by reverse-evaporation method. Their results showed that inside the liposomes no fluorescence self-quenching of quantum dots was not observed. Later Al-Jamal et al. (2008), prepared lipid-quantum dot bilayer vesicles. They integrated commercially available CdSe/ZnS core/shell quantum dots within the liposome membranes. They prepared thin lipid film with the QDs and then hydrated it as a result they integrated QDs with the liposomes membrane. Their results suggest that integration of quantum dots within the liposome membrane improves the photostability of QDs in storage and against UV exposure.

In this study keeping all the variants in mind MLV and SUV liposomes were prepared using phosphatidylcholine, cholesterol and dodecylamine (to provide positive charge), or DOPS (dioleoyl-sn-glycero-3-phospho-L-serine) (to provide negative charge).

In order to track liposomes Quantum Dots with CdTe cores were loaded into the liposomes. To prevent cell growth doxorubicin was selected and Bevacizumab was tested as the antiangiogenesis agent. These were tested on Saos2 human osteosarcoma cells and HUVEC human vascular endothelial cells under *in vitro* conditions alone or in co-culture.

1.7 Aim, Approach and Novelty of the Study

The aim of this research was to achieve cancer therapy using a 2-pronged approach. One was to deliver an anticancer agent to the tumor cells to crosslink the DNA and to block replication and the other was to prevent angiogenesis (blood vessel growth) at the tumor site. In order to achieve this, two different types of liposomes labeled with Quantum Dots were prepared. One type carried Bevacizumab, ‘an anti-angiogenesis’ agent to lower and thus normalize the blood vascularization. And the second carried an anti-cancer drug, Doxorubicin, to inactivate the cancer cells. Here three different concepts were brought together in the design of one drug delivery system: (i) imaging of the cancer cells and tracking of the liposomes, (ii) normalization of tumor blood vessels and (iii) inactivation of the cancer cells to achieve an effective anticancer treatment.

In the literature there is no delivery system design involving these 3 active agents to use in cancer therapy at the same time.

CHAPTER 2

MATERIALS AND METHODS

2.1 Materials

Cholesterol (5-cholesten-3 β -ol), Calcein (3, 3'-bis [N,N-bis(carboxymethyl)aminomethyl] fluorescein) and Doxorubicin hydrochloride were purchased from Sigma-Aldrich Co (Germany) and used without further purification.

Lecithin (1.2-diacyl-sn-glycero-3-phosphocholine) (PC) (from egg yolk), citric acid, potassium dihydrogen phosphate and potassium monohydrogen phosphate were obtained from Merck AG (Germany). Chloroform (CHCl₃) was the product of Lab-Scan Analytical Sciences (Dublin, Ireland). Dimethyl sulfoxide (DMSO) and Triton-X 100 were obtained from AppliChem. Trypan blue (0.4 %) and Alamar blue® were purchased from Invitrogen Inc. (USA). MTS (Cell Titer® Nonradioactivity Cell Proliferation Assay) kit was obtained from Promega Co (USA). Sodium sulfite (98 %, ACS) was obtained from Sigma-Aldrich (Germany). Osteosarcoma cells (Saos2) (ATCC, HTB-85) was purchased from American MesoEndo Growth Medium was obtained from Cell Applications Inc. USA. Type Cell Collection (ATCC). Human umbilical vein endothelial cells (HUVEC) were kindly provided by Prof. Dr. Gamze Torun Kose of Yeditepe University (Istanbul, Turkey).

Sephadex G 50-80 was purchased from Sigma-Aldrich Co (Germany) and swollen in excess potassium phosphate buffer (0.05 M, pH 7.4) before use. Nunc™ OptiCell Cell Culture System was purchased from Thermo Scientific (USA). Coomassie Plus Bradford Assay was obtained from Pierce (USA) POPC (1-Palmitoyl-2-oleoylphosphatidylcholine), Dodecylamine, DOPS (1,2-dioleoyl-sn-glycero-3-phospho-L-serine) and fluorescence lipid (1-oleoyl-2-{6-[(7-nitro-2-1,3-benzoxadiazol-4-yl)amino]hexanoyl}-sn-glycero-3-phosphocholine) were obtained from Avanti Polar Lipids Inc (USA). Bevacizumab (Altuzan) (25 mg/mL) was purchased from Roche Pharma (Basel, Switzerland).

DMEM-High glucose, DMEM-High glucose modified, fetal bovine serum (FBS), trypsin-EDTA (0.25 %) (HyClone) and SnakeSkin pleated dialysis tubing (10000 molecular weight cut off) were purchased from Thermo Scientific (USA).

CdTe water dispersed quantum dots were kindly provided by Assoc. Prof. Dr. Hilmi Volkan Demir of Bilkent University (Ankara, Turkey).

2.2 Methods

2.2.1 Preparation of Liposomes

Lipids of the liposomes are dissolved in chloroform, poured into a round bottom flask (50 mL) and the flask is attached to the rotary vacuum evaporator (Bibby Sterilin, RE-100, UK) (Figure 14). The temperature is fixed to 39°C (should not exceed the boiling temperature of the solvent) and the speed of rotation is fixed to 8-10. The process is continued until the complete removal of the solvent and formation of a thin lipid film (TLF). The flask is flushed with nitrogen to remove the traces of solvent. Spontaneous liposome formation takes place when the lipid film is hydrated with the drug solution.

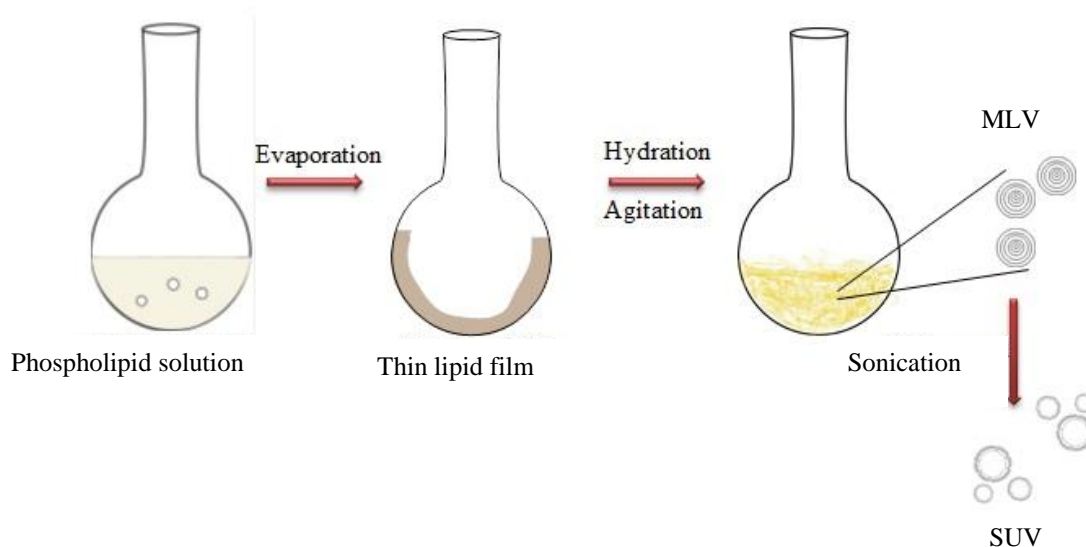


Figure 14. Schematic representation of SUV liposome preparation.

Hydration was performed with agitation for 5 min on vortex (Heidolph Reax Top, Germany) and drug encapsulation was achieved. Multilamellar Vesicles (MLV) are obtained after addition drug solution and vortexing. After formation of MLV, liposome solution sonicated for 5 min with 30 s intervals at 20 watts. To separate liposomes from the untrapped material; gel permeation chromatography (GPC) is applied. Ultrasonication step is done in ice to avoid temperature increase and oxidation of the lipids.

After separation of liposomes by GPC using Sephadex G50-80 beads the optical densities of the eluates were measured at 410 nm with UV spectrophotometer (Shimadzu, UV-1201, Japan) to detect the fractions with the liposome. When a fluorescence matter such as calcein is loaded into the liposomes, this is measured with spectrofluorometer (Shimadzu, RF-5000, Japan).

2.2.1.1 Active and Passive Loading of Doxorubicin into Liposomes

After TLF formation two different methods are used for the loading of material into liposomes; active and passive loading.

Passive loading:

After formation of TLF, hydration of the film was carried out as described in section 2.2.1.

Active Loading (Freeze-Thawed Liposomes- FAT):

After formation of lipid layer, multilamellar vesicles were formed by hydrating with 100 mM citric acid (pH 4.0) and vortexing. Then the mixture was frozen (-80°C) and thawed (60°C) 3 times. Thus, transmembrane pH gradient was obtained. Warm Doxorubicin solution (65°C) and liposomes were mixed and incubated at 65°C for 10 min (Liu et. al., 2001). Then to discard the citric acid, gel permeation chromatography is applied.

2.2.2 Preparation of Liposomes for Surface Interaction Studies

2.2.2.1 Preparation of Extruded Liposomes

Extrusion produces liposomes by forcing aqueous suspensions through polycarbonate filters with defined pore size. MLV are directly used for the preparation of extruded liposomes. MLV were filtered with the filters having 800 nm pore size then extruded liposomes were filtered with the filters having 400 nm cut-off size. The prepared liposomes were directly used for further experiments.

2.2.2.1.1 Charged Liposome Production

Charged liposomes were produced with the use of charged phospholipid ingredients. Multilamellar vesicles and extruded liposomes were prepared as charged liposomes according to following ratio:

- 69 % POPC (1-palmitoyl-2-oleoyl phosphatidylcholine)
- 20 % Dodecylamine (Positive charge) or 20 % 1,2-dioleoyl-sn-glycero-3-phospho-L-serine (DOPS) (Negative charge)
- 10 % Cholesterol
- 1% Fluorescence lipid (1-oleoyl-2-{6-[(7-nitro-2-1,3-benzoxadiazol-4-yl)amino]hexanoyl}-sn-glycero-3-phosphocholine) (18:1-06:0 fatty acid labeled)

Lipids were dissolved in chloroform and thin lipid film was prepared with rotary evaporator. Multilamellar liposomes were prepared by hydration of lipid film with 1 mL of 150 mM KCl + 10 mM 3-(N-morpholino) propane sulfonic acid buffer (MOPS), pH 7.0 for 5 minutes. Extruded liposomes were prepared from multilamellar liposomes using 400 nm filters in extruder.

2.2.3 Characterization of liposomes

2.2.3.1 Size distribution of liposomes

Dynamic Light Scattering (DLS) was used to investigate the particle size distribution, effect of QD loading, time and frequency of sonication on liposome size. These were performed with aqueous solution of liposomes at room temperature and 90° using a Malvern CGS-3 (UK) DLS system.

2.2.3.2 Encapsulation efficiency calculation

Encapsulation efficiency (EE) determination is used to quantify the amount of calcein, QDs, Doxorubicin and Bevacizumab in the liposome. Triton X-100 is used for the purpose of disrupting the liposomes.

$$EE (\%) = \frac{\text{Amount of fluorescent compound in Liposomes } (\mu\text{g})}{\text{Amount of fluorescent compound added to the liposome preparation medium } (\mu\text{g})} \times 100 \dots\dots\dots(I)$$

2.2.3.3 *In situ* release studies

In situ release studies were conducted at 37°C on an orbital shaker at 50 rpm. Liposome suspension was placed in a 5 cm long dialysis bag (10,000 molecular weight cut off) with addition of 1 mL phosphate buffer (10 mM, pH 7.4) and immersed into 50 mL phosphate buffer. Aliquots (3 mL) from the medium were analyzed at predetermined points to determine the release profiles. Calcein, quantum dots and doxorubicin content of the medium were determined by spectrofluorometer with λ_{ex} : 494 nm, λ_{em} : 517 nm for calcein, λ_{ex} : 488 nm, λ_{em} : 614 nm for quantum dots and λ_{ex} : 470 nm, λ_{em} : 590 nm excitation and emission wavelengths, respectively. Bevacizumab content was determined using the Bradford assay. Briefly, Coomassie dye binds the protein resulting in spectral shift. After incubation at room temperature, the absorbance at 595 nm was determined.

2.2.4 QD Preparation

CdTe quantum dots suspended in water were kindly provided by Assoc. Prof. Dr. Hilmi Volkan Demir of Bilkent University (Ankara, Turkey). The synthesis carried out in their labs was as follows: In aqueous CdTe synthesis, Cd (ClO₄)₂·6H₂O was dissolved in Milli-Q water and TGA was added to the mixture. NaOH was added dropwise to the mixture to increase the pH to 11.8-12.0. With this mixture became clear or slightly turbid. For the preparation of tellurium precursor, Al₂Te₃ was deaerated by passing Ar gas. To produce H₂Te gas, deaerated H₂SO₄ was slowly poured into Al₂Te₃ then the gas was carried by a slow Ar flow and bubbled through the mixture containing cadmium precursor. To obtain the the desired nanocrystal size, the mixture was refluxed at 100°C. Selective precipitation was used for the separation step after cooling to room temperature (Mutlugun et al., 2010). The QDs used were CdTe nanocrystals suspended in water. In this study the QD were used had a mean diameter of 3.473 nm and the suspension was 11.37 μM.

2.2.5 *In vitro* Studies

In order to study interaction of the nanoparticles with and to examine the interaction between liposomes and nanoparticles, Saos2 cells were used for the *in vitro* studies. Saos2 cells were grown in RPMI medium with 10% Fetal Bovine Serum, 100 units/mL- 100 mg/mL of Pen/Strep antibiotic and 1 μg/mL of Amphotericin B for the fungal contamination. HUVEC cells were grown in DMEM low glucose with the same amount of serum and antibiotics. Cells were incubated at 37°C in humidified CO₂ incubator (5% CO₂).

2.2.5.1 Cell Proliferation Assay

Three different colorimetric assays were used to determine cell viability, cell proliferation experiments.

Principle of the “Cell Titer® Nonradioactivity Cell Proliferation Assay” (MTS Assay): MTS assay is the conversion of MTS/PES solution into a water-soluble formazan that absorbs light at 490 nm. At predetermined time points, the media were discarded and the wells were washed with sterile media and MTS/PES solution (0.5 or 1 mL, 10% MTS/PES reagent in low glucose DMEM) was added on the cells. The cells were incubated for 2 h at 37°C in the CO₂ incubator. An aliquot of 200 μL was transferred into a 96 well plate and absorbance of the product of MTS assay was determined at 490 nm with Elisa Plate Reader (Model Maxline, Molecular Devices, USA). The absorbance was

correlated with the cell number using a calibration curve constructed with known cell numbers (Appendix A).

“Alamar Blue Cell Proliferation Assay” was used for the continuing culture of the live cells. It is based on detection of color produced by metabolic activity (related to cell number) of the cells. Oxidized form of Alamar Blue is reduced by mitochondrial enzyme activity and this reduction causes a color shift (from blue to red) which can be detected with a spectrophotometer.

At each time point, the wells were washed twice with sterile PBS and incubated for 1 h with Alamar Blue solution (10% DMEM colorless) at 37°C and 5% CO₂. Then supernatant (200 µL) was transferred to a 96 well plate and absorbance was determined at 570 and 595 nm. The wells were washed with PBS again and culture medium added to the wells and incubation was continued. Percent of reduction calculated as follows:

$$\text{Dye Reduced (Percent)} = \frac{((\epsilon_{\text{ox}})_{\lambda_2} \times A_{\lambda_1}) - ((\epsilon_{\text{ox}})_{\lambda_1} \times A_{\lambda_2})}{((\epsilon_{\text{red}})_{\lambda_1} \times A'_{\lambda_2}) - ((\epsilon_{\text{red}})_{\lambda_2} \times A'_{\lambda_1})} \times 100 \dots\dots(\text{II})$$

where,

A_{λ_1} = Absorbance of test well at $\lambda_1 = 570$ nm

A_{λ_2} = Absorbance of test well at $\lambda_2 = 595$ nm

A'_{λ_1} = Observed absorbance of negative control well (blank)

A'_{λ_2} = Observed absorbance of negative control well

$(\epsilon_{\text{ox}})_{\lambda_2} = 117.216$

$(\epsilon_{\text{red}})_{\lambda_1} = 155.677$

$(\epsilon_{\text{ox}})_{\lambda_1} = 80.586$

$(\epsilon_{\text{red}})_{\lambda_2} = 14.652$

Extinction coefficients for the wavelengths used.

The calibration curves with known numbers of cells were determined to correlate the percent reduction with cell numbers (Appendix B).

MTT viability assay was also used for the determination of cell number. MTT acts as artificial electron acceptor and leads to shut down of the respiratory chain. Wells were rinsed with sterile PBS and 1 mL of MTT solution (1 mg/mL) added. After 3 h incubation in CO₂ at 37°C, formazan crystals produced by cells were dissolved using acidified isopropanol (1 mL). Solutions (200 µL) were removed and absorbances measured spectrophotometrically at 550 nm.

2.2.6 Microscopy

Confocal Laser Scanning Microscopy (CSLM, Leica DM2500, Germany) was used in the study of liposome-cell interactions. CSLM uses lasers for excitation of the specimen and in this study specimens were excited with three argon lasers, 488 nm, 532 nm, 633 nm. Confocal microscope only illuminates a few points on the specimen and eliminates the fluorescence signals that are out-of-focus. Time lapse microscopy (live cell imaging) was used for the detection of the cell migration, cell growth and cell- DDS interaction. In this study live cell imaging was only used for the interactions between cell-liposomes.

2.2.6.1 Live Cell Imaging

Real time observation of interaction between liposomes and live cells were performed in POC chamber system (H. Saur, Reutlingen, Germany) or OptiCell™ Cell Culture System (Nunc, Roskilde, USA).

Cells were incubated on cover glasses (42 x 0.16 mm, POC cell chamber system) placed in a tissue culture petri plate containing 3 mL growth medium. One cover glass with cells was aseptically transferred and placed into the POC cell chamber (Figure 15), and liposome containing growth media (~ 2 mL) were added to the chamber.

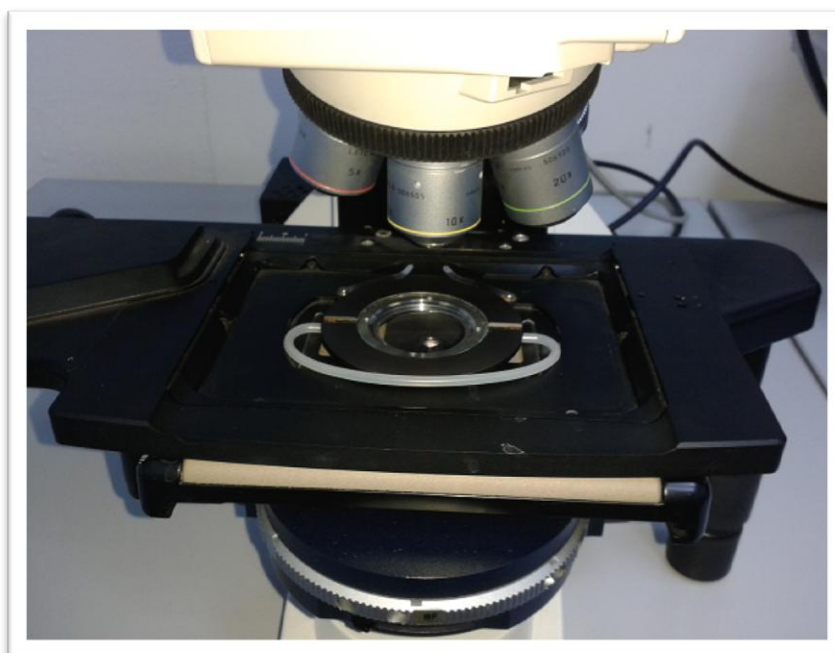


Figure 15. POC cell chamber system in the Confocal Scanning Light Microscope

The OptiCell has polystyrene membranes having 75 μm thicknesses and total 100 cm^2 surface area. These are permeable to O_2 , CO_2 , and N_2 gas. The membranes do not interfere with the laser light of confocal microscope and fluorescence.

2.2.7 Characterization of Liposomes by Transmission Electron Microscopy (TEM)

QD loaded SUV liposomes were examined with TEM by negative staining with 2% uranyl acetate on 300 mesh copper grids. TEM images of were obtained at 120 kV using a FEI Tecnai G² Spirit Bio (TWIN) microscope (METU Central Lab).

2.2.8 Preparation of Surfaces with Modified Chemistry

In order to investigate the binding capacity preferences of the liposomes patterned surfaces produced by photolithography were used. Photolithography is a process used in microfabrication and in microelectronics industry to selectively transfer designs onto surfaces. It uses UV exposure to transfer a geometric pattern through a photo mask onto a light sensitive photo resist coated on a substrate. A series of chemical treatments to erode and etching engraves the exposure pattern into the material underneath the photoresist. Figure 16 shows the scheme for patterned surface production by photolithography production.

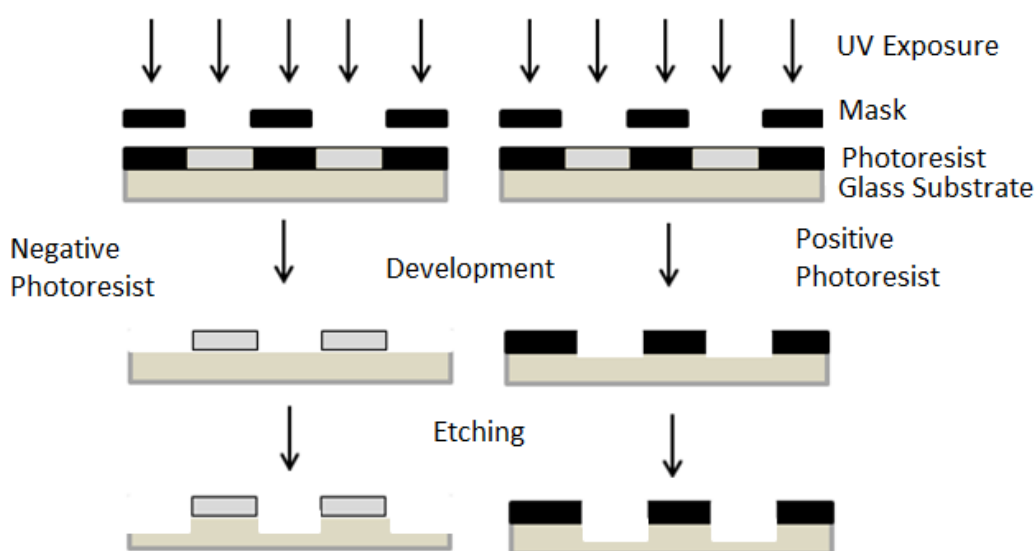


Figure 16. Schematic representation of photolithography process (adapted from Gates et. al., 2005).

Figure 16 shows that the negative photoresist is crosslinked and thus stabilized by exposure to UV and the positive is degraded. So the first gives the same pattern whereas the positive creates the reverse.

2.2.9 Preparation of Surfaces with Polymer Brushes

In order to prepare polymer brushes on polytetrafluoroethylene (PTFE, Teflon) films, they were first exposed to extreme ultraviolet (EUV) radiation producing radicals in a pattern on the surface of the substrate (Padeste et. al., 2006). Then the samples were treated with solutions of monomers and degassed to remove oxygen. Heat leads to initiation of graft polymerization of the polymer brush at the sites originally exposed to the EUV because of the active compounds like radicals and ions created there (Padeste et. al., 2006). Figure 17 shows the scheme for the polymer brush production.

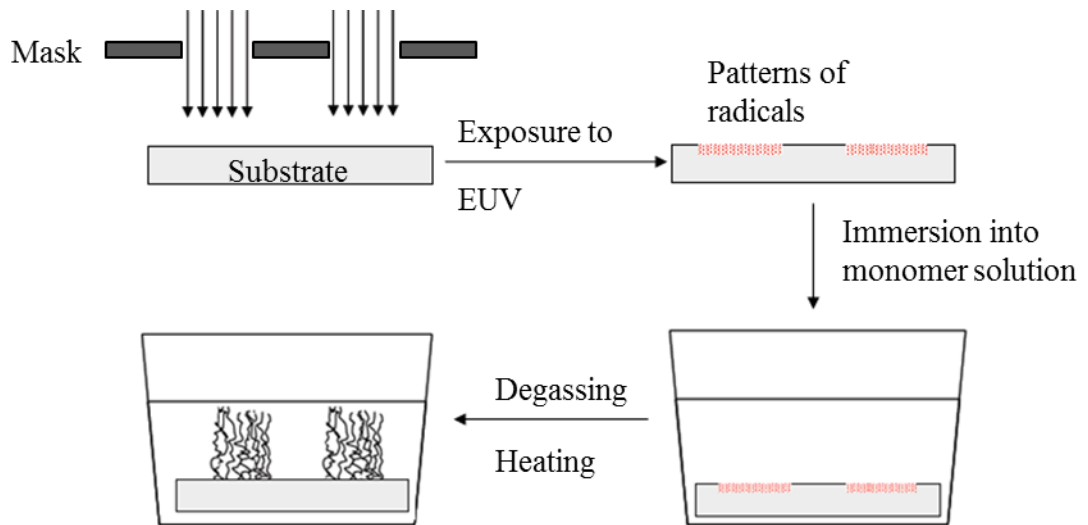


Figure 17. Schematic representation of polymer brush preparation through EUV exposure (from Padeste et. al., 2006)

In this study, for the production of negative polyelectrolyte brushes poly(methacrylic acid) was used.

2.2.10 Statistical Analysis

Student's t-test was used for statistical analysis and minimum confidence level was 95% (p value lower than 0.05).

CHAPTER 3

RESULTS AND DISCUSSION

3.1 Investigation of Liposome Surface Interaction

Liposomes were developed in this study with the purpose of interaction with surfaces and eventually with cells. For this purpose, surfaces with various charges and liposomes with different charges were prepared. Liposomes and surfaces can be prepared so that they carry opposite charges so that they are attractive to each other and these liposomes can bind to modified or patterned surfaces. In these experiments both MLV and SUV liposomes were used.

3.1.1 Selection of Compounds for Patterning Surfaces and Reacting with Liposomes

The surface-liposome interaction experiments were carried out after preparing the partially photoresist coated surfaces with photolithography were coated with polyions and then the photoresist were removed (lift-off) from the surface and then other chemical compounds could be coated on the surface or left as glass. Since liposomes were expected to have preferences because of their charge bound to certain regions and with the use of fluorescence microscope (liposomes had a fluorescent lipid in the bilayer) the preferences or the interactions could be observed. Figure 18 shows the schematic representation of polymer coating and photoresist removal off process.

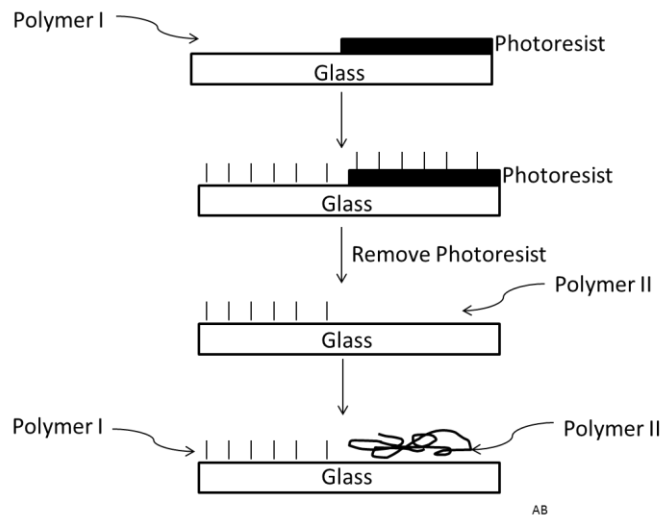


Figure 18. Schematic representation of polymer coating on half photoresist coated glass slide. Polymer I was applied onto the partially photoresist coated surfaces, the photoresist was then removed and Polymer II was applied to coat the other side.

For investigation of surface interactions of liposomes, slides coated with photoresists bands 3, 5 and 10 μm wide were used.

Fluorosilane-1:fluorosilane-3 (FS) (1:1) or (3-aminopropyl) trimethoxysilane–tetramethoxysilane (APTMS) was applied by gas phase deposition under vacuum. After photoresist removal procedure, slides were incubated with polystyrene sulfonate (PSS) polymer solution to coat with a polyanionic polymer. Figure 19 shows the interaction of PSS coated surface with cationic liposomes. Cationic liposomes were bound to the PSS coated surfaces effectively.

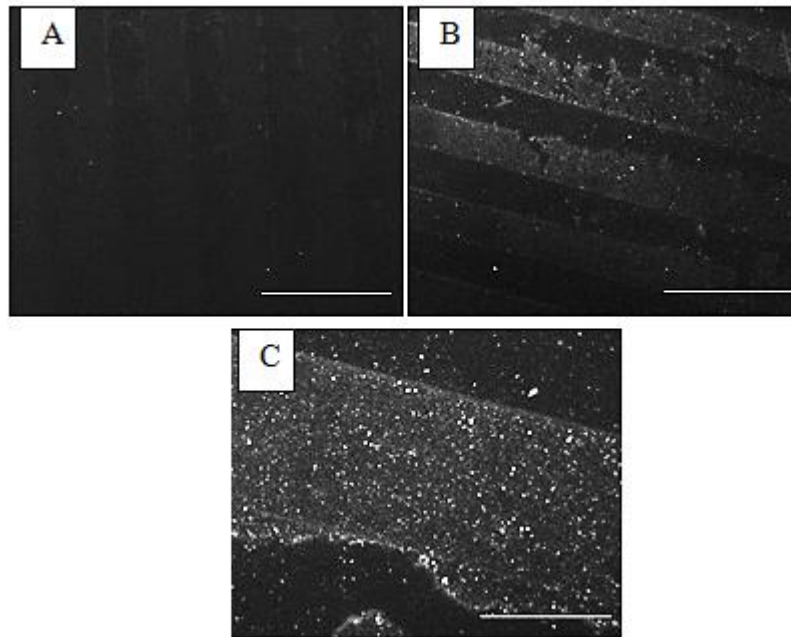


Figure 19. Liposome attachment on FS (no charge) and APTMS (positive charge) surfaces treated with polystyrenesulfonate (PSS) solutions. A) FS treated with PSS (10 x), B) APTMS treated with PSS (10 x), C) APTMS treated with PSS (40 x) (Scale bar 5 μm).

Figure 19 shows the result of PSS attachment on the surface; it indicates that liposomes have preferences to the APTMS-PSS covered surface. Figure 20 shows the binding mechanism of the cationic liposomes onto the PSS coated surface.

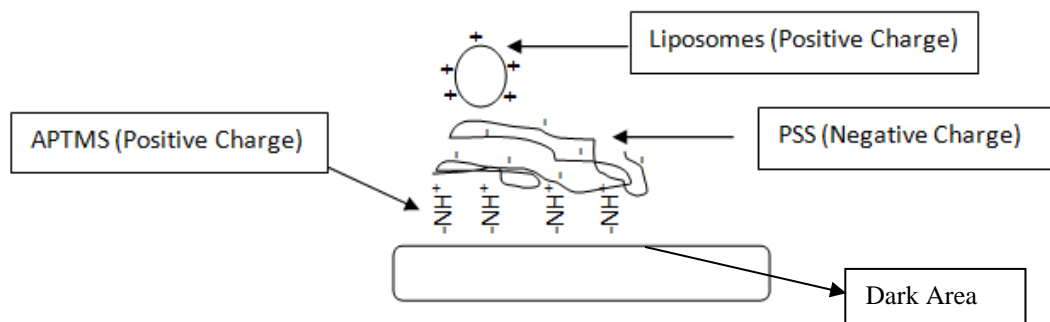


Figure 20. Scheme of the liposomal binding.

Figure 21 shows the surfaces treated with fluorosilane or coated with (3-glycidoxypropyltrimethoxysilane) GTMS and poly(allylamine) PAA. Anionic liposomes

did not attach to the fluorosilane deposited surface reacted with GTMS and PAA covered surfaces because these surfaces had at the top the PAA which was a polycation. Figure 21 shows the absence of interaction between the polyanionic liposome and the fluorosilane deposited regions on the surface; these liposomes bound to PAA covered regions.

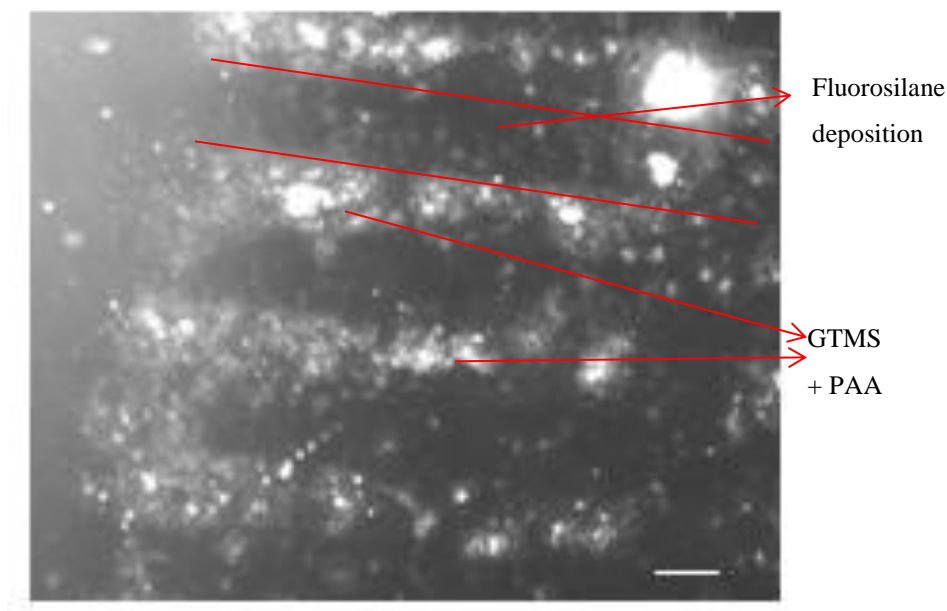


Figure 21. Liposomal binding to fluorosilane deposited GTMS (3-glycidoxypropyltrimethoxysilane) and poly(allylamine) (PAA) covered surfaces with anionic liposomes. (Scale bar 5 μm).

Figure 22 shows the schematic representation for the interaction mechanism between GTMS- PAA covered surfaces and anionic liposomes.

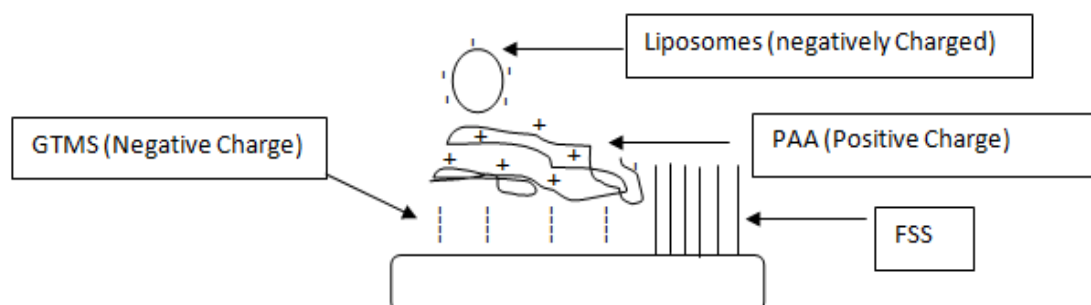


Figure 22. Scheme of the liposomal binding on fluorosilane deposited surface.

3.1.2 Liposome Behavior on Polymer Brushes

Polymer brushes are surface anchored polymer chains that extend away from the surface with a high enough chain density and resembling a brush (Padeste et. al., 2004). The brushes are usually started polymerization with reactive monomers from reactive sites in the support material as was described in Materials and Methods section. Figure 23 shows the light micrograph of polymer brush surface structure.

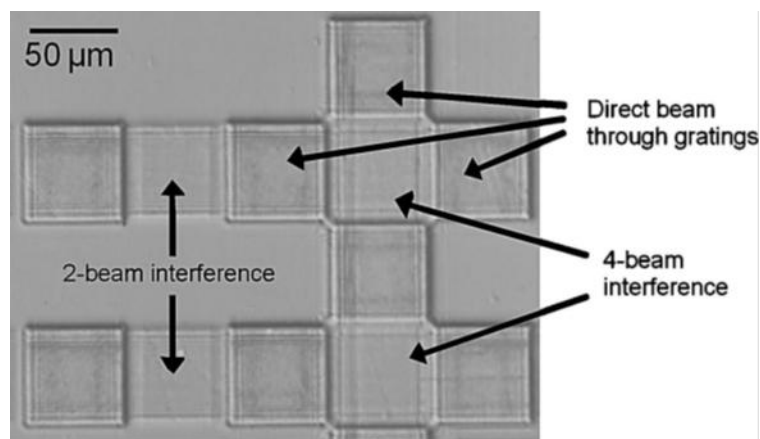


Figure 23. Light micrograph of surface structures produced with the micro-/ nano-grafting technique (from Padeste et. al., 2004).

In certain regions the high intensity of direct EUV (extreme ultraviolet) beams leads to an increase in the thickness of the grafted material on the surface. In these regions, the grafted chains are packed in such a way that they mainly extend perpendicular to the surface away from (Padeste et. al., 2004). The number of reactive sites increase as the dose increases and this leads to an increase in the number of grafted polymer chains. Thus, the chains extend in a perpendicular direction and a thick graft is developed (Padeste et. al., 2004).

In this study, EUV light in a synchrotron-based interference set up was used to create the radicals on polytetrafluoroethylene (PTFE, Teflon) surfaces to initiate the polymerization.

3.1.2.1 Liposome Behavior on Negative Polyelectrolyte Polymer Brush Surfaces

In this section polymethacrylic acid (PMA) polymer brushes were used to investigate the interaction. Similarly in the study of Kepczynski et al., (2005) the interaction between liposomes and PMA was studied.

PMA brushes were prepared on PTFE surfaces. PMA is a weak polyanion and its brushes were incubated for 10 min at room temperature with both extruded and multilamellar cationic liposomes. Figure 24 shows the fluorescence micrographs of the Teflon surface with PMA brush covered surface incubated with multilamellar, positive charged liposomes. Liposomes had a fluorescence lipid in their lipid bilayer, therefore, fluorescence microscopy could be used to examine the extent of interaction by visualizing the liposome-attached sites.

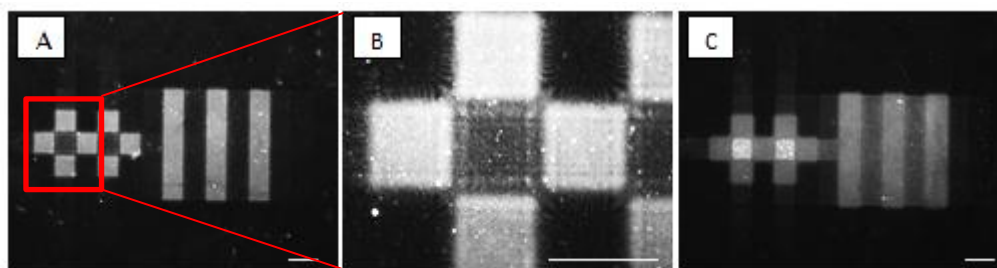


Figure 24. Cationic multilamellar liposome attachment on surfaces with PMA brush regions. A) Multilamellar liposomes (10x), B) Magnification of A (40x), C) Multilamellar liposomes with different lengths of brush polymer (10x). The light regions are where on surfaces with PMA brushes were formed.

Figure 24 shows that cationic MLV liposomes were bound on the polymer brush coated surfaces according to their surface structures. Polymer brushes had the same chemistry throughout the surface but some regions had different length polymers, the difference being in the nanometer scale (Padeste et. al., 2004). The liposomes apparently are bound to the brushes in accordance with the polymer lengths (Figure 24)

Figure 25 shows the fluorescence micrographs of the Teflon surfaces heated with PMA brushes incubated with extruded positive charged liposomes.

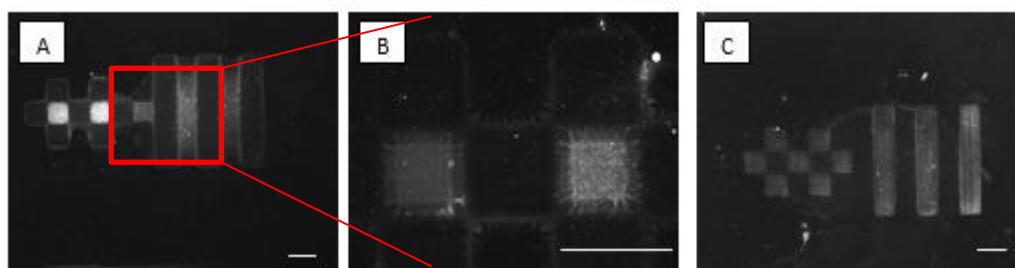


Figure 25. Cationic extruded liposome attachment on surfaces with PMA brush regions. A) Extruded liposomes (10x), B) Magnification of A (40x), C) extruded liposomes interacting with polymers of different length (10x).

Figure 25 shows that cationic extruded liposomes bound on the polymer brush surfaces. Figure 24 and Figure 25 indicate that the cationic liposomes whether MLV or SUV (due to extrusion) were attached only to the negative charged polymer because the liposomes had positive charge.

To check the interaction between liposomes and polymer brush surfaces after 24 h of incubation, liposomes were incubated with buffer solution at room temperature for 24 h after treating the surface. Figure 26 shows that the cationic MLV liposomes have remained attached to the surface for duration of 24 h.

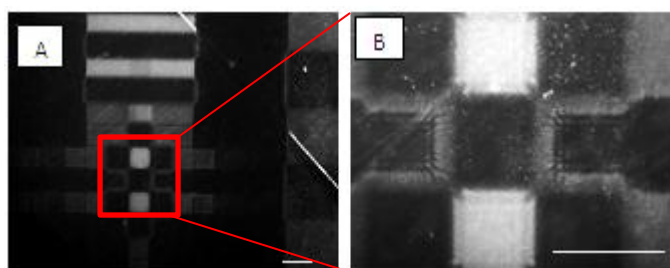


Figure 26. Presence of cationic MLV liposomes on polymer brush regions of the Teflon surface after 24 h incubation in the buffer solution. A) Multilamellar liposomes (10x), B) Magnification of A (40x).

Figure 27 extruded bilayer liposomes also remained attached to the surface 24 h.

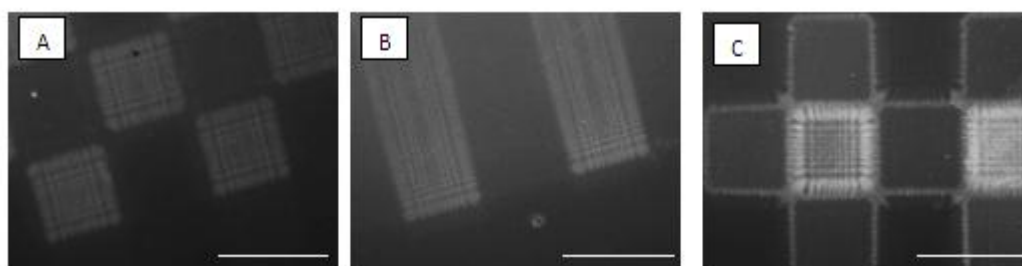


Figure 27. Attachment of cationic extruded bilayer liposomes on polymer brush regions on the Teflon surface after 24 h incubation in the buffer solution. A) Extruded liposomes (40x), B) and C)

Figure 26 and Figure 27 show that the cationic liposomes remained attached to polymer brushes even after 24 h in PBS proving the strength of the ionic bond between the cationic liposome and the negative brush regions on Teflon.

Figure 28 presents the same but 48 h after of contacting and shows that the fluorescence decreased to some extent especially in MLV liposomes. Extruded liposomes

are reportedly physically more stable than the unextruded ones like MLV and therefore persisted in the PBS medium in attached form (Zelphati et. al., 1998).

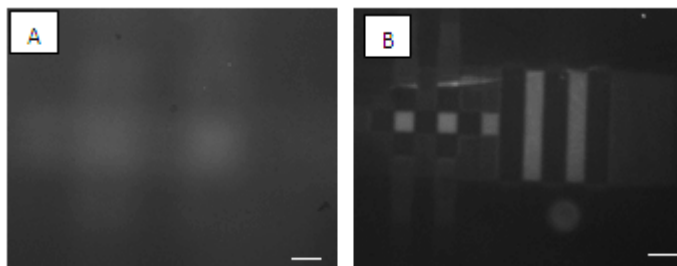


Figure 28. Cationic liposomes attached on polymer brush surfaces after 48 h in buffer solution. A) Multilamellar liposome (10 x), B) Extruded liposome (10 x)

The extent or strength of PMA binding to liposomes was pH dependent and, Oto et. al., 1995 studied the pH dependent binding of liposomes to PMA. They used this feature to investigate the aggregation of liposome by binding to PMA. These results show that PMA polymer brushes can be used to localize liposomes on predetermined regions on a surface for purposes of drug delivery, or serve as a sensor, or used in the release of liposomes (and drugs) triggered by pH changes. In the context of this study these liposomes can be used to attach to cells which generally have negative charges.

3.2 Preparation of Liposomes

Gel Permeation Chromatography (GPC) was used to separate liposomes from untrapped compounds. Sephadex G 50- 80 was packed in a 30 cm long 1 cm wide column. The eluates (4 mL/ tube) were collected by fraction collector using just the gravity. Liposome presence in eluates was determined at $\lambda = 410$ nm which was also investigated with fluorescence intensity (model drug calcein) at $\lambda_{ex} = 494$ nm and $\lambda_{em} = 517$ nm using a spectrofluorometer. The data obtained from absorption and fluorescence intensity were plotted against eluate number (Figure 29).

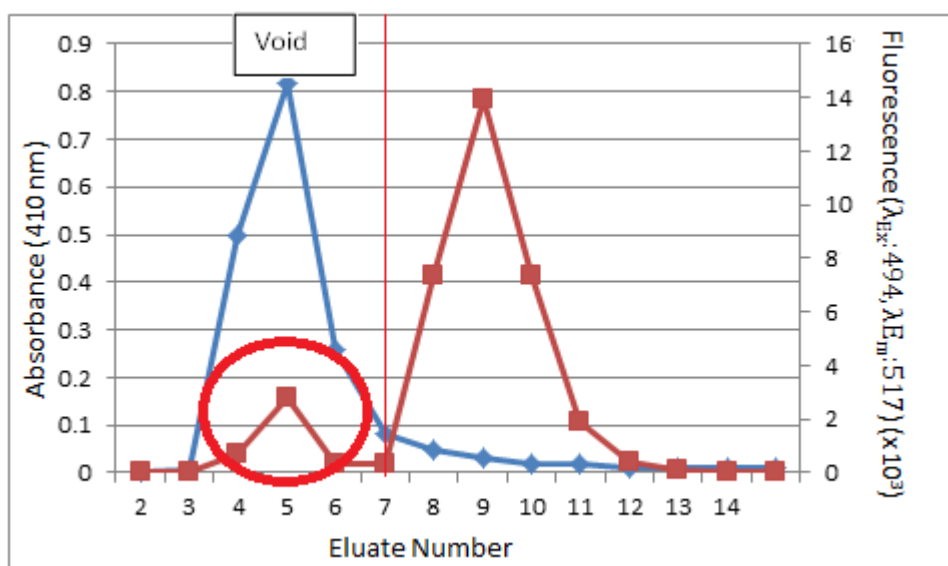


Figure 29. GPC of calcein loaded liposome

The UV absorbance (blue) indicates the void where the liposomes are concentrated. The fluorescence intensity (red) shows the distribution of calcein in the void fraction indicating entrapped calcein and the second peak (eluate 9) shows the untrapped (or free) calcein.

The UV-Vis spectrophotometric determination of the liposomes shows that liposomes were located in eluates in tubes 3-7, which is also the void volume. The fluorescence intensity chromatogram shows two distinct peaks; the first (eluates 3-7) shows the encapsulated calcein, liposomal calcein, and the second one (eluates 7-12) shows the untrapped calcein. The overlapping section of the peaks (shown in red circle) indicates the liposomes with entrapped calcein.

3.3 Preparation of Quantum Dot Labeled Liposomes

In 2006, Chu and Lui used liposomes as templates in the preparation of nanocapsules and nanospheres carrying CdSe Quantum Dots (QD). They found that liposomes could act as a template for the nucleation of CdSe starting from the ions. They suggested that at low concentrations of Cd²⁺ ion, CdSe was formed on the outer surface of the liposomes. After some time these covered the liposome and formed a CdSe coat. However, in the case of high Cd²⁺ concentration, Cd²⁺ ions bound the polar head groups of phospholipids and formed a domain structure in the vesicle membrane. This led to an increase in the permeability of the lipid membranes and Cd²⁺ ions penetrated into the liposomes.

Studies with both hydrophobic CdSe/ZnS core/shell QD incorporated in the lipid bilayer (Al-Jamal et. al., 2008) and hydrophilic functionalized QD encapsulated in the liposomes (Al-Jamal et. al., 2008 (2)) showed that both types of liposomes label the tumor cells. In this study liposomes loaded QD were preferred and studied.

3.4 Preparation of CdTe labeled liposomes

Quantum dots with CdTe cores were used to label the liposomes. These QDs were water soluble and kindly provided by Assoc. Prof. Dr. Hilmi Volkan Demir (Bilkent University, Ankara, Turkey).

Peng's method was used to calculate the diameter and concentration of CdTe quantum dots (Yu et al., 2003). Peng's method suggested that determination of extinction coefficient of CdTe nanocrystals using the following equation

$$D = (9.8127 \times 10^{-7})\lambda^3 - (1.71147 \times 10^{-3})\lambda^2 + (1.0064)\lambda - (194.84) \dots \dots \dots (III)$$

where λ (nm) is the wavelength of the first exciton and it is 576 nm according to the absorption spectrum presented Figure 30.

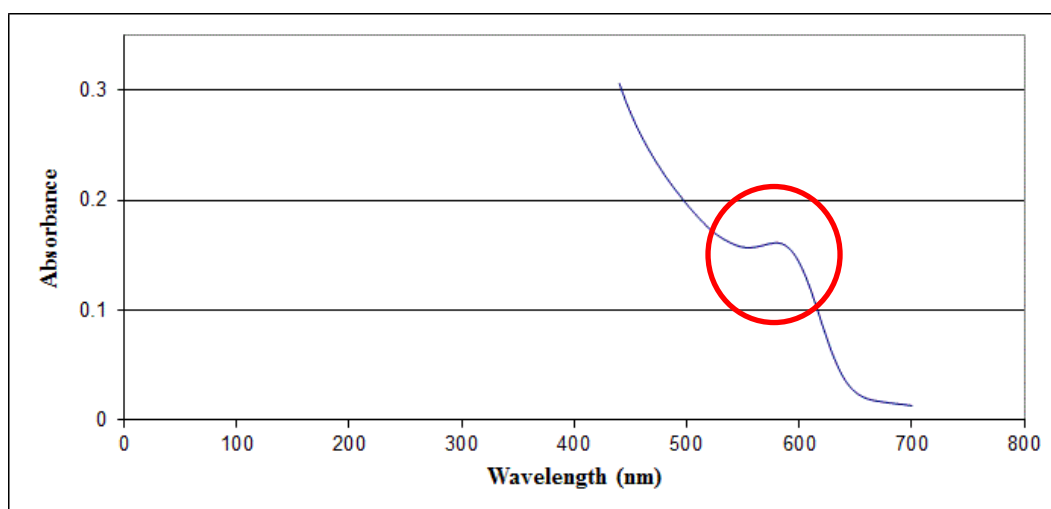


Figure 30. Absorption spectrum of CdTe Quantum Dots between 0-800 nm

Figure 30 shows the first exciton of the CdTe quantum dot (red circle), the excitation wavelength should be lower than this first exciton.

Beer- Lambert law: $A = \epsilon LC \dots \dots \dots (IV)$

where, A is the absorbance at the peak position of the first exciton, C is the molar concentration of the CdTe nanocrystals, and L is the path length (cm) of beam used within the sample and L was fixed at 1 cm in these experiments, and ϵ is the molar extinction coefficient of CdTe.

The diameter of CdTe quantum dots was found as 3.473 nm and the concentration of the CdTe solution that was provided was 11.37 μM . Figure 31 shows the calibration curve for CdTe quantum dot fluorescence.

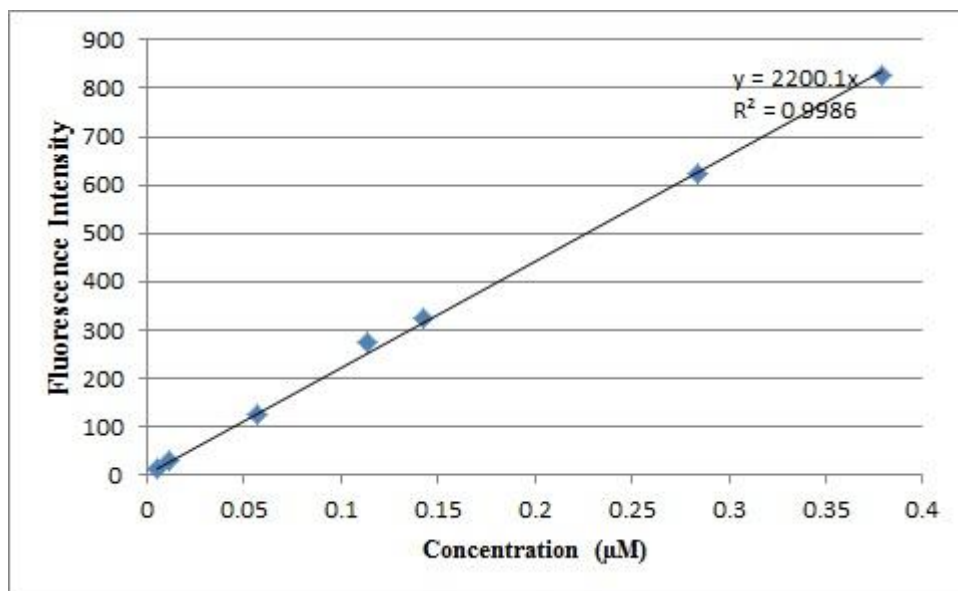


Figure 31. Calibration curve for CdTe quantum dots at λ_{ex} 488 nm and λ_{em} 614 nm

Figure 32 shows the eluates after GPC. In this figure eluates were exposed to day light and UV light to investigate the effect of liposome encapsulation on fluorescence of the QDs.

Figure 32 shows the first 10 eluates obtained with GPC which indicates that eluates are turbid due to the scattering by liposomes. The fluorescence in Figure 32B shows that under UV exposure the optical properties of QDs were not altered by loading in liposomes.

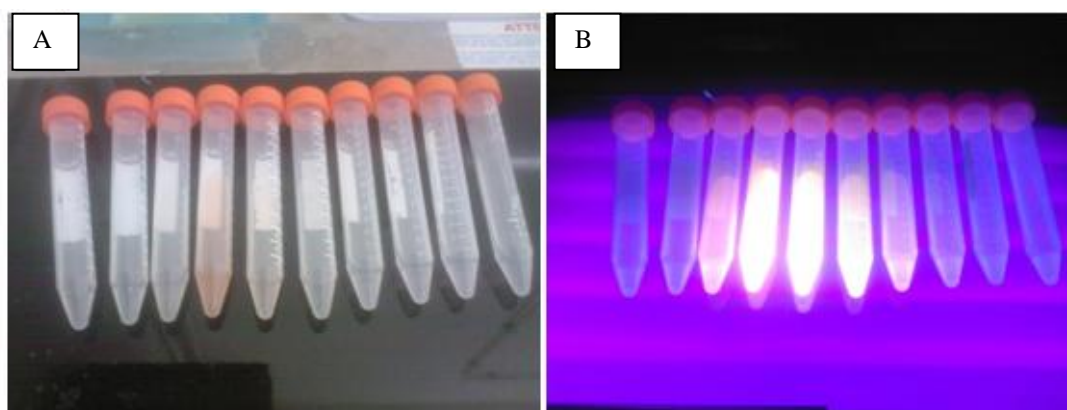


Figure 32. GPC eluates of QD loaded SUV. A) Visible light, B) UV λ_{ex} : 352 nm

Figure 33 shows the fluorescence of free QDs, empty liposomes, and QD-loaded liposomes under UV exposure. It shows that liposomes did not quench the fluorescence of the quantum dots.

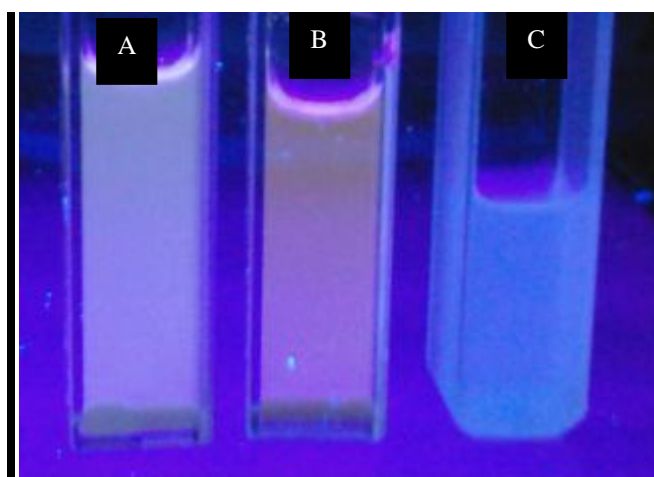


Figure 33. The effect of UV exposure on liposome, QDs and QD-loaded liposomes. A) QD-loaded liposomes, B) Free QDs, C) Empty liposomes.

In Figure 33 the fluorescent emission of the quantum dots which comes from CdTe can be observed. The turbidity was due to the scattering by liposomes and the QD-loaded liposomes present both turbidity and fluorescence emission.

CdTe loaded liposomes were observed with a confocal scanning laser microscope (CSLM) using different laser beams. Sample was partially dried in the air and the micrographs were obtained at the wet-dry border of solution.

The CLSM results showed that, QDs were not excited with 633 nm but were excited upon exposure to the other two lasers (458 nm and 543 nm) as expected (Figure 34). The first exciton of the CdTe nanocrystals was around 573 nm and excitation of these nanoparticles had to be lower than the first exciton. Therefore, these results indicated that the fluorescence of the QD-loaded liposomes in the micrographs was only due to the QD presence.

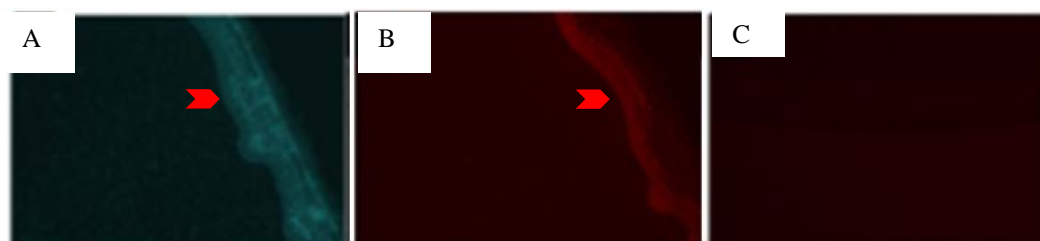


Figure 34. CSLM and transmission microscopy of QD-loaded liposomes exposed to light source with different wavelengths. A) 458 nm laser, B) 543 nm laser, C) 633 nm laser. (x20).

The QD-loaded liposomes were further observed with confocal microscope (Figure 35).

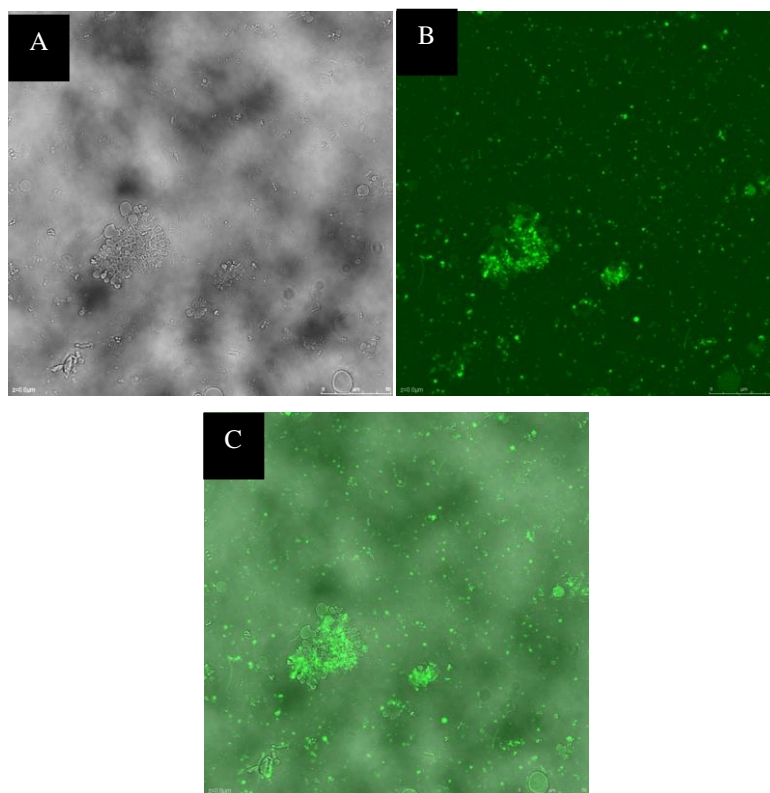


Figure 35. Micrographs of liposomes loaded with QD. A) Transmission, B) Confocal, C) Overlay (x40).

Figure 35(A) shows a transmission micrograph where the liposomes were located, and in Figure 35 (B) the micrograph shows the location of the QDs. Figure 35 (C) is an overlay, and it shows that the QDs were co-localized with the liposomes. In other words, this is a visual proof that the QDs are entrapped in the MLV. It can, therefore, be said that QD-loaded liposomes can be used as a joint drug delivery-imaging tracking agent. Multilamellar liposomes had approximately 1 μm mean diameter, and SUV are much smaller and they are too small to be observed by confocal laser scanning microscope; therefore the micrograph shows the agglomerated liposomes and not the individual liposomes.

Figure 36 indicates the interaction between QD-loaded liposomes and Saos2 human osteosarcoma cells.

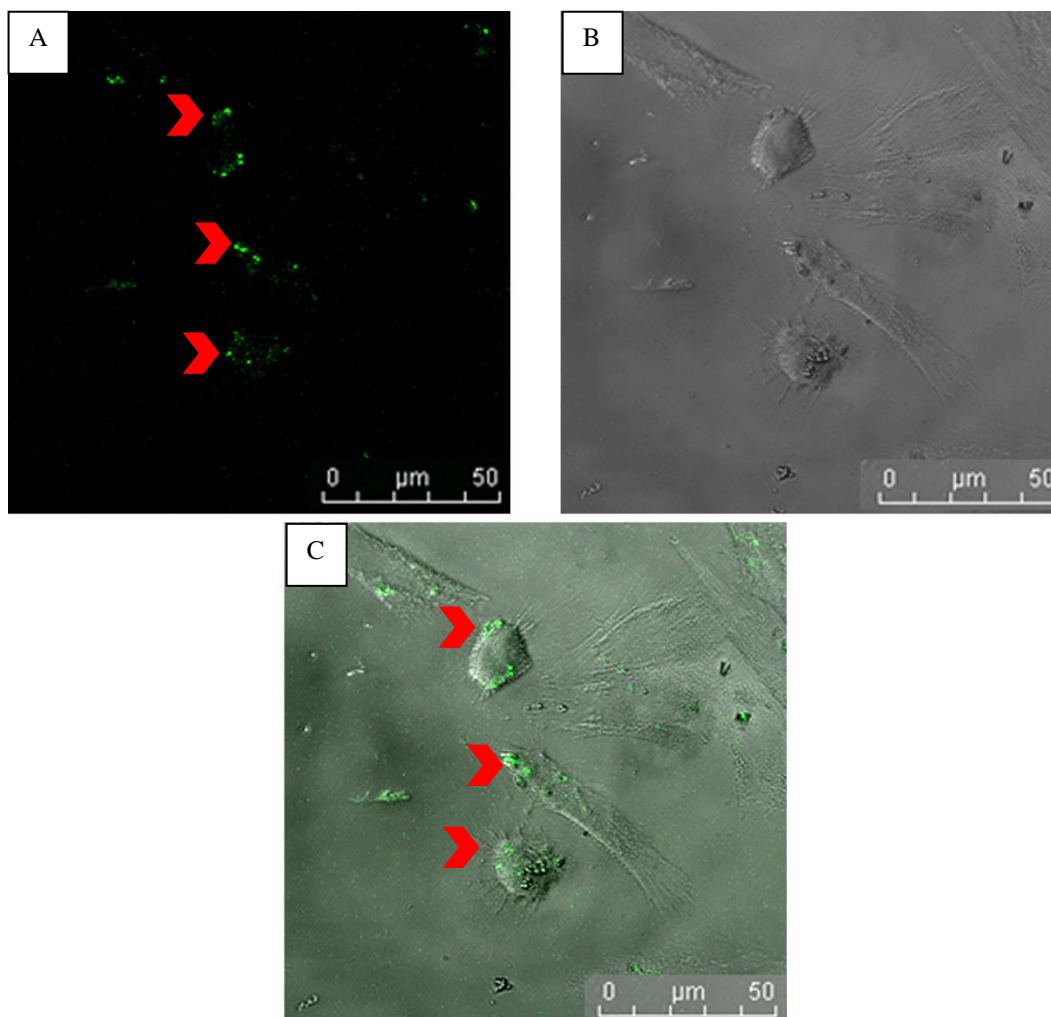


Figure 36. Micrographs of Saos2 cells with QD-loaded liposome. a) Confocal at 488 nm, b) Transmission, c) Overlay. (x40). Arrow heads show the Saos2 cells.

Figure 36 shows the interaction between the QD-loaded liposomes with cancer cells. The fluorescence emission seen in these micrographs were due to the presence of QD loaded liposomes surrounding the cells. Prior to imaging Saos2 cells washed to remove the unbound liposomes, therefore, it can be deduced that QD-loaded liposomes interact with the Saos2 cells which is in agreement with the studies of Al-Jamal et. al., 2008 (1) and (2).

Figure 37 and Figure 38 show the control micrographs of Saos2 cells without and with liposomes.

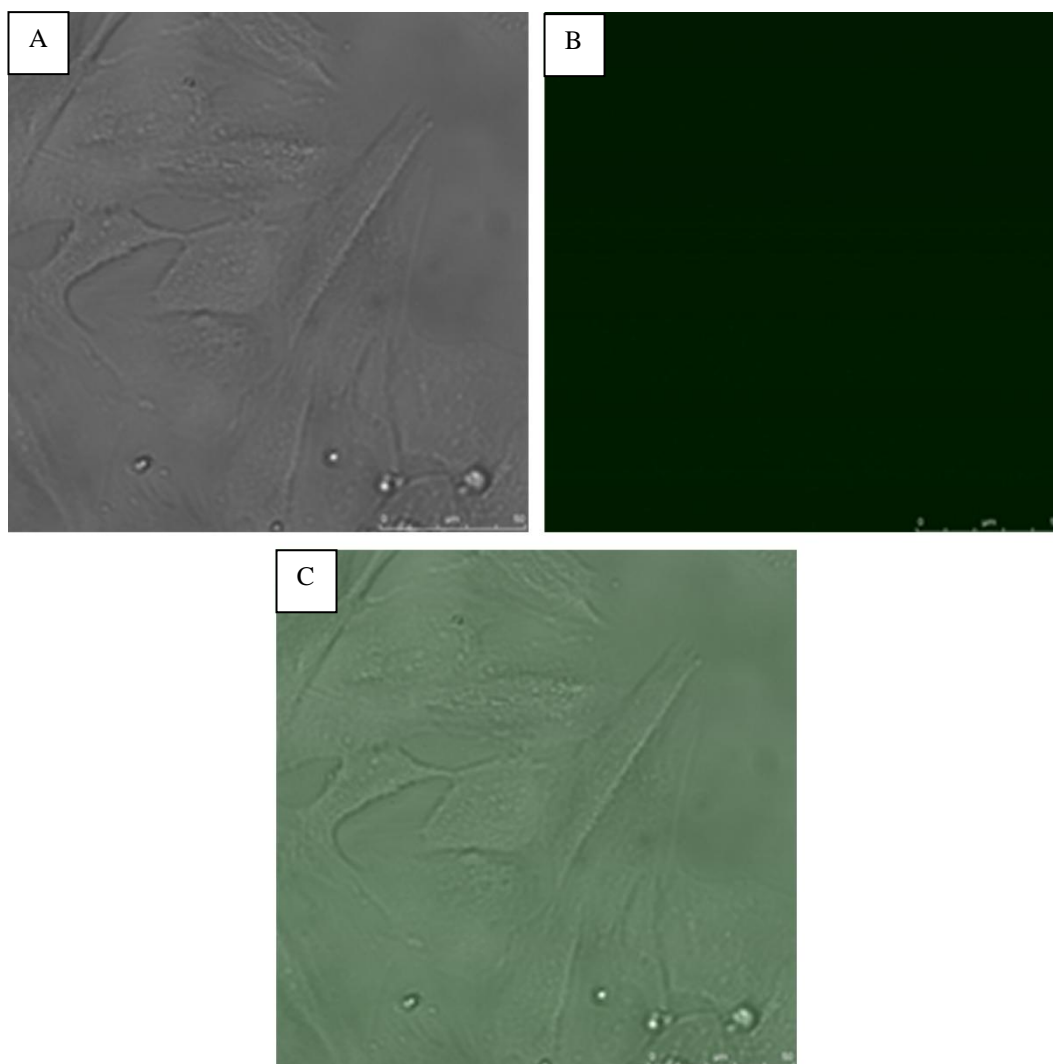


Figure 37. Control micrographs of Saos2 cells in the absence of liposomes. A) Transmission, B) Confocal at 488 nm, C) Overlay (x40).

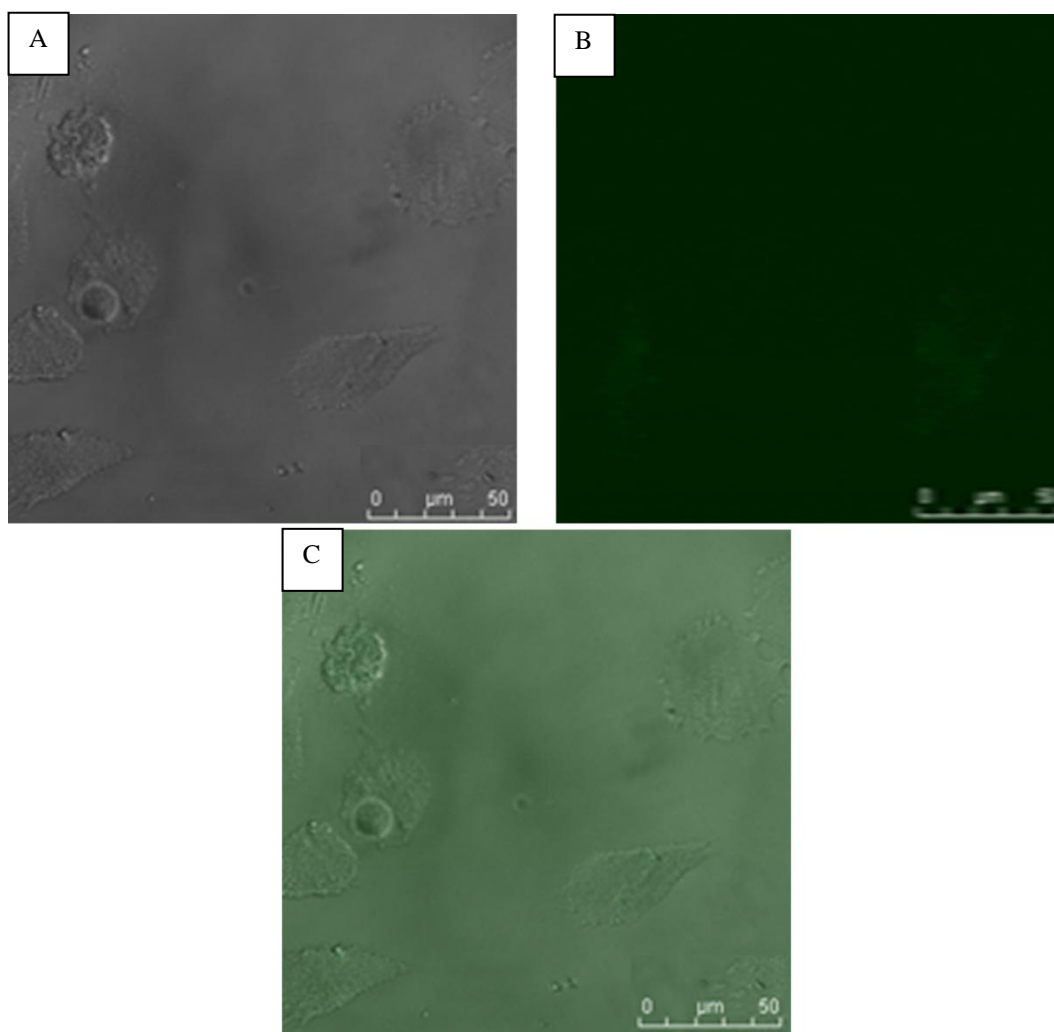


Figure 38. Control micrographs of Saos2 cells with empty liposomes. A) Transmission, B) Confocal at 488 nm, C) Overlay at 488 nm(x40).

Figure 38 indicates the PB loaded liposomes (not carrying any fluorescent molecules) had no fluorescence emission under the confocal microscope. This shows that there was not any autofluorescence emission from liposomes (Figure 37) or cells themselves (Figure 38) and therefore, the QDs can be used with liposomes in tracking the liposomes under the microscope.

3.4.1 Separation of Free QDs from Liposome Loaded QDs

After preparation of the QD-loaded liposomes GPC was carried out for the separation of unloaded material. Normally compounds not entrapped in liposomes are eluted at eluate numbers much later than the voids where the liposomes are eluated. In this study the same elution profile from the GPC column for both the liposomes and QDs

indicated that liposomes and QDs cannot be properly perfectly separated from each other by using GPC (Figure 39).

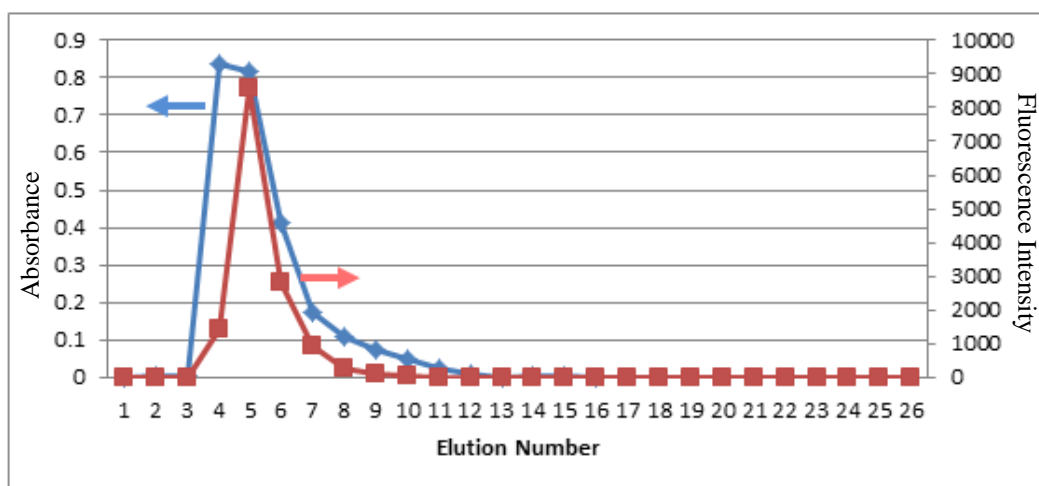


Figure 39. GPC of loading of liposomes with QD. UV-Vis spectrophotometry (blue, 410 nm) and spectrofluorimetry (red, λ_{ex} : 497 nm, λ_{em} : 514 nm).

In order to achieve the separation of untrapped QDs from liposomes carrying QDs eluates 4, 5 and 6 were centrifuged at 1×10^4 g for 10 min and washed three times with buffer (10 mM, pH 7.4, PB). After the first centrifugation, supernatant was analyzed for fluorescence. The pellets was washed three times and then dispersed in 250 μ L running buffer (PB) and the fluorescence intensity was measured. The results are presented in Table 4.

Table 4. The fluorescence intensities of eluates 4, 5 and 6.

Sample	Fluorescence Intensity (λ_{ex} : 497 nm, λ_{em} : 514 nm)		
	Tube 4	Tube 5	Tube 6
Before centrifugation	1458	8586	2820
Supernatant	992	6484	1840
Pellet (dispersed)	331	356	42

Table 4 indicates that quantum dots did not precipitate, whereas liposomes did. Therefore, liposomes can be separated from free quantum dots with centrifugation. These show that the fluorescence intensity of the pellets were due to the QD loaded in the liposomes and it is also calculated that 6.5% of the fluorescence was associated with the liposomes.

3.4.2 Determination of Liposome Size with Dynamic Light Scattering

Dynamic Light Scattering (DLS) experiments were performed to study the liposome particle size distribution, and determine the effect of QD loading on the size distribution. Because for the delivery of liposomes *in vivo*, especially for the EPR effect, size is very critical. DLS experiments were done using aqueous solutions of liposomes and at room temperature and at the 90 degree.

Thin lipid films were prepared using 1 mL of PC:Chol (7:3). Hydration of TLF was done with 0.5 mL of QD in PB or PB solutions. The system was vortexed for 5 min to remove the TLF from the vessel wall, and prepare Multilamellar Liposomal Vesicles (MLV). This suspension was sonicated at 20 watts for 5 min in ice to form the SUV. All liposomal preparations were first centrifuged at 1×10^4 g, 4°C for 10 min and GPC was carried out to separate the free QD from the QD loaded in the liposomes.

Figure 40 and Table 5 show the results of the GPC and DLS results of unloaded (PB-loaded) MLVs.

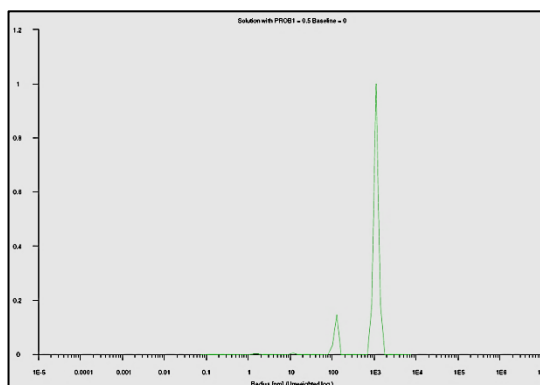


Figure 40. A representative DLS of size distribution for unloaded MLV.

Table 5. DLS results of unloaded MLV.

Peak No	Weight of Peak [%]	Mean Diameter [nm]
1	0.2	1.5
2	0.4	11.7
3	11.5	123
4	87.9	1116

Table 5 shows that the main bulk of the PB-loaded MLV had a diameter of 1116 nm or 1.11 μm , which is an expected value for a MLV. The size distribution of the MLV liposomes was very narrow.

Table 6 indicates DLS results of QD-loaded MLV prepared in a similar fashion but loaded with QD.

Table 6. Average size and size distribution of QD-loaded MLV (DLS)

Peak No	Weight of Peak [%]	Mean Diameter [nm]
1	0.5	0.1
2	0.3	5.7
3	10.5	109
4	88.8	1013

Here again 4 peaks were detected with DLS and only the larger 2 had significant proportion. It is observed that the main peak of the QD-loaded MLV had a mean diameter of 1013 nm or roughly 1.0 micrometer. It is concluded that the unloaded and QD-loaded MLV both had mean diameters of around 1.0 micron; these values are very close to each other and it appears that QDs did not make a difference in the diameter. This is good in the context of *in vivo* (and *in vitro*) use.

SUVs were also studied with DLS. Table 7 indicates that there are 3 peaks with the unloaded (PBS loaded) SUV and the mean diameter was 82.7 nm. The size distribution of the SUV liposomes had quite a narrow range; 99.3% of the liposomes were in the range of 82.7 nm. The size obtained is in a range quite suitable for EPR effect where the nanoparticles benefit from the “leaky” blood vessels of solid tumors.

Table 7. Mean diameter of unloaded SUV.

Peak No	Weight of Peak [%]	Mean Diameter [nm]
1	0.3	0.1
2	0.4	5.0
3	99.3	82.7

The QD loaded SUV also showed (Table 8) 3 peaks and the major peak was around 100 nm like the unloaded SUV but an interesting observation was that the presence of a small (6.8%) fraction of large SUV in the size of 340 nm.

Table 8. DLS results of QD-loaded SUV

Peak No	Weight of Peak [%]	Mean Peak Position [nm]
1	0.5	0.09
2	92.7	99.46
3	6.8	340

The mean diameters of QD loaded and QD-free SUV were around 100 nm. Nanoparticles used for drug delivery to cancer tumors are expected to be less than 200 nm in order to take the advantage of enhanced permeation and retention (EPR) effect. The current SUV liposomes appeared to be suitable for such an application. The MLV sizes were also in the expected range also much lower than the size that macrophages phagocytose; thus, their circulation time will not be decreased for this reason.

3.4.3 Morphological Characterization of QD Loaded Liposomes by Transmission Electron Microscopy (TEM)

Quantum dot loaded liposomes were examined using TEM by negative staining with uranyl acetate as dark regions (Figure 41 and Figure 42). The TEM of the QD loaded liposome samples showed a hollow circular structure with a dense boundary showing the membranes of the liposomes. The crystalline flakes on the outside of the liposomes appear to be salt crystals due to the PBS in which the liposomes were suspended. In Figure 41 QD-loaded MLV liposomes are presented.

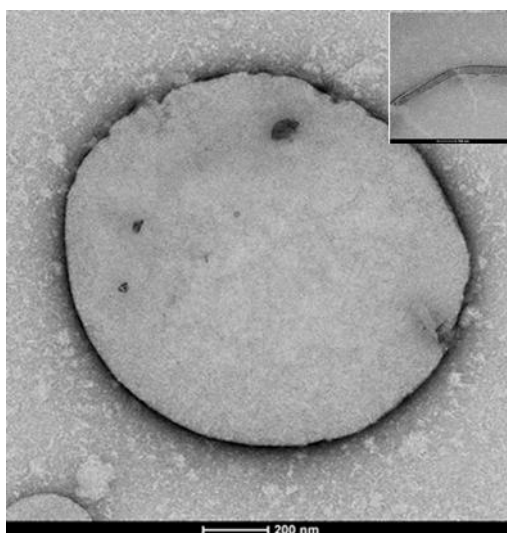


Figure 41. TEM images of QD loaded MLV Liposomes, inset: Multilamellar lipid layer structure. Stained with uranyl acetate for the lipid membrane components.

Before observing the samples under TEM dehydration step should be carried out that leads to distortion on the shapes. Freeze fracture method can be utilized with cryo electron microscopy for non-distorted visualization (Torchilin and Weissig, 2003).

Figure 41 shows that QD loaded MLV liposomes had a diameter range of 1 μm . The size data is in agreement with that obtained from DLS measurements.

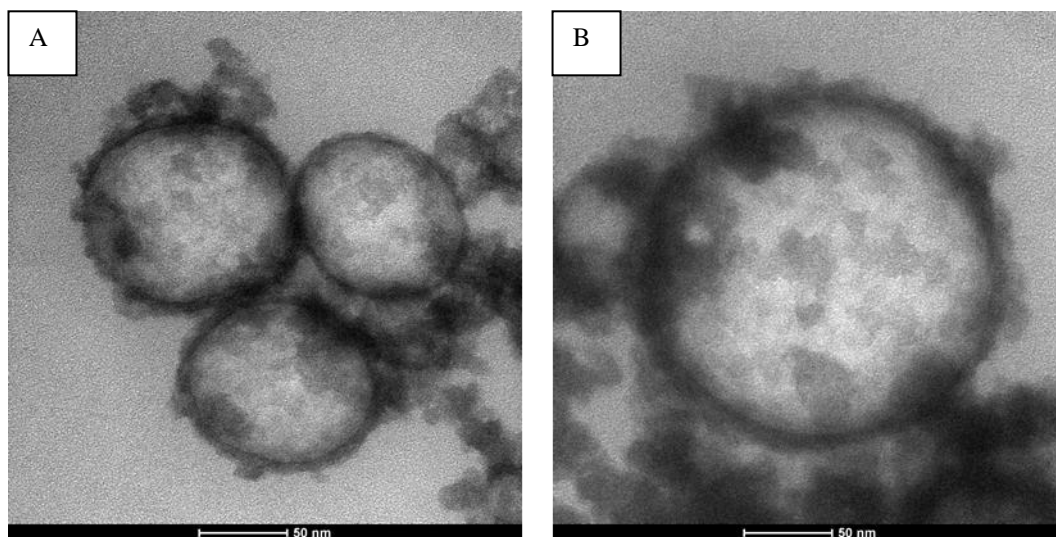


Figure 42. TEM images of QD loaded SUV Liposomes (x 150,000). Stained with uranyl acetate for the lipid membrane components.

The Figure 42 shows that QD loaded SUV had a diameter range of 100-200 nm and SUVs had spherical morphology and unilamellar structures. The size data is in agreement with that obtained from DLS measurements.

3.5 Cytotoxicity of Free QD and QD Loaded in Liposomes

It is well known that quantum dots are cytotoxic but in order to be able to serve as imaging and tracking tools, their toxicity has to be partially or fully decreased. It was expected that encapsulation in liposomes would also serve this purpose. Saos2 cells were used as the test cells since they are a cancer cell line and were seeded at a density of 5×10^4 cells/well into 24 well plate in RPMI medium to study the cytotoxicity of QD-loaded SUV. After 24 h of cell seeding, free QD suspension, QD-loaded in liposomes, and control, unloaded liposomes were seeded into these wells.

At 24 and 48 h after adding the suspensions light microscopy was used to determine the dead Saos2 cells by checking their structural deformation. Figure 43 and Figure 44 show the light microscope images of Saos2 cells at 24 and 48 h after adding the suspensions.

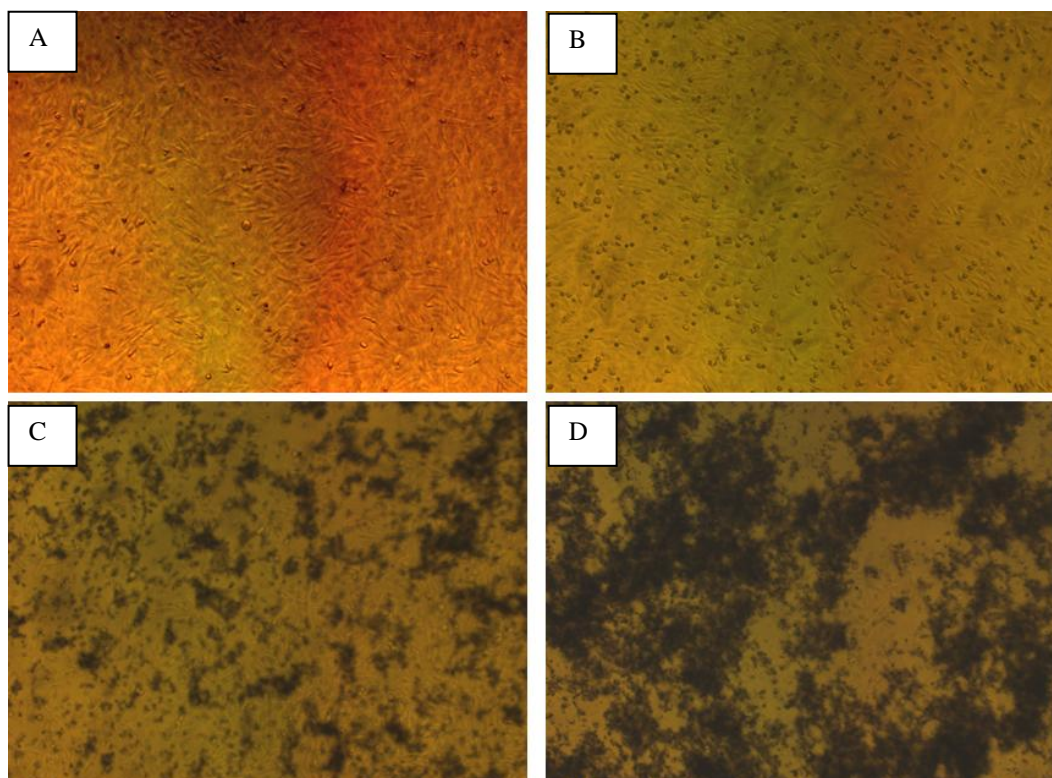


Figure 43. Light microscope images of Saos2 cells after 24 h of incubation. a) Saos2 cells, b) Saos2 cells with free Quantum Dots, c) Saos2 cells with Quantum Dot-loaded liposomes, d) Saos2 cells with unloaded liposomes (4x).

Figure 43 shows the cell morphology under light microscopy after 24 h of incubation. In the control (Figure 43A) where only Saos2 were present, the cells appear attached and spindle-like, thus like typical Saos2 cells. Their circularity is around 0, indicating that they were more elliptical than circular. However, in Figure 43B, the free QD added wells, the cells appear to be detached and round, with a circularity of one, a value indicating unhealthy Saos2 cells. Figure 43C and D contain the liposomes and the cells were not easily visible. This prevents a clean conclusion but this level of liposome presence appears to be not appropriate as the other viability test would later show.

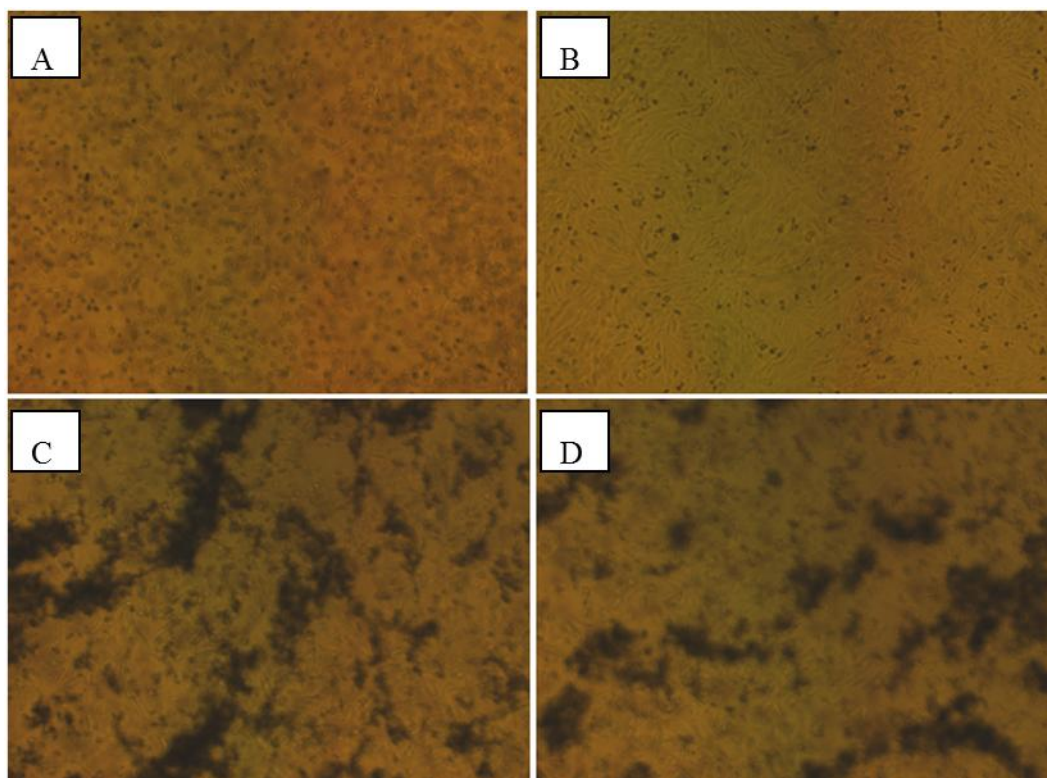


Figure 44. Light microscopy images of Saos2 cells after 48 h of incubation. A) Saos2 cells, B) Saos2 cells with Quantum Dots, C) Saos2 cells with quantum Dot-loaded liposomes, D) Saos2 cells with unloaded liposomes (4x).

Figure 43 showed that Quantum Dot added culture medium induced a cytotoxic effect due to QDs as morphological deformation. The cells, which were seeded with QD-liposomes, however, showed almost no morphological deformation. These results are in agreement with the cell viability tests (Figure 46). Therefore, a preventative effect of liposomes against QD toxicity was observed in these two sets (24h and 48h) of microscopy.

In order to investigate the cytotoxicity of liposomes themselves, Saos2 cells were prepared with a cell number of approximately 5×10^4 in RPMI medium and seeded in 24 well tissue culture flasks. Unloaded MLVs and SUVs were prepared as described in Material and Methods section. 24 h after addition of liposome suspensions, cell numbers were determined with MTS cell proliferation assay. All the *in vitro* studies were done with duplicates.

Figure 45 shows the result of cell proliferation (MTS) tests for the unloaded MLV and SUV liposomes.

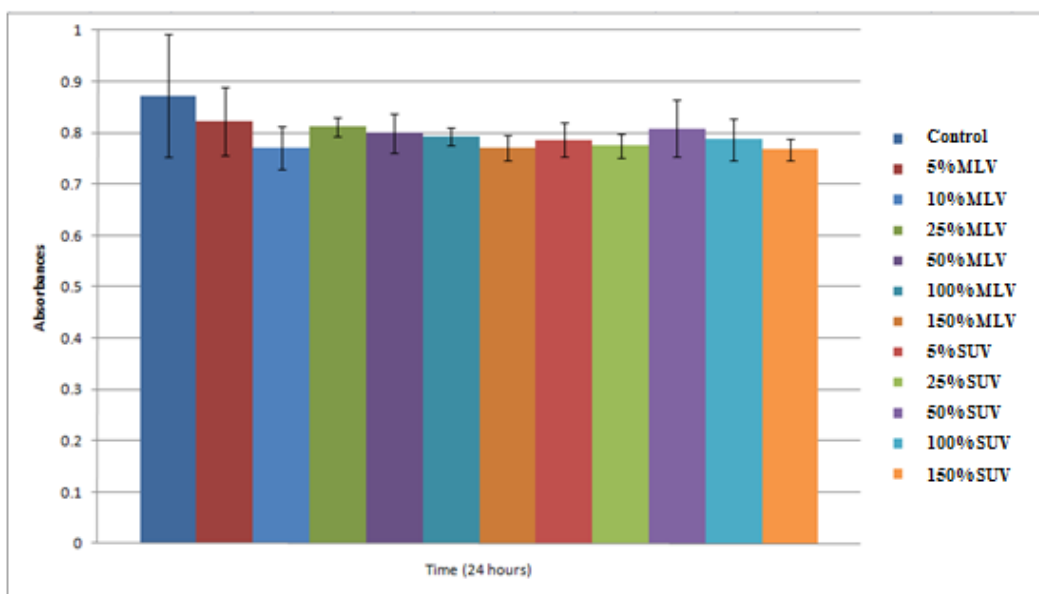


Figure 45. MTS results of unloaded liposomes with Saos2 cells.

The Figure 45 indicates that unloaded liposomes regardless of the liposome type had no significant cytotoxic effect on Saos2 cells and therefore liposomes can be used as the carriers for QDs transportation.

A similar test, but this time involving QDs was carried out 48 hours after addition of QD and liposome suspensions were added into the wells containing the Saos2 and cell viability was determined with MTS cell proliferation assay (Figure 46).

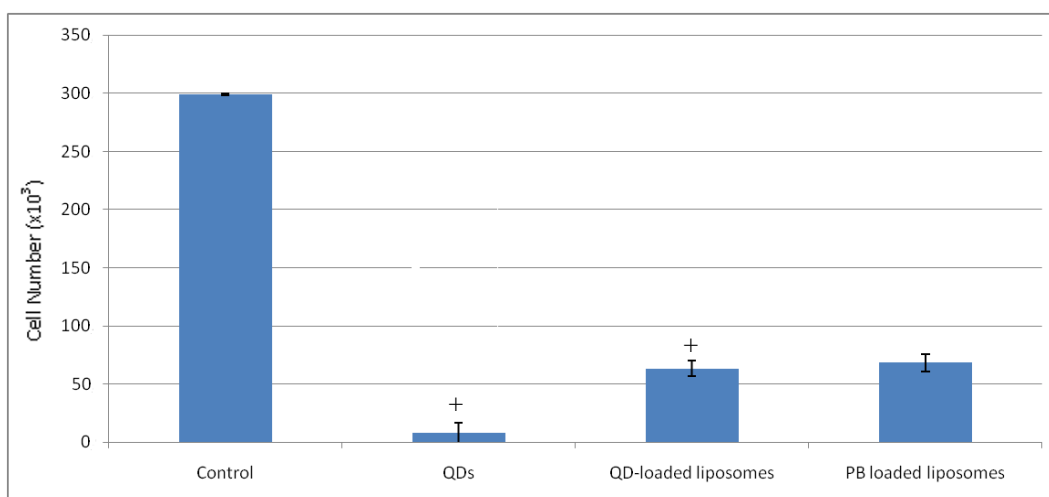


Figure 46. Influence of Quantum Dots on the proliferation of Saos2 cells (MTS test) loaded into SUV liposomes or free. After 48 h incubation with the cells. (+) indicates the significant difference (p value lower than 0.05). (n=2)

Figure 46 indicates that liposomes also decreased the cell viability to a significant extent (to 20%) but not as much as free QDs. QD loaded liposomes and free QD were statistically different than each other (p value was lower than 0.05). QDs affected the cell viability and killed almost all the inoculated cells after 48 h. However, when loaded with QD, the liposomes were not statistically more toxic than the unloaded liposomes (p value was higher than 0.05). This indicates the amount of liposomes as were seen in Figure 43 and Figure 44 were excessive and led to cell death and the liposomes masked the toxicity of the QDs. It can also be deduced from Figure 46 that, the amount of liposomes used in the test was not suitable for cell growth; liposomes might have decreased the oxygen transfer in the medium and suppressed cell growth.

MLV are multilayer liposomes while SUV have only one bilayer. In order to investigate the effect of MLV on the cytotoxicity of QD, Saos2 cells (5×10^4) in RPMI were seeded in 24 well tissue culture plates. After 24 h of incubation with MLV loaded with QD, the cell numbers were determined with MTS cell proliferation assay. All the *in vitro* studies were done in duplicates. Table 9 shows the testing conditions (concentrations and volumes of materials added to the liposomes) that were investigated for cytotoxicity.

Table 9. The test conditions for the influence of MLV on QD cytotoxicity

Treatment Medium (μL), Ingredient (μM)	Test Medium								
	Control			QDL			QD		
PBS	20	50	100	-	-	-	-	-	-
QDL, QD	-	-	-	20, 0.23	50, 0.57	100, 1.14	-	-	-
Free QD, QD	-	-	-	-	-	-	20, 0.23	50, 0.57	100, 1.14

QDL: QD-loaded MLV

Figure 47 shows the MTS results of the above mentioned test with QD-loaded MLV liposomes.

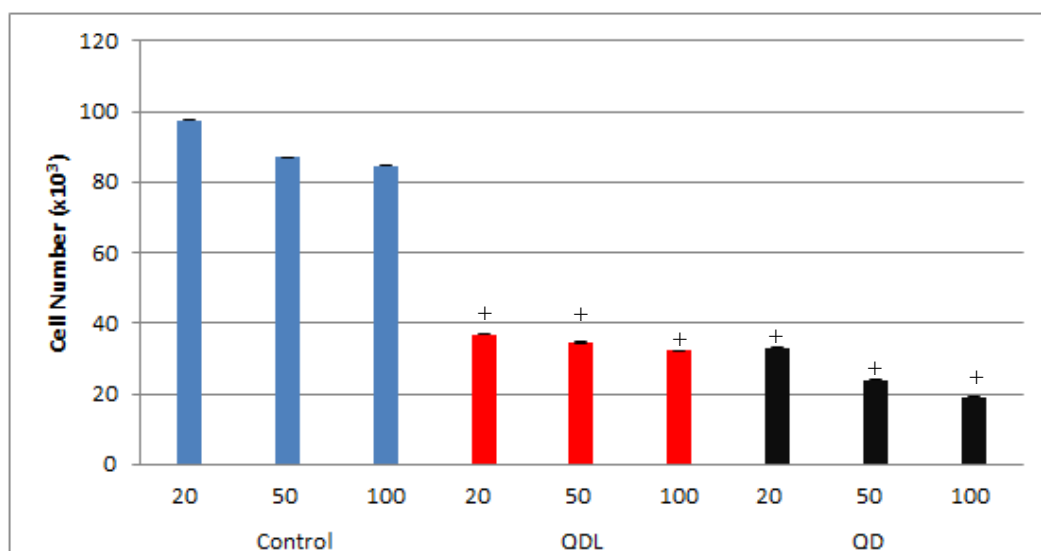


Figure 47. MTS results of control (no QD, blue), free QDs (red) and QD loaded in MLV liposomes (QDL, black) allowed to interact with Saos2 cells for 24 h. The numbers are volumes (μL) of the test solutions added to the wells. (+) indicates the significant difference (p value lower than 0.05). (n=2)

After 24 h of exposure to 0.23 μM, 0.57 μM and 1.14 μM free QDs or QD encapsulated MLV liposomes, it is observed that encapsulating the QDs in liposomes protect the cells from the cytotoxic effect of QDs. For all the concentrations studied, the cytotoxic effects of Quantum Dots were decreased by 10-20%. All the free QD concentrations studied were significantly different from the liposomal QDs with the p value lower than 0.05.

In order to investigate the prevention of cytotoxicity of QD by encapsulation in SUV liposomes, Alamar Blue proliferation assay tests were also performed. Saos2 cells (3×10^4 in RPMI medium) were seeded on 24 well tissue culture plates and they were exposed for 24 h to different concentrations of QD-loaded liposomes and free QDs, and cell numbers were determined using Alamar Blue cell proliferation assay (Figure 48). In the control only buffer solution was added. Buffer loaded liposomes were used to observe the effect of presence of liposomes on the Saos2 cells. These studies were done in duplicates.

After 24 h of exposure to 10, 100, 200, 300, and 500 nM QDs free or loaded in liposomes, it was observed with 10 nM QD-loaded liposomes ~81% cell viability was retained while buffer loaded liposomes had 85%, and free QD had 61% cell viability. Thus unloaded liposomes or liposomes with QD did not show high cytotoxicity but the free QD had a distinctly lower viability. This result indicates that when the QD concentration is 10 nM, liposomes can decrease the cytotoxic effect of the free CdTe

QDs by about 30%. As the added QD amount increases, however, the cytotoxic effect of the QDs increase but the protective capability of the encapsulation in liposomes start becoming ineffective. This is especially important when with 500 nM QDs liposomal protection was 10% which was much higher with MLVs (Figure 47). It can be therefore be stated MLVs have a significant protective capability whereas the SUVs, possibly due to the lower number of bilayer, are less able to protection. All liposomal QD concentrations and free QD concentrations significantly different than each other (p values were lower than 0.05).

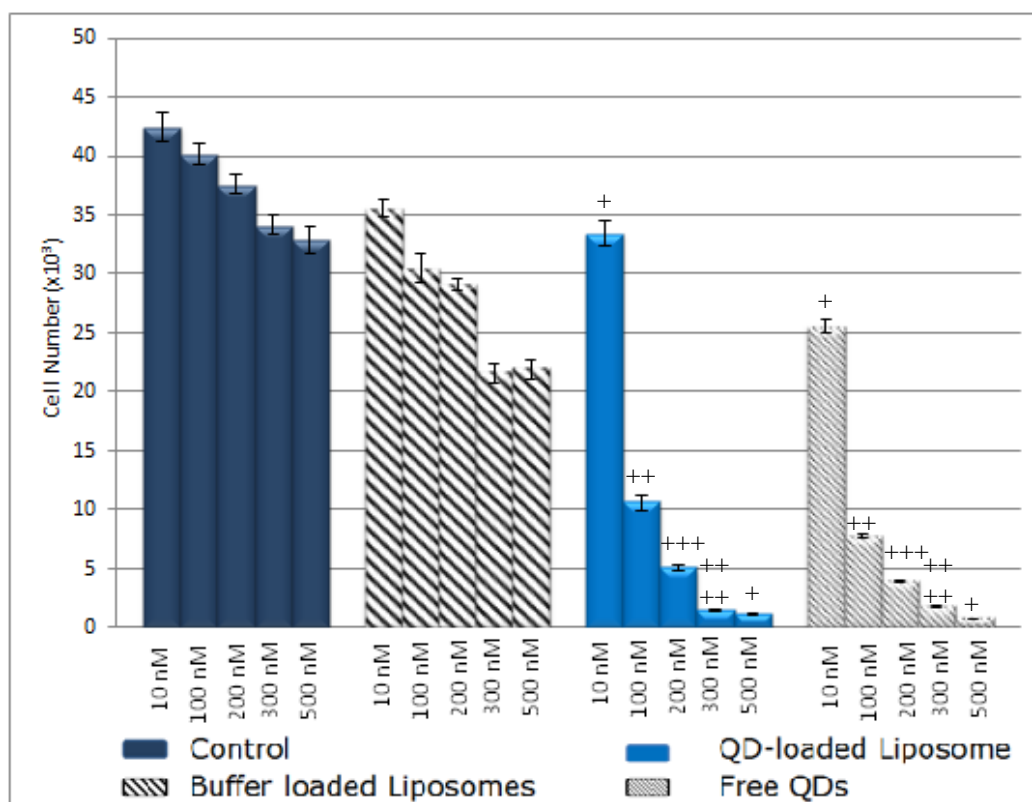


Figure 48. Alamar Blue cell viability test for the exposure of Saos2 cells to free QDs and SUV encapsulated QDs. Exposure duration 24 h. Seeding density 30,000 cells/well. (+) indicates the significant difference (p value lower than 0.05). (n=2)

The survival rate of the cells decreased as the QD concentration increased in both conditions whether encapsulated in liposomes or free form. Yang et. al., in 2009 found that encapsulation in the liposomes decreased the cytotoxicity of CdTe quantum dots. Although the results were depending on the optical micrographs, they found that liposomes decreased the cytotoxicity of the QDs even at the low concentrations. The suggestion was encapsulation prohibits the release of Cd²⁺ ions and decreased the cytotoxicity of the QDs.

Schroeder et. al., 2007, identified a micellar form of a QD-phospholipid complex called lipodots and found that lipodots increased the fluorescent capacity of the QDs. Hydrophobic QDs existed in phospholipid monolayer and this helped increase in quantum yield and cytotoxicity was not detected for up to 72 h of incubation *in vitro*. And they suggested that lipodots could be used for detection of the tumor *in vivo*.



Figure 49. Confocal Micrograph of Saos2 cells treated with 100 nM QD loaded SUV liposomes. Test duration: 24 h. (x60)

QD loaded liposomes were examined under confocal microscopy and it was observed that these liposomes were internalized by the Saos2 cell and localized around the nucleus (Figure 49). This is a visual proof for the cells being penetrated by the liposomes.

3.6 Real Time Observation of Neutral and Positively Charged MLV Liposome-Cell Interactions

In order to study the influence of charge on the interactions MLV liposomes with Saos2 cells, the MLV were loaded with a fluorescent molecule, calcein, and studied

with CLSM using the 488 nm laser for excitation. Since in gene transfer and other cell interactions a positive charge is preferred, the study was conducted with positive charged (cationic) liposomes, and for comparison with neutral (no net charge) liposomes. The live cell imaging system set up was a closed system, with no input or output of solution or gas.

Figure 50 shows the interaction of neutral MLV with the Saos2 cells studied in the live cell imaging system. It is observed that the neutral liposomes and the cells were distant to each other implying that they did not interact with each other.

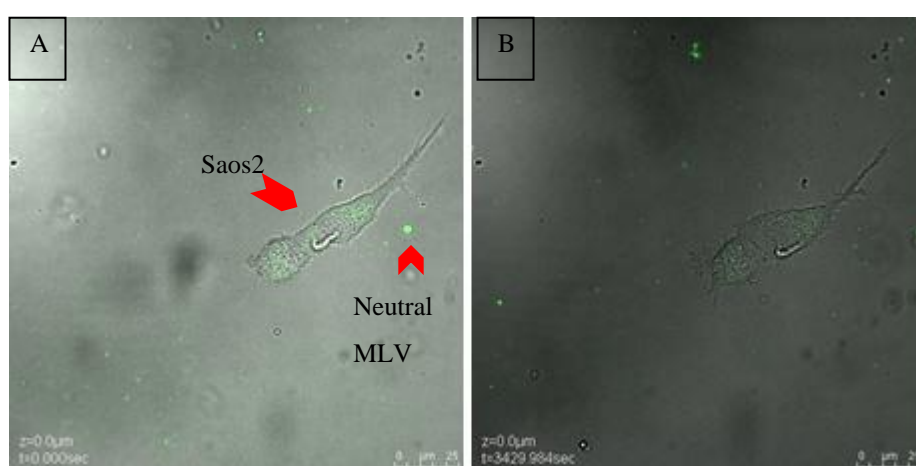


Figure 50. CLSM micrographs of Saos2 cells in interaction with calcein loaded neutral MLV liposomes. Duration of interaction. A) 0 min, B) 60 min. (63x)

In order to observe the influence of charge on the interactions MLV liposomes with Saos2 cells were loaded with fluorescent molecule (calcein) or cytotoxic drug (Doxorubicin) and studied with CLSM using 488 nm laser for excitation.

Figure 51-Figure 53 present the results of the test between calcein-loaded cationic liposomes and the Saos2 cells. Here, the single cell seen in the center of the micrograph is followed for 3 h at a rate of 4 frames per minutes.

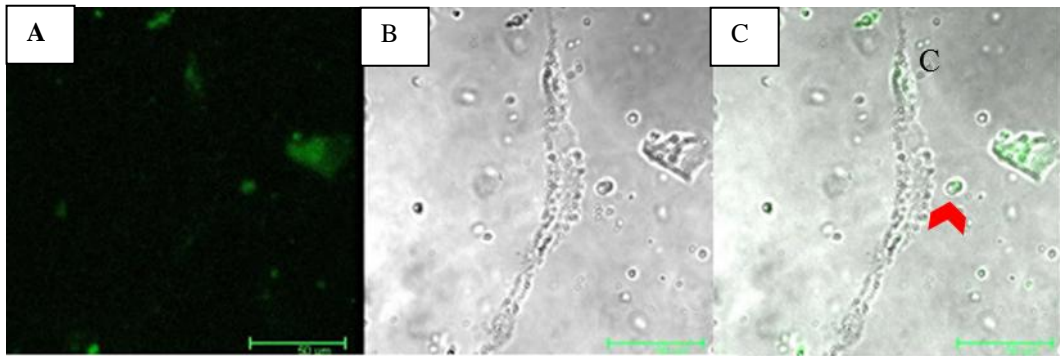


Figure 51. CLSM and transmission micrographs of Saos2 cells in the presence of calcein loaded cationic MLV liposomes. Interaction time: 0. A) Confocal micrograph, B) Transmission micrograph, C) Overlay micrograph. (60x) Arrow heads show the MLV. C denotes the Saos2 cell.

Figure 51 shows the beginning of the incubation in the chamber. There were fluorescence signals from the cell itself but no liposomes are found near the cells.

After 88 min of incubation, MLV liposomes were seen to be bound to the cell.

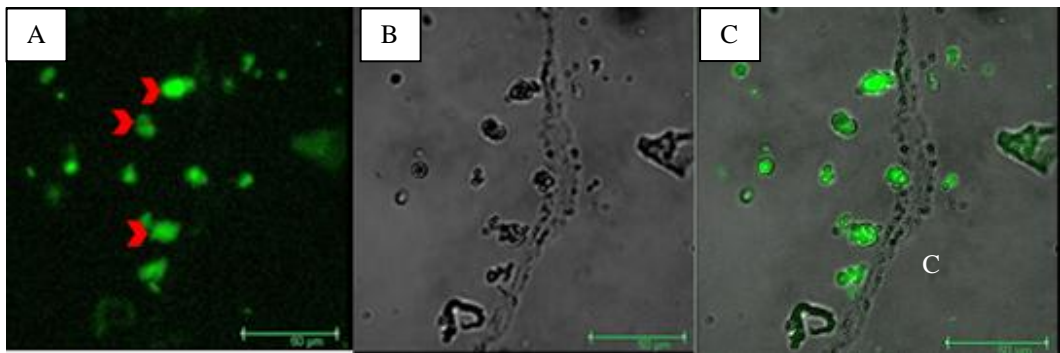


Figure 52. CLSM and transmission micrographs of Saos2 cells in the presence of calcein loaded cationic MLV liposomes. Interaction time: 88 min. A) Confocal micrograph, B) Transmission micrograph, C) Overlay micrograph. (60x) Arrowhead shows the MLV and C denotes the Saos2 cells.

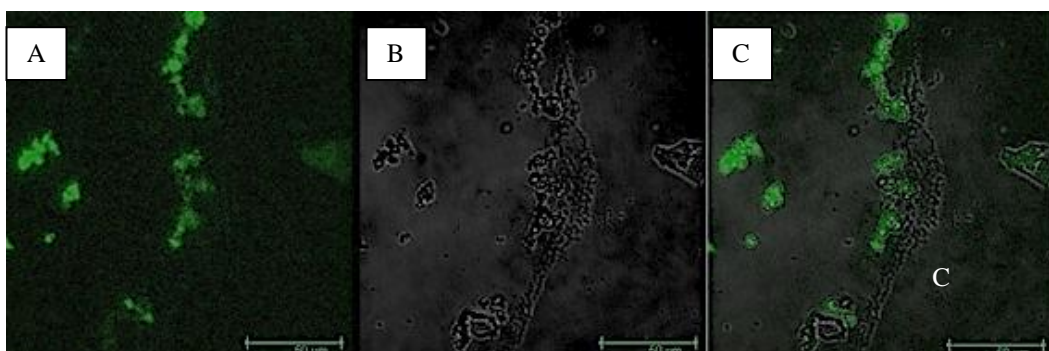


Figure 53. CLSM and transmission micrographs of Saos2 cells in the presence of calcein loaded cationic MLV liposomes. Interaction time: 180. A) Confocal micrograph, B) Transmission micrograph, C) Overlay micrograph. (60x) Arrowhead shows the MLV and C denotes the Saos2 cells.

At the end of the 3 h incubation many MLV liposomes (or their clusters) were observed to be associated with the cell showing that liposomes were effectively bound to Saos2 cells especially when they had a positive charged molecule in their structure (or, in other words when they are cationic).

This study has shown for the first time through real-time CLSM microscopy that cationic liposomes attach to Saos2 cells.

3.6.1 Real Time Observation of Anticancer Agent Doxorubicin Loaded Neutral MLV Liposomes

Interaction between doxorubicin loaded liposomes and Saos2 cells was also studied observed under real time conditions with CLSM using the Opticell™ as a closed system except for the gas transfer. The microscope was set to scan every 15 s for 16 h. The 488 nm laser was used for the excitation of doxorubicin (λ_{ex} : 470 nm and λ_{em} : 590 nm) loaded liposomes and emission band width was 500-800 nm.

Figure 54 shows both locations of the cells and their confocal micrograph at time zero. In the confocal micrograph four cells can be seen in the middle of the frame and doxorubicin loaded liposomes (or their clusters) are seen as green specks. This micrograph shows the beginning of the real time observation and there appears to be no attachment of the liposomes to the Saos2 cells.

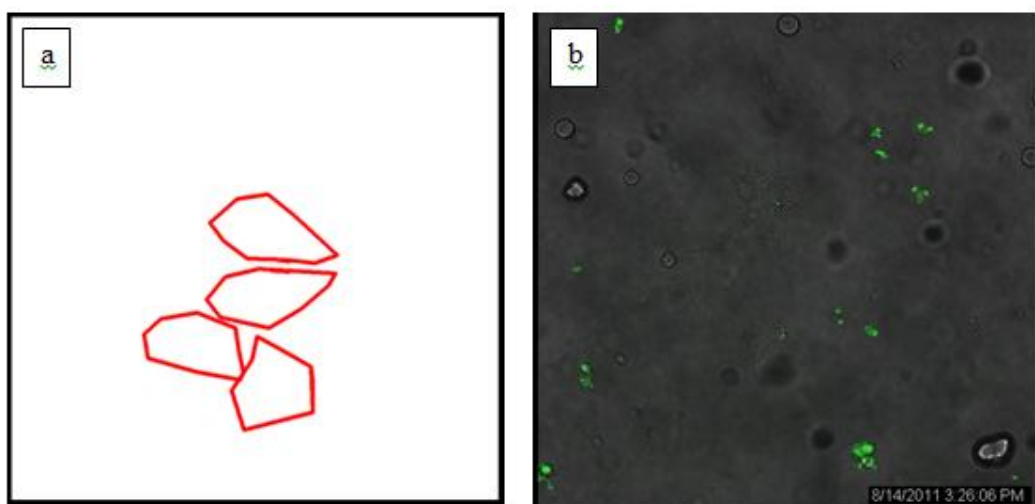


Figure 54. Time zero for the real time observation a) Location map of the cells, b) CLSM overlay micrographs showing Saos2 and doxorubicin loaded neutral liposomes, 0 min. (40x)

Figure 55 shows doxorubicin loaded liposomes and Saos2 cells approximately 4.5 h later showing one of the liposomes in contact with a Saos2 cell. Liposome in contact with the cell is indicated in the micrograph within a red circle.



Figure 55. Doxorubicin loaded liposome in contact with Saos2 cell (within red circle). (40x)

Figure 56 shows a total of two doxorubicin loaded liposomes in contact with two Saos2 cells and Figure 57 shows 3 liposomes in contact with Saos2 cells. Liposomes in contact with the cells are indicated in the micrograph within red circles.

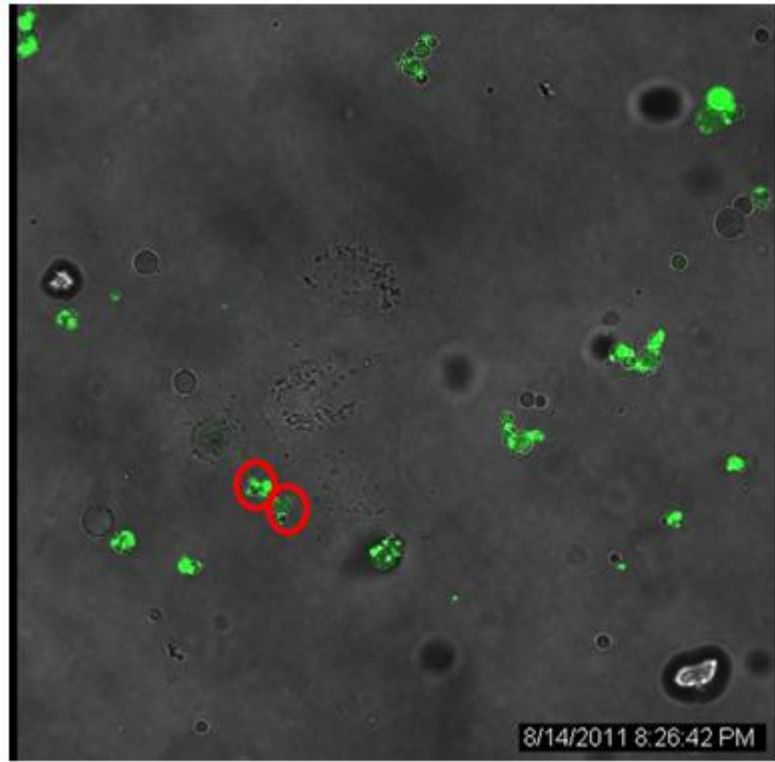


Figure 56. Doxorubicin loaded liposomes in contact with the Saos2 cells. (40x)



Figure 57. Three doxorubicin loaded liposomes in contact with three Saos2 cells. (40x)

Figure 58 shows bound doxorubicin loaded liposomes starting to change places with respect to the nuclei of Saos2 cells.



Figure 58. Liposomes move on the cells. (40x)

Figure 59 shows another doxorubicin loaded liposome (or liposomal aggregate) in contact with the cell (in the lower left corner).

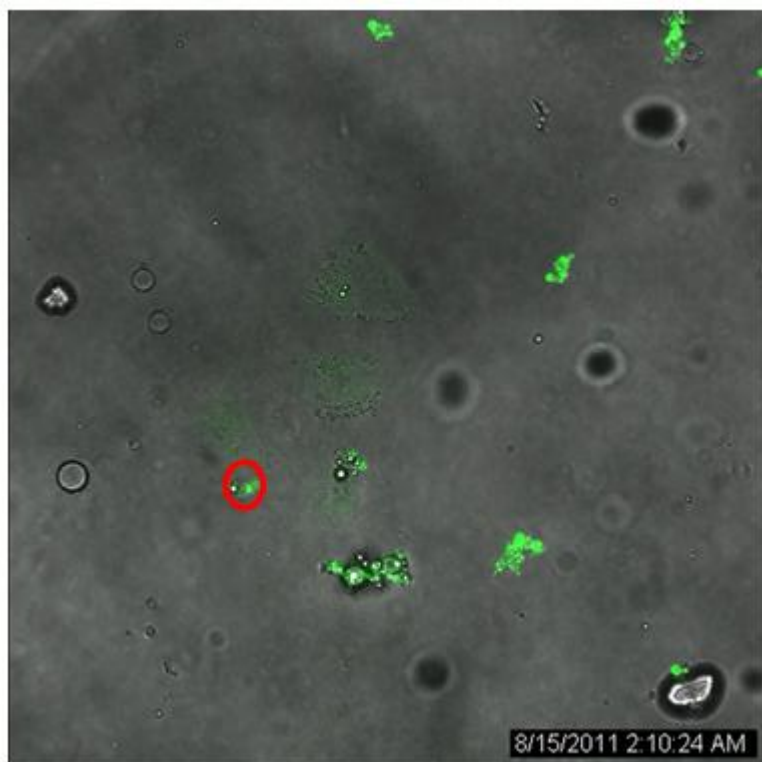


Figure 59. Another liposome in contact with a cell. (40x)

Figure 60 shows that after 846 min the Saos2 cells are in contact with the neutral MLV liposomes and the cells start to shrink possibly as a result of doxorubicin released from the liposomes.

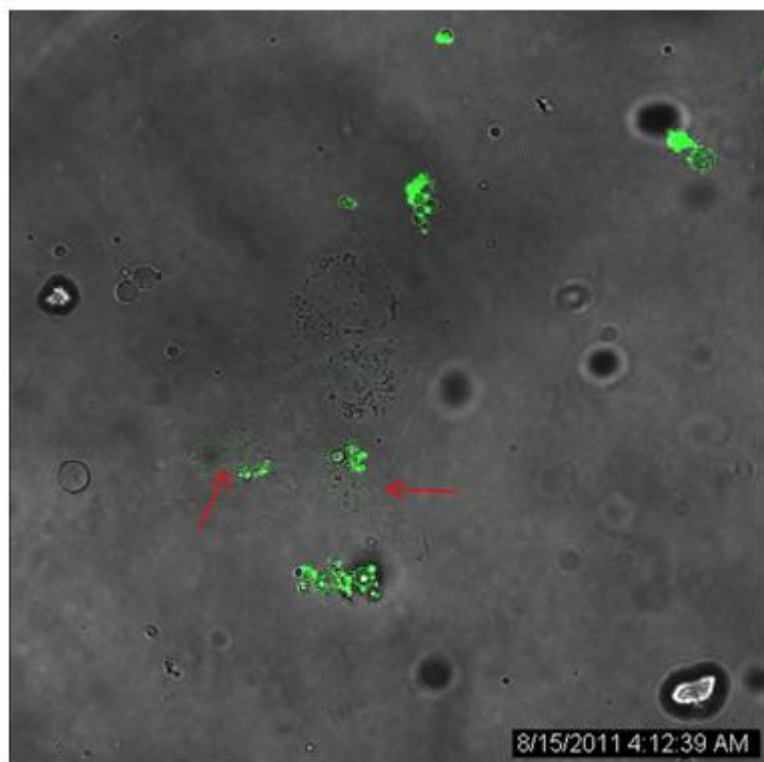


Figure 60. Saos2 cells start to shrink time of exposure: 846 min. (40x)

Figure 61 shows that one of the cells that was in contact with the liposomes take a spherical shape, which generally means that the cell is dead.

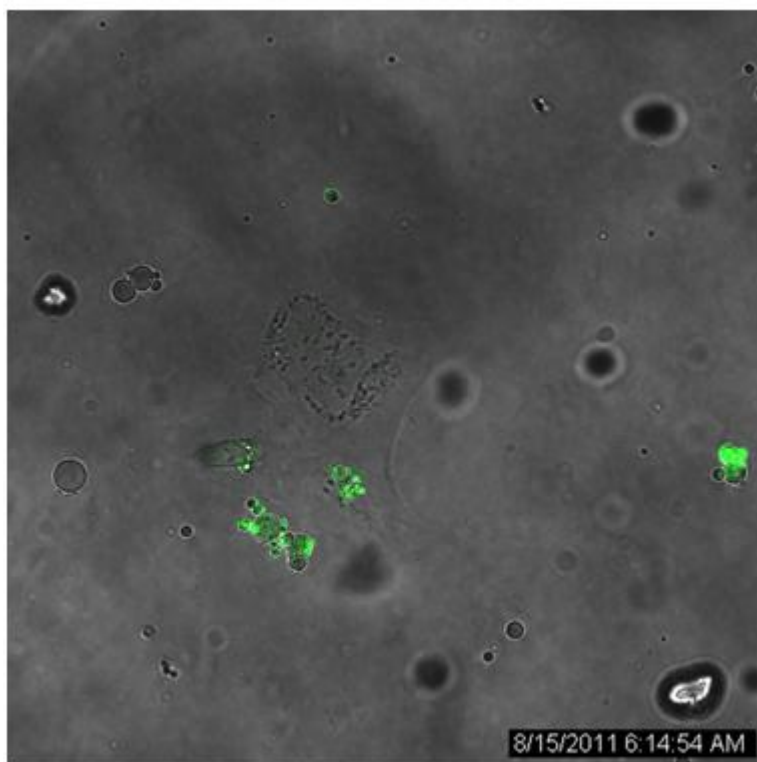


Figure 61. Dead Saos2 cell. t: about 16 h. (40x)

At the end of the observation period many liposomes were seen to surround the cell, and the cell was dead. Figure 54- Figure 61 show that doxorubicin loaded neutral MLV were bound to at least three of Saos2 cells and led to their deaths.

This study has shown for the first time through real-time CLSM microscopy attachment of doxorubicin loaded liposomes to Saos2 cells and leading to their deaths.

At the end of the real time observation of the interaction between Saos2 and Doxorubicin loaded liposomes, the interaction was observed in z dimension. The 3D scanning was performed in 8.8 μm thickness.

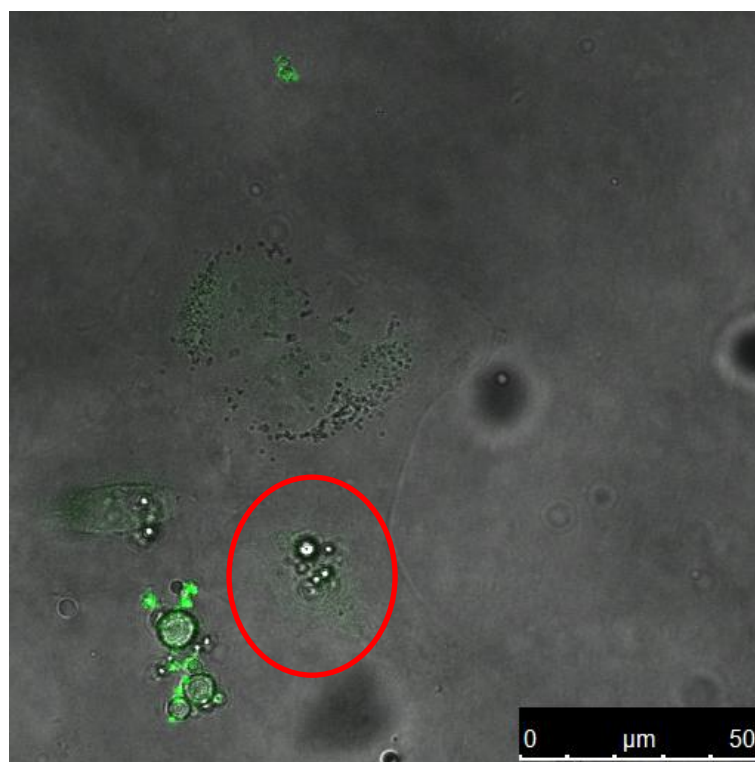


Figure 62. End of the real time observation. Indicated region with a circle was scanned for 8.8 μm thickness.

Figure 63 shows the -4.8 μm depth of the scanning. In this region no signal was detected.

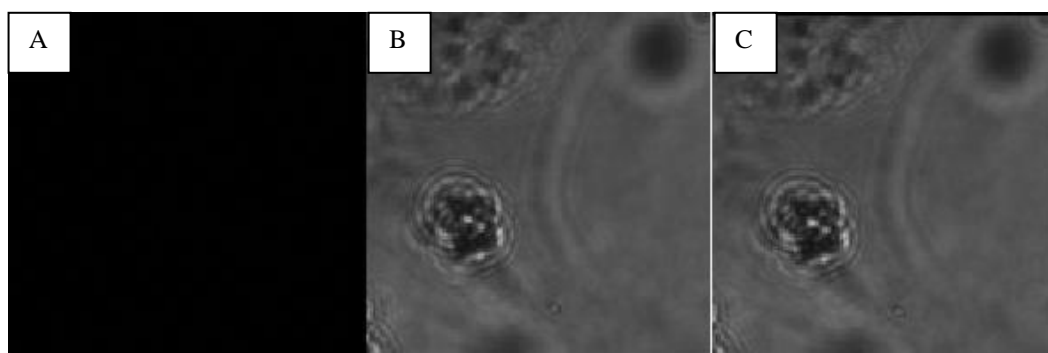


Figure 63. 3D scanning of Saos2 cell interacting with the Doxorubicin loaded liposomes $z: -4.8 \mu\text{m}$. A) Confocal micrograph, B) Transmission micrograph, C) Overlay micrograph.

Figure 64 shows the interaction at $z = 0 \mu\text{m}$ and it can be seen that confocal micrograph was in the focus and emission from Doxorubicin was determined. The transmission micrograph shows the cell in the focus.

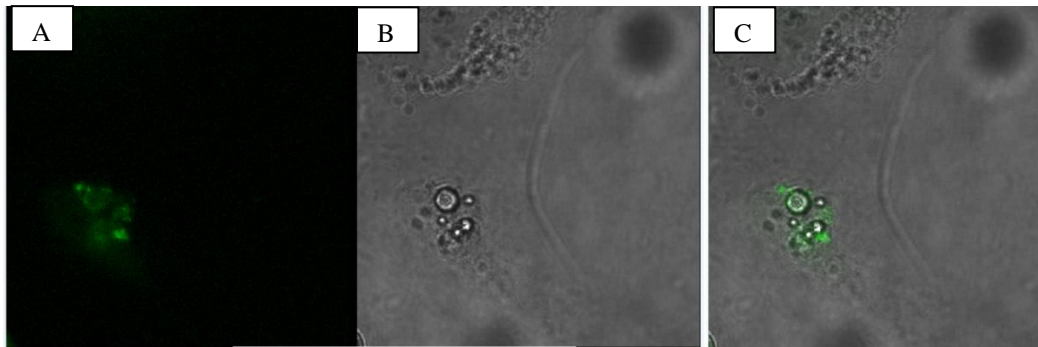


Figure 64. 3D scanning of Saos2 cells with the Doxorubicin loaded liposomes $z:-0 \mu\text{m}$
 A) Confocal micrograph, B) Transmission micrograph, C) Overlay micrograph.

In this figure it can be deduced that Saos2 cell and the Doxorubicin loaded liposomes were in the same height in z direction. This means Doxorubicin loaded liposomes are in contact with the Saos2 cells, which can be also seen in the real time observation section.

Figure 65 shows 3D scanning at z direction +4 and at this height no emission was detected from the Doxorubicin (liposome), and the cell is not in the focal point.

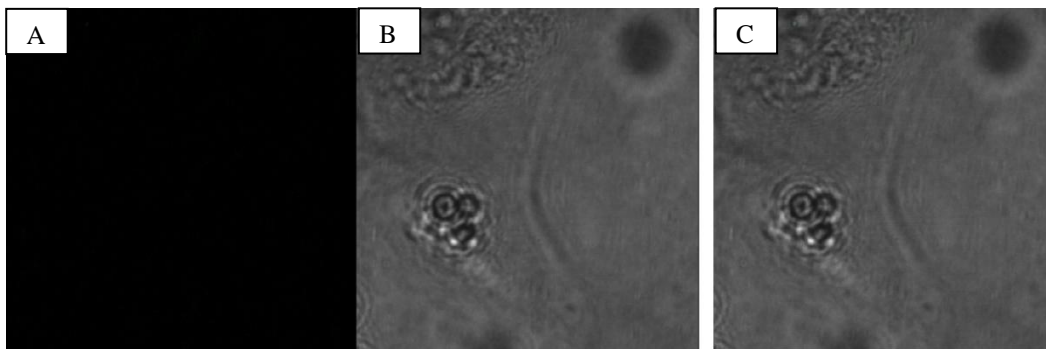


Figure 65. 3D scanning of Saos2 cells with the Doxorubicin loaded liposomes $z= +4 \mu\text{m}$.
 A) Confocal micrograph, B) Transmission micrograph, C) Overlay micrograph.

Figure 66 shows the 3D projection of the interaction in this figure it can be said that liposomes were located around the cell nucleus but it can not be deduced whether they are inside or not.

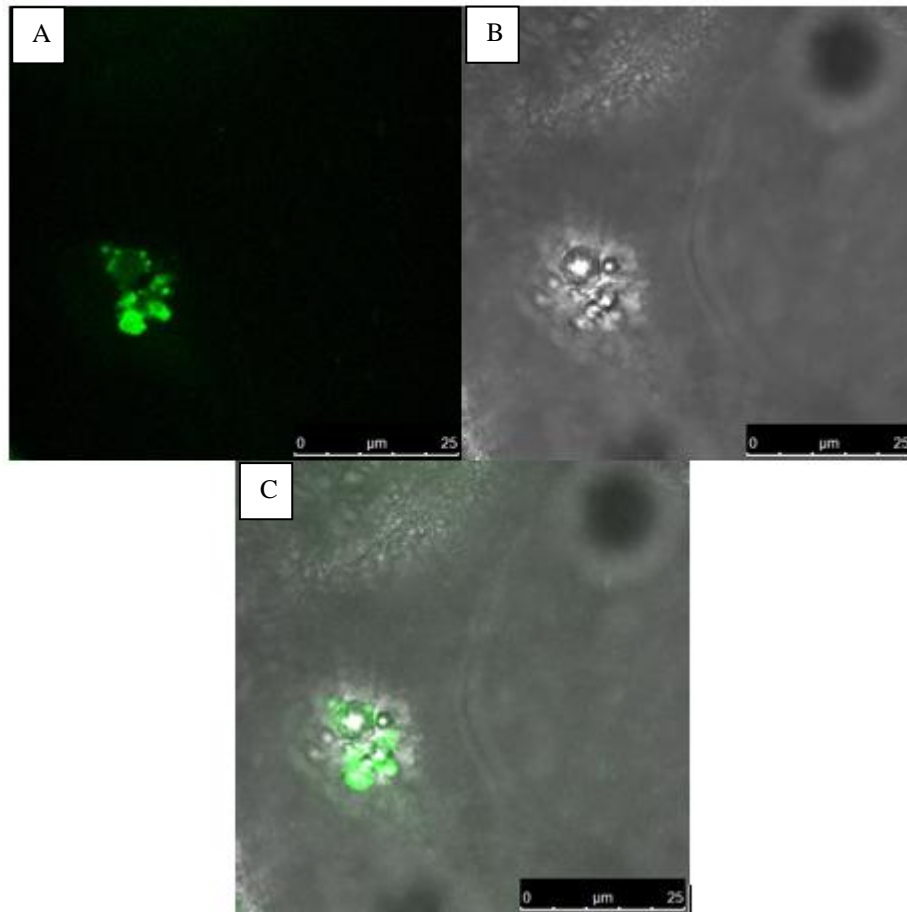


Figure 66. 3D projection of 3D scanning of the Saos2 and Doxorubicin interaction A) Confocal micrograph, B) Transmission micrograph, C) Overlay micrograph.

Figure 67 shows the lateral view of 3D projection, in this figure liposomes were interacting with the cell. The green line under the liposomal emission originating from Doxorubicin released from the liposomes and delivered into the cell.

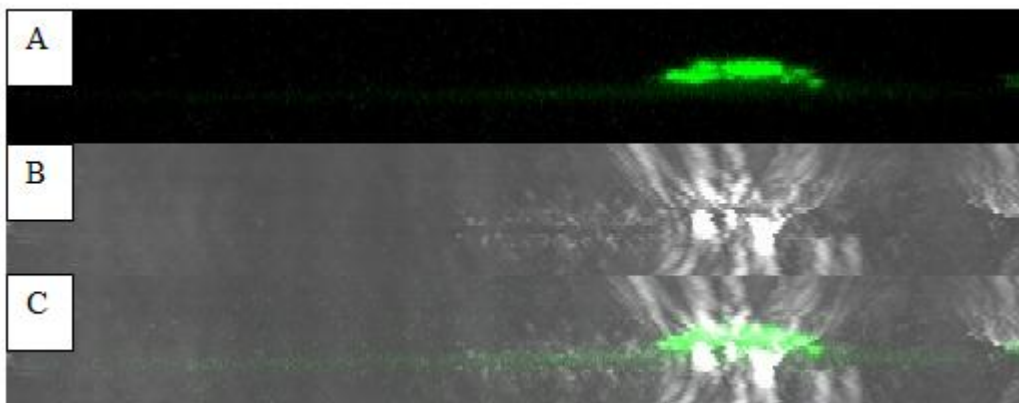


Figure 67. CLSM and transmission micrographs lateral 3D projection. A) Confocal micrograph, B) Transmission micrograph, C) Overlay micrograph.

Figures from the real time observation experiments indicated that liposomes whether positively or neutral interact with the Saos2 cells but the time of the first binding change. Positively charged liposomes bind earlier than the neutral liposomes.

3.7 *In situ* and *In vitro* Studies with Doxorubicin

Passive loading of SUV

Thin lipid films were prepared with PC:Chol (7:3) and hydrated with Doxorubicin solution and the release of doxorubicin these SUVs into buffer at 37⁰C was studied.

It is observed that the release of Doxorubicin took place for a period of about 50 h with a gradually decreasing rate and the half life was around 5 h. This rate is very similar to Higuchi models prediction and is acceptable because an initial high dose followed by a lower dose is preferred for most treatments.

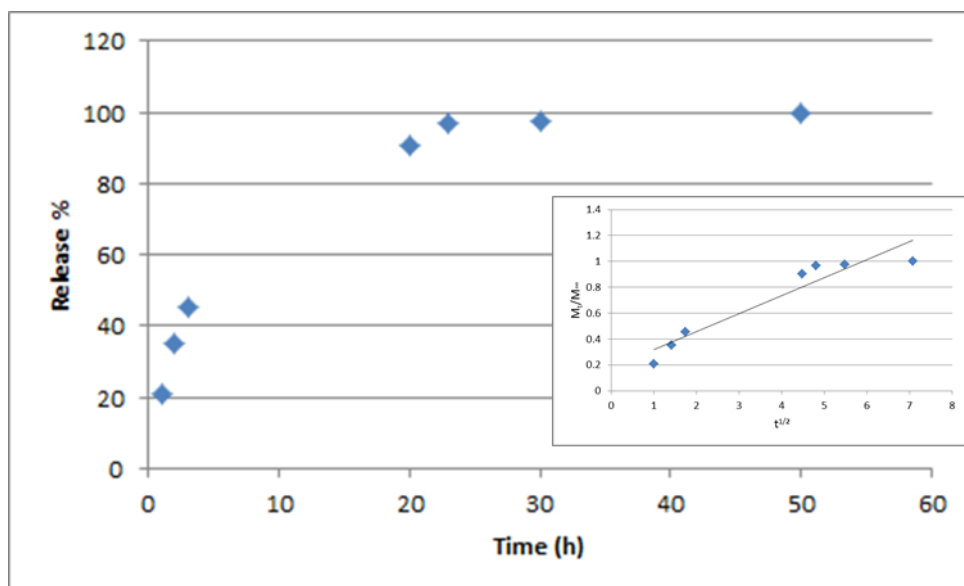


Figure 68. Release of Doxorubicin from passive loaded neutral SUV liposomes, inset Higuchi's release model prediction.

Active loading (Freeze and Thawed Liposomes- FAT):

Figure 69 shows the doxorubicin release profile of the FAT SUVs in buffer at 37⁰C. Active loaded SUV behaved in a similar fashion to the passive loaded SUVs except that the release duration was lower (around 40 h) and the half life was about 4 h.

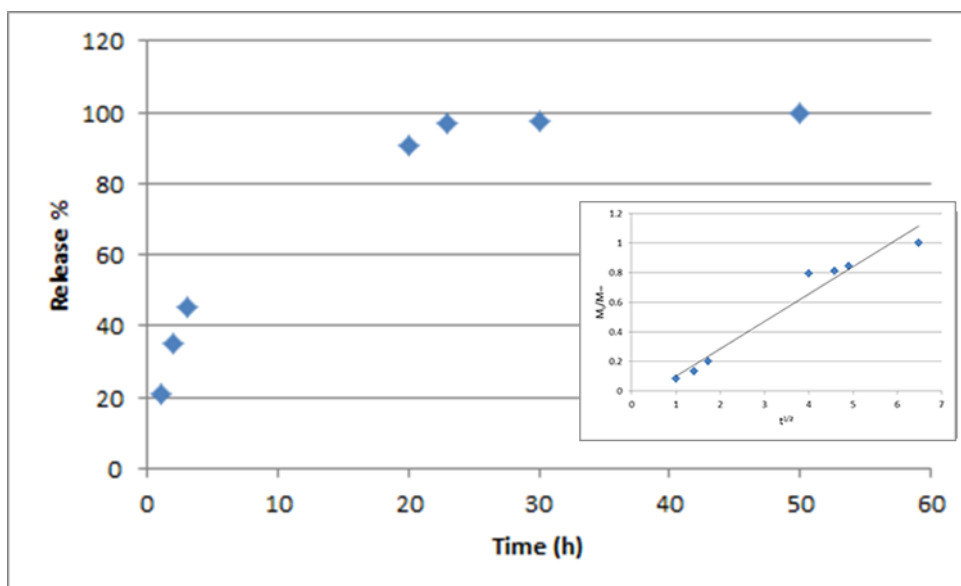


Figure 69. Release of Doxorubicin from FAT SUV liposome vs. Time inset Higuchi's release model prediction.

3.7.1 *In vitro* Testing of Toxicity of Free Doxorubicin on Saos2 Cells

Figure 70 shows the Saos2 cell response to different concentrations (0.1 μM - 3 μM) of free doxorubicin as tested with Alamar Blue assay. It is observed that the drug is very potent and kill 60-95 % of the cells within 24 h and almost all in 48 h.

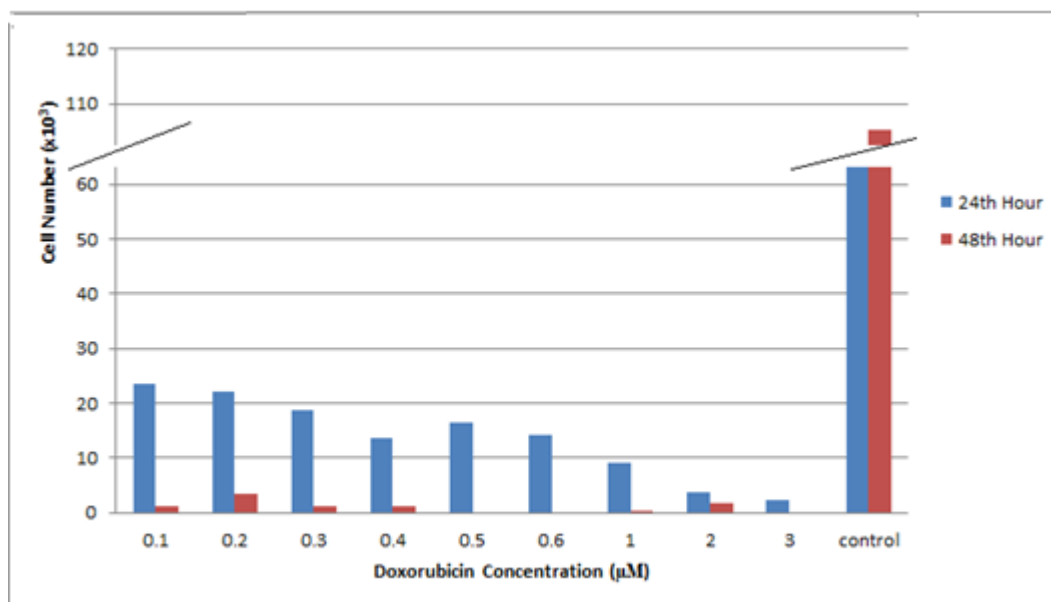


Figure 70. Effect of concentration of Doxorubicin on viability of Saos2 as determined with Alamar Blue test after 24 and 48 h incubation. Cell seeding density 3×10^4 /well in RPMI medium. (n=2)

Then *in vitro* studies were carried out to study the influence of loading Doxorubicin in MLV liposomes (Figure 71). Saos2 cells (5×10^4 /well in RPMI medium) and FAT Doxorubicin-loaded MLVs (Dox-L) were incubated for 24 h and then viability assay was applied. All the concentrations of doxorubicin significantly different from the control (p values were lower than 0.05). All the *in vitro* studies were done with duplicates.

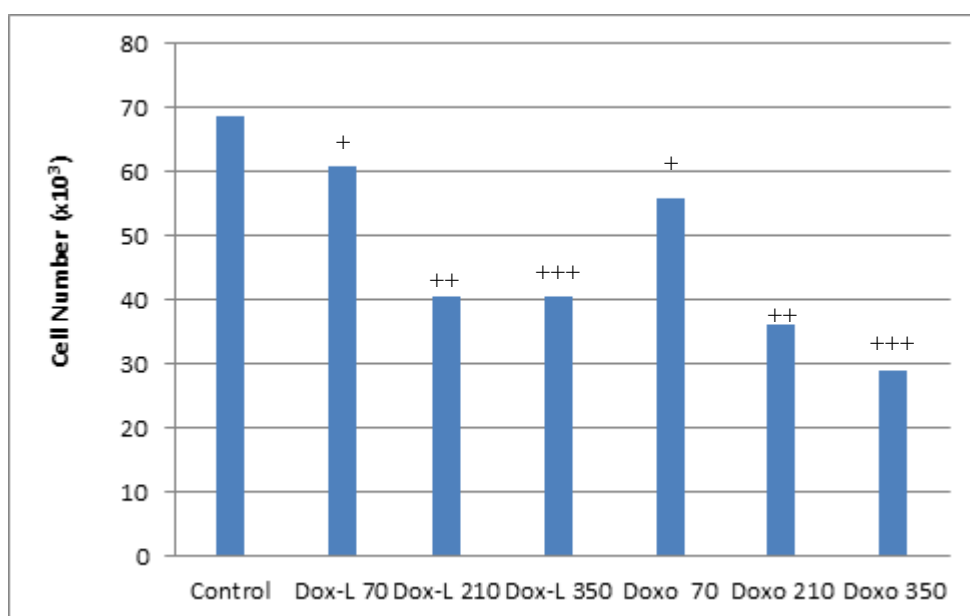


Figure 71. MTS results of Control cells, free Doxorubicin and FAT doxorubicin-loaded MLV liposomes with Saos2 cells. Time of exposure: 24 h. The numbers are concentrations in nM. Doxorubicin-loaded MLVs (Dox-L), Free Doxorubicin (Doxo). (n=2)

After 24 h of exposure to free doxorubicin or doxorubicin loaded in MLV liposomes a dose-dependent decreased in cell numbers was observed. 70 nM doxorubicin whether encapsulated or free was not very toxic; liposomal formulation caused a 11% decrease in viability whereas the free doxorubicin caused a 19% decrease. When the dose became 5 times higher (350 nM) these decreases were 41% and 57%, respectively. All the results of the same concentrations had significantly different from each other (p value were lower than 0.05). These results indicate that doxorubicin when supplied free is immediately available and toxic whereas the liposomal formulation as was shown in the release studies to release its content gradually. These explain why liposomal anticancer agents are preferable. Thus, although they also lead to the death of cells, liposomes still provide some protection for the cells against the cytotoxic effect of doxorubicin.

3.8 *In Situ* and *In vitro* Studies with Bevacizumab

Bevacizumab is a compound that is used as an angiogenesis inhibitor and acts by inhibiting the activity of VEGF by chemically binding to it and preventing VEGF's interaction with the receptors on endothelial cells such as HUVECs. *In vitro* studies were carried out in order to investigate the possibility of a direct effect of Bevacizumab on HUVECs proliferation. HUVECs (3×10^4 /well in DMEM low glucose medium) and free Bevacizumab were incubated for 24 h and then Alamar Blue cell

viability assay was carried out (Figure 72). All the *in vitro* studies were done in duplicates.

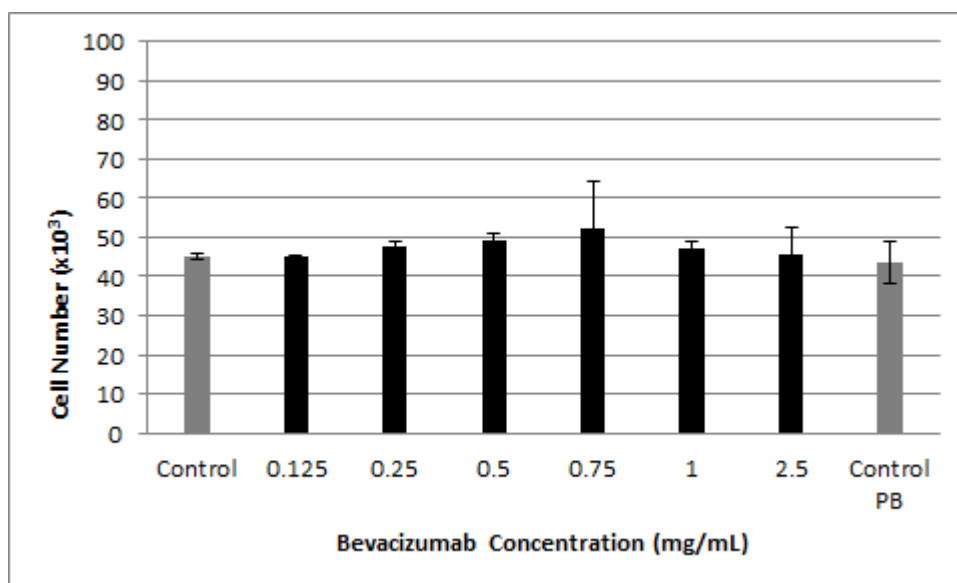


Figure 72. Influence of Bevacizumab concentration on the proliferation of HUVEC (Alamar test). After 24 h incubation. Control contains only the cells, Control PB contains the phosphate buffer in the amount of Bevacizumab added. Cell seeding density: 30,000/well. (n=2)

It is observed that all the samples show a significant cell number increase (from 30,000) within 1 day. This increase was not changed with the presence or the dose of the drug, therefore, it can be stated that Bevacizumab did not suppress the proliferation of HUVECs. After 1 day of exposure to Bevacizumab there was not a significant change in the cell numbers in comparison to the control (p values were higher than 0.05). Although Kuester and Campbell in 2009 found the maximum amount of antibody that did not suppress the proliferation to be 500 µg/ml, the used concentration 2.5 mg/ml five times higher than the concentration the drug did not affect cell proliferation.

The effect of Bevacizumab on the proliferation in HUVEC and Saos2 co-cultures were also investigated. Figure 73 shows the light micrograph of the two healthy cell populations in the co-culture. HUVEC (1.5×10^4 /well) and Saos2 cells (1.5×10^4 /well), both in DMEM Low glucose medium, and Bevacizumab were incubated for 24 h and then proliferation was determined with Alamar blue test (Figure 74).

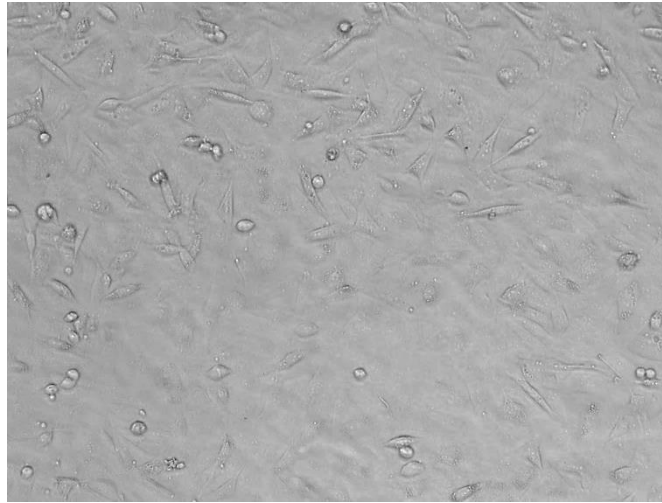


Figure 73. Light micrographs of HUVEC and Saos2 in the co-culture system. 24 h after incubation in DMEM low glucose medium (x10). The round cells are HUVEC and spindle shaped cells are Saos2.

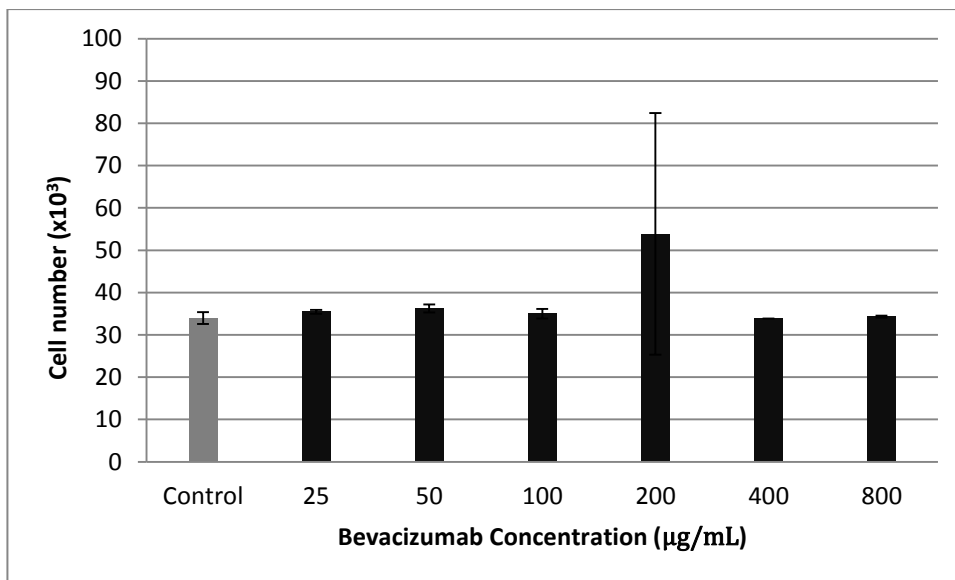


Figure 74. Effect of Bevacizumab concentration on the proliferation of HUVEC and Saos2 cells in a co-culture system. Time of incubation 24 h. Medium: DMEM low glucose (n=2). Cell seeding density: 30,000/well.

The test used is based on the determination of the reduction of Alamar blue in the mitochondria, and therefore, even though the cells are counted with this approach their phenotype can not be stated. Since a total of 30,000 cells were seeded, the increase observed in Figure 74 is not as great as it was in Figure 72. The figure indicates that

Bevacizumab in the concentration range of 25-800 µg/mL did not suppress the proliferation of the cells. According to the action mechanisms Saos2 would produce VEGF and lead to an increase in HUVEC proliferation. When Bevacizumab was added, this would bind to VEGF and prevent the increase in HUVEC number (Figure 75). Since no significant cell number increase was observed between control and the others (p values were higher than 0.05), no effect can be assigned to the drug. This implies that either insufficient amounts of Bevacizumab was provided (this is not very likely when compared with literature), or not distinct amounts of VEGF was secreted by Saos2 or the drug used was inactivated (it is an antibody and therefore this is likely).

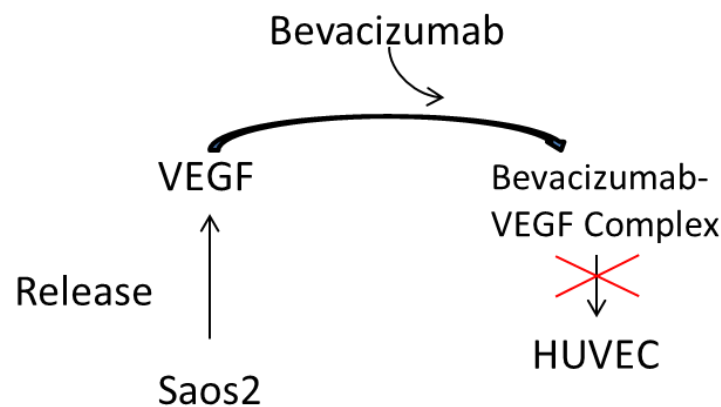


Figure 75. Schematic illustration of VEGF effect mechanism

The drug Bevacizumab was shown in the above tests to be ineffective but normally it is expected to be more effective when delivered with liposomes because entrapment in liposomes would improve targeting, help preserve its integrity and prolong its delivery time (and effective duration). Bevacizumab loaded in SUV liposomes were used to study the proliferation along with free drug. The encapsulation efficiency of the liposomes found to be $8.6\% \pm 1.8\%$. In this test VEGF (50 pg/mL) was also added to the medium. In angiogenesis endothelial cells, smooth muscle cells and pericytes have roles. Growth factors such as: interleukin-1 (IL-1), tumor necrotic factor- α (TNF- α) and VEGF also take action in angiogenesis. But VEGF is the most potent growth factor in angiogenesis. Therefore addition of VEGF can simulate the tumor vascularization. Han et. al., 2009 used VEGF on HUVECs to simulate the angiogenesis. HUVECs (3×10^4 /well in DMEM low glucose medium), Bevacizumab (free), and Bevacizumab loaded in SUV liposomes were incubated for 24 h and then tested for their effect on cell (HUVEC) proliferation.

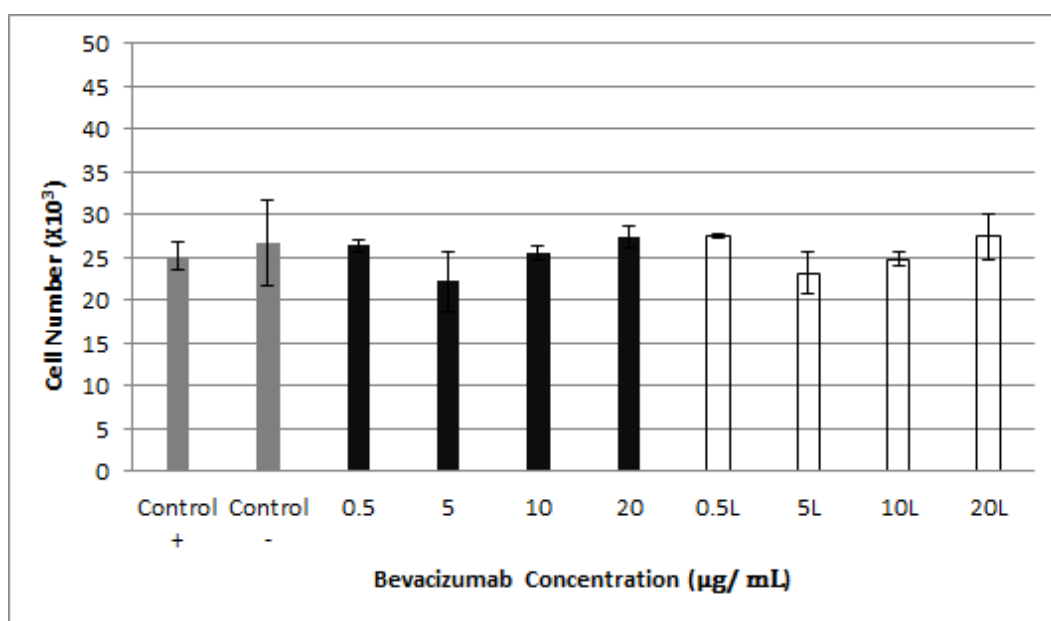


Figure 76. Influence of Bevacizumab concentration and encapsulation in liposomes on the viability of HUVEC (Alamar test). 0.5-20 indicate the dose for free Bevacizumab, and 0.5L-20L for liposome encapsulated Bevacizumab. VEGF was added into the control indicated with (+) and to all the other samples (except control (-)). Cell seeding density: 30,000/ well. (n=2)

Figure 76 shows that a 1 day exposure to Bevacizumab did not suppress the proliferation of HUVECs. Addition of VEGF to the medium did not improve HUVEC proliferation either. Thus, it is observed that under the test conditions VEGF did not improve the proliferation of the HUVEC and Bevacizumab did not show any adverse (suppressive) effect either. Actually a detrimental effect of Bevacizumab was expected in the case of VEGF added samples because Bevacizumab would bind the VEGF and prevent its positive effect on HUVEC proliferation. Since there was no significant difference between the controls (all p values were higher than 0.05.), the activity of VEGF on HUVEC also becomes questionable. In the literature the addition of VEGF (10 ng/mL) into the culture medium increased the proliferation of HUVECs by 15% compared to the control group after 24 h (Han et. al., 2009). The used VEGF concentration in the present study was 200 fold less than that used in the study of Han et. al., and the ineffectiveness in the proliferation of HUVECs may be because of low the dose used.

After the investigation of the effect of Bevacizumab on HUVEC proliferation and the contribution of Bevacizumab to this stage, another growth activating agent, Endothelial Cell Growth Supplement from bovine pituitary (ECGS) was added to the culture medium (100 µg/mL). HUVECs (3×10^4 /well in DMEM low glucose medium),

Bevacizumab and Bevacizumab loaded SUV liposomes were incubated for 24 h and then proliferation was studied (Figure 77).

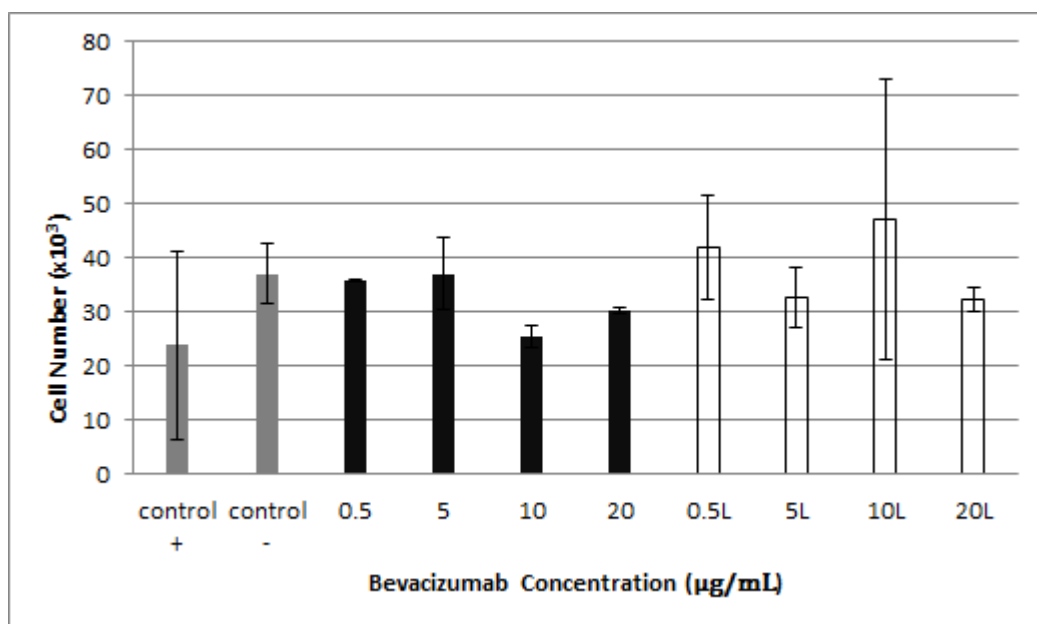


Figure 77. Influence of the concentration of Bevacizumab on HUVEC proliferation in the presence of ECGS. 0.5L- 20L are the dose in liposome encapsulated Bevacizumab samples. ECGS was added in control indicated with (+) and all the other samples except control (-). Cell seeding density: 30,000/well. (n=2)

After a 1 day of exposure to ECGS on the medium did not affect the proliferation of HUVECs (Figure 77). All the samples showed a cell number increase regardless of the Bevacizumab concentration implying again the ineffectiveness of the drug and of the ECGS. Presence of the liposomes led to slightly higher cell numbers but these were not statistically significant, all p values were higher than 0.05.

The experiments carried out with HUVEC; co-cultivation, VEGF addition and ECGS addition did not increase the proliferation of HUVECs. There were no significant differences between the drug added samples and control cells. It may also be because of the cell line used; HUVECs may lose their features under the laboratory conditions and may not give positive response to stimulating factors.

After observing the ineffectiveness of Bevacizumab on HUVEC cells, Human Internal Thoracic Artery Endothelial Cells (HITAEC) were investigated. The effect of Bevacizumab on the proliferation of HITAEC and Saos2 co-cultures were investigated. HITAEC (1.5×10^4 /well) and Saos2 cells (1.5×10^4 /well), both in MesoEndo Growth Medium, and Bevacizumab were incubated for 24 h and then proliferation was studied with Alamar blue cell viability test (Figure 78).

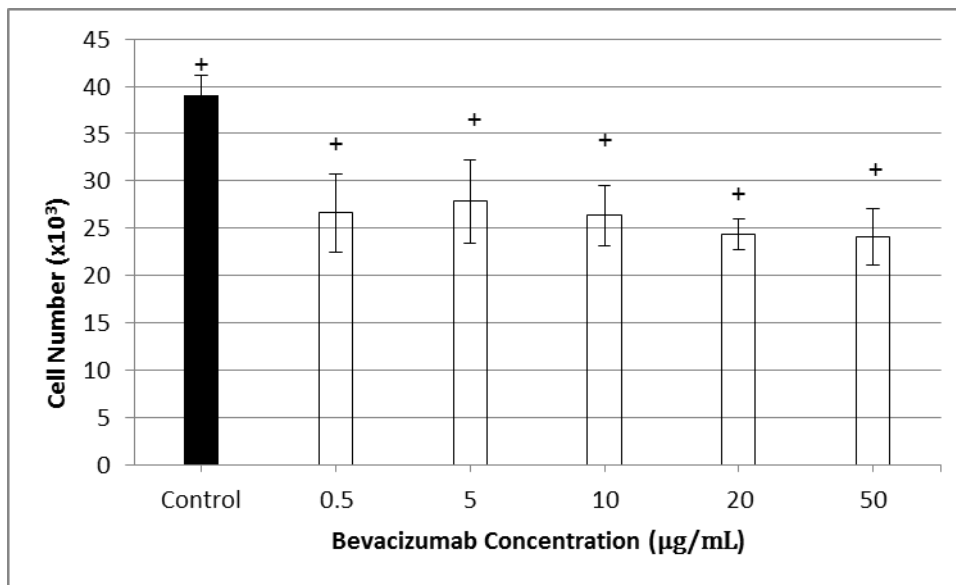


Figure 78. Influence of the concentration of Bevacizumab on HITAEC and Saos2 cells proliferation in a co-culture system. Time of incubation 24 h. Medium (MesoEndo Growth Medium): 0.5- 50 are the dose used Bevacizumab samples. Cell seeding density: 30,000/well. (+) indicates significant difference (p value lower than 0.05). (n=2)

Figure 78 shows that a 1 day exposure to Bevacizumab suppressed the proliferation of HITAECs. Addition of Bevacizumab to the medium was effective at all the concentrations tested causing a decrease of about 30%. The cell number of the control significantly higher than the others (Student's t-test with minimum confidence level of 95%, p value lower than 0.05). In the co-culture system Saos2 was used as a VEGF producer and HITAEC as a blood vessel endothelial cell. Although *in vitro* the proliferation assay did not show the angiogenic effect, it shows that if the cell proliferation were suppressed *in vitro*, it would suppress the angiogenic effect under *in vivo* conditions.

CHAPTER 4

CONCLUSION

Liposomes are used as carriers of bioactive molecules because they can mask the activities and protect the structure of their contents. In this study SUV liposomes were loaded with for use as both bioactive agent carrier and also as a tracking system. The effect of QD loading on liposomes, liposomes was studied *in situ* and *in vitro*. QD loading did not change size of the SUV and MLV liposomes and the liposomes did not change the optical (light emission) properties of the quantum dots. It was found that liposomes could decrease the cytotoxicity observed with the untrapped quantum dots. MLV were shown to be more protective than the SUV liposomes possibly due to the presence of the multi-layer of lipids.

The interactions of the liposomes and substrates with charged surfaces were shown before testing their effect on liposomes. It was shown that these surfaces effectively bind the oppositely charged liposomes. The bound liposomes were stable in this state for 48 h. These interactions showed that these liposomes, with and without charges can be used to localize them on predetermined regions for the purpose of drug delivery and also for binding opposite charged cells.

For the detection of the interaction between MLV liposomes with various charges and Saos2 cells real time observations were made and the interactions were successfully shown for the first time in literature. The positively charged liposomes bound to the human osteosarcoma cells faster than the neutral charged liposomes. This real time observation also showed that the liposomes in the culture medium released their content slowly and the cells were observed to gradually lose their membrane integrity and release the fluorescent agent. The real time observation also indicated that liposomes whether neutral or positively charged, interact with the cells but the speed of this interaction changes according to their charge.

Doxorubicin incorporated into liposomes was shown to be more cytotoxic than empty liposomes but less than the free doxorubicin. These results indicated that liposomes protect the cells from the drug by achieving a gradual release, which is the main feature of a drug delivery system.

Future Work:

Although the scope of this thesis contains simultaneous delivery of an anticancer drug, an antiangiogenesis agent and the imaging agent QDs from liposomes, the antiangiogenic agent Bevacizumab selected for this purpose did not perform as

excepted on HUVEC. The endothelial proliferation tests should be repeated using another antiangiogenesis agent and a preferably new endothelial cell type in place of HUVEC. It should then be tested *in situ*, *in vitro* and *in vivo*, preferably using rabbits.

REFERENCES

Allen T. M. and Cullis P. R., Liposomal drug delivery systems: from concept to clinical applications. *Adv Drug Deliv Rev.*, 65- 1, 36-48, 2013.

Al-Jamal W.T., Al-Jamal K.T., Tian B., Lacerda L., Bomans P.H, Frederik P.M, Kostarelos K., Lipid-Quantum Dot Bilayer vesicles enhance tumor cell uptake and retention *in vitro* and *in vivo*, *Acs Nano* 2, 408-418, 2008.

Al-Jamal W. T., Al-Jamal K. T., Bomans P. H., Frederik P. M., Kostarelos K. Functionalized-quantum-dot-liposome hybrids as multimodal nanoparticles for cancer. *Small*, 4- 9, 1406- 1415, 2008 (2).

Aluri S., Janib S. M., Mackay J. A., Environmentally Responsive Peptides as Anticancer drug carriers, *Adv Drug Deliv Rev.*, 61-11, 940-952, 2009.

Baba A. I. and Cătoi C., *Comparative Oncology*, The Publishing House of the Romanian Academy, 2007.

Baeriswyl V., and Christofori G., The Angiogenic Switch in Carcinogenesis. *Semin. Cancer Biol.* 19, 329–337, 2009

Banerjee R., Liposomes: Applications in Medicine, *J Biomater Appl.*, 16-1, 3-21, 2001.

Bangham A. D., Standish M. M., and Watkins J. C., Diffusion of Univalent Ions Across The Lamellae of Swollen Phospholipids, *Journal of Molecular Biology*, 13- 1, 238–252, 1965.

Bharali D. J. and Mousa S. A., Emerging Nanomedicines for Early Cancer Detection And Improved Treatment: Current Perspective and Future Promise, *Pharmacol Ther.*, 128-2, 324-335, 2010.

Brigger, I., Dubernet, C., Couvreur, P., Nanoparticles in Cancer Therapy and Diagnosis, *Adv. Drug Delivery Rev.*, 54, 631-651, 2002.

Bukowski, T. J. and Simmons J. H., Quantum Dot Research: Current State and Future Prospects, *Solid state and materials sciences*, 27, 119-142, 2002.

Carmeliet P. and Jain R. K., Molecular Mechanisms and Clinical Applications Of Angiogenesis, *Nature*, 19; 473- 7347, 298-307, 2011.

Caterina D. R. and Libby P., *Endothelial Dysfunctions and Vascular Disease*, Wiley-Blackwell, MA, USA, 2007.

Chan W. C., Maxwell D. J., Gao X., Bailey R. E., Han M., Nie S., *Luminescent Quantum Dots for Multiplexed Biological Detection and Imaging*, *Current Opinion in Biotechnology*, 13, 40–46, 2002.

Chen C. S., Yao J. and Durst R. A., *Liposome Encapsulation of Fluorescent Nanoparticles: Quantum Dots and Silica Nanoparticles*, *Nanoparticle Research*, 8-6, 1033-1038, 2006.

Chu M. and Liu G., *Synthesis of Liposomes Templated CdSe Hollow and Solid Nanospheres*, *Materials Letters*, 60, 11 – 14, 2006.

Cirli O. O. and Hasirci V., *UV-Induced Drug Release from Photoactive REV Sensitized by Suprofen*, *J. Controlled Release*, 96, 85-96, 2004.

Demirbag B., Kardesler S., Buyuksungur A., Kucukturhan A., Eke G., Hasirci N., and Hasirci V., *Nanotechnology in Biomaterials: Nanoparticulates as Drug Delivery Systems*, *Bionanotechnology II: Global Prospects*, CRC Press, NW, USA Ch. 11, 2011.

Duda D. G., Batchelor T. T., Willett C. G., Jain R. K., *VEGF-Targeted Cancer Therapy Strategies: Current Progress, Hurdles and Future Prospects*, *Trends in Molecular Medicine*, 13-6, 223-230, 2007.

Ferrara N., Hillan K. J., Gerber H. P., Novotny W., *Discovery and Development of Bevacizumab, an Anti-VEGF Antibody For Treating Cancer*, *Nat. Rev. Drug Discov.* 3-5, 391–400, 2004.

Forough R., *New Frontiers in Angiogenesis*, Springer, 2006.

Elbayoumi T. A., Torchilin V. P., *Current Trends in Liposome Research, Liposomes Methods and Protocols Volume 1: Pharmaceutical Nanocarriers*, Humana Press, London, UK, Ch. 1, 2010.

Folkman J., *Tumor Angiogenesis: Therapeutic Implications*, *Nature Engl. J. Med.*, 285, 1182–1186, 1971

Gabizon, A., Price, D. C., Huberty, J., Bresalier, R. S., Papahadjopoulos, D., *Effect Of Liposome Composition And Other Factors On The Targeting Of Liposomes To Experimental Tumors: Biodistribution And Imaging Studies*. *Cancer Res.*, 50- 19, 6371–6378, 1990.

- Gao J. and Xu B., Applications of Nanomaterials Inside Cells, *Nano Today*, 4, 37-51, 2009.
- Gates B.D., Xu Q., Stewart M., Ryan D., Willson C.G., Whitesides G.M., New Approaches To Nanofabrication: Molding, Printing, And Other Techniques, *Chemical Reviews* 105- 4, 1171-1196, 2005.
- Geidel C., Schmachtel S., Riedinger A., Pfeiffer C., Müllen K., Klapper M., Parak WJ., A General Synthetic Approach For Obtaining Cationic And Anionic Inorganic Nanoparticles Via Encapsulation In Amphiphilic Copolymers. *Small*, 7- 20, 2929-2934, 2011.
- Goldmann E., The Growth Of Malignant Disease In Man And The Lower Animals, With Special Reference To The Vascular System, *Proc. R. Soc. Med.* 1, 1–13, 1908.
- Han M. Y., Gao X. H., Su J. Z., Nie S., Quantum-Dot-Tagged Microbeads for Multiplexed Optical Coding of Biomolecules, *Nat Biotechnol*, 19, 631–635, 2001.
- Han Y. S., Lee J. E., Jung J. W. and Lee J. S., Inhibitory Effects Of Bevacizumab On Angiogenesis And Corneal Neovascularization, *Graefes Arch Clin Exp Ophthalmol*, 247, 541–548, 2009.
- Hanahan D., and Folkman J., Patterns and Emerging Mechanisms of The Angiogenic Switch During Tumorigenesis, *Cell* 86, 353–364, 1996.
- Hanahan D. and Weinberg R. A., The Hallmarks of Cancer, *Cell*, 100- 1, 57–70, 2000.
- Hanahan D. and Weinberg R. A., Hallmarks of Cancer: The Next Generation, *Cell*, 144- 5, 646-674, 2011
- Hasirci V., Vrana E., Zorlutuna P., Ndreu A., Yilgor P., Basmanav F. B., Aydin E., Nanobiomaterials: A Review Of The Existing Science And Technology, And New Approaches, *J Biomater Sci Polym Ed.*, 17-11, 1241-1268, 2006.
- Ioannou D. and Griffin K. D., Nanotechnology and Molecular Cytogenetics: The Future Has Not Yet Arrived, *Nano Rev.* 1, 5117, 2010
- Jackson S.M., Jones M.N., Lyle I.G., The Measurement Of Phospholipid Adsorption From Liposomal Dispersions Onto Glass Surfaces, *Colloids and Surfaces*, 20-3, 171–186, 1986.
- Jain R. K., Normalization of Tumor Vasculature: An Emerging Concept in Antiangiogenic Therapy *Science*, 307, 58-62, 2005.
- Jain R. K., Taming Vessels to Treat Cancer, *Scientific American*, 298- 1, 56-63, 2008.

Jain R. K. and Carmeliet P., SnapShot: Tumor Angiogenesis, *Cell*, 149- 6, 1408-1408, 2012.

Jaimeson T., Bakhshi R., Petrova D., Pocock R., Imani M., Seifalian A. M., Biological Applications of Quantum Dots. *Biomaterials*, 28, 4717–4732, 2007.

Jemal A., Bray F., Center M. M., Ferlay J., Ward E., Forman D., Global Cancer Statistics, *CA Cancer Journal for Clinicians* 61-2, 69-90, 2011.

Kepczyński M, Karewicz A, Górnicki A, Nowakowska M., Interactions Of Porphyrin Covalently Attached To Poly(Methacrylic Acid) With Liposomal Membranes, *J Phys Chem B*. 109- 3, 1289-94, 2005.

Kirpotin, D. B., Drummond D. C., Shao Y., Shalaby M. R., Hong K., Nielsen U. B., Marks J. D., Benz C. C., and Park J. W., Antibody Targeting of Long Circulating Lipidic Nanoparticles Does Not Increase Tumor Localization But Does Increase Internalization in Animal Models, *Cancer Res*, 66, 6732-6740, 2006.

Kuesters G. M. and Campbell R. B., Conjugation of Bevacizumab to Cationic Liposomes Enhances Their Tumor-Targeting Potential. *Nanomedicine (Lond)*, 5- 2, 181-192, 2010

Kumar R., Bakowsky U., Lehr C.M., Preparation and Characterization of Cationic PLGA Nanospheres as DNA Carriers, *Biomaterials*, 25- 10, 1771-1777, 2004.

Kumari A., Yadav S. K., Yadav S. C., Biodegradable Polymeric Nanoparticles Based Drug Delivery Systems, *Colloids and Surfaces B: Biointerfaces*, 75, 1-18, 2010.

Leu A. J., Berk D. A., Lymboussaki A., Alitalo K., Jain R. K., Absence Of Functional Lymphatics Within A Murine Sarcoma: A Molecular And Functional Evaluation, *Cancer Res.*, 60, 4324–4327, 2000.

Liu Z., Cheung R., Wu X. Y., Ballinger J. R., Bendayan R., Rauth A. M., A Study Of Doxorubicin Loading Onto And Release From Sulfopropyl Dextran Ion-Exchange Microspheres, *Journal of Controlled Release* 77, 213–224, 2001.

Liu Y., Miyoshi H., and Nakamura M., Nanomedicine For Drug Delivery And Imaging: A Promising Avenue For Cancer Therapy And Diagnosis Using Targeted Functional Nanoparticles, *Int J Cancer*, 120-12, 2527-2537, 2007.

Maeda H., Greish K., Fang J., *The EPR Effect And Polymeric Drugs: A Paradigm Shift for Cancer Chemotherapy in the 21st Century*, Springer, Heidelberg, Germany, 2006.

Maeda H, Wu J, Sawa T, Matsumura Y, Hori K., Tumor Vascular Permeability And The EPR Effect In Macromolecular Therapeutics: A Review, *J. Controlled Release*, 65, 271–284, 2000.

Maeda H., Vascular Permeability In Cancer And Infection As Related To Macromolecular Drug Delivery, With Emphasis On The EPR Effect For Tumor-Selective Drug Targeting, *Proceedings of the Japan Academy, Series B, Physical and Biological Sciences* 88, 53-71, 2012.

Marcuccia F., Cortic A., How To Improve Exposure Of Tumor Cells To Drugs — Promoter Drugs Increase Tumor Uptake And Penetration Of Effector Drugs, *Advanced Drug Delivery Reviews*, 64 (1), 53–68, 2012.

Matsamura Y., Maeda H. A., New Concept For Macromolecular Therapeutics In Cancer Chemotherapy: Mechanisms Of Tumorotropic Accumulation Of Protein And The Antitumor Agent SMANCS, *Cancer Res.*, 46, 6387-6392, 1986.

Medintz I. L., Uyeda H. T., Goldman E R., and Mattoussi H., Quantum Dot Bioconjugates For Imaging, Labelling And Sensing, *Nature Materials* 4, 435 – 446, 2005.

Michalet X., Pinaud F.F., Bentolila L.A., Tsay J.M., Doose S, Li J.J., Sundaresan G, Wu A.M., Gambhir S.S., Weiss S., Quantum Dots For Live Cells, *In Vivo* Imaging, And Diagnostics, *Science*, 307-,5709, 538-544, 2005.

Murray C. B., Norris D. J., et al., Synthesis And Characterization Of Nearly Monodisperse Cde (E=S, Se, Te) Semiconductor Nanocrystallites, *J. Am. Chem. Soc.*, 115, 8706-8715, 1993.

Mutlugun E., Samarskaya O., Ozel T., Cicek N., Gaponik N., Eychmuller A., and Demir H.V., Highly Efficient Nonradiative Energy Transfer Mediated Light Harvesting In Water Using Aqueous CdTe Quantum Dot Antennas, *Optics Express* 18, 10720, 2010.

Nishiyama M., and Eguchi H., Recent Advances in Cancer Chemotherapy: Current Strategies, Pharmacokinetics, and Pharmacogenomics, *Advanced Drug Delivery Reviews* 61, 367–368, 2009.

Novosel E. C., Kleinhans C., Kluger P. J., Vascularization is the Key Challenge in Tissue Engineering, *Adv Drug Deliv Rev.*, 63,300-11, 2011

Olivier J.C., Drug Transport to Brain with Targeted Nanoparticles, *J Am. Soc. for Experim, NeuroTherapeutics*, 2, 108-119, 2005.

Oto E. K., Zalipsky S., Quinn Y. P., Zhu G. Z., Uster P. S., Poly(methacrylic acid)-Induced Liposome Aggregation For Measuring Drug Entrapment. *Anal Biochem.* 229-1,106-111, 1995.

Padeste C., Solak H., Brack H. P., Slaski M., Alkan Gürsel S., and Scherer G. G., Patterned Grafting Of Polymer Brushes Onto Flexible Polymer Substrates, *J. Vac. Sci. Technol. B*, 22, 3191, 2004.

Padeste C., Farquet P., Potzner C., Solak H. H., Nanostructured Bio-Functional Polymer Brushes, *J Biomater Sci Polym Ed.*, 17- 11, 1285-1300, 2006.

Pankhurst Q. A., Connolly J., Jones S.K., Dobson J., Applications of Magnetic Nanoparticles in Biomedicine, *J. Phys. D: Appl. Phys.* 36, 167–181, 2003.

Park E. K., Lee S. B., Lee Y. M., Preparation And Characterization Of Methoxy Poly (Ethylene Glycol)/Poly (Caprolactone) Amphiphilic Block Copolymeric Nanospheres For Tumor-Specific Folate-Mediated Targeting Of Anticancer Drugs, *Biomaterials*, 26, 1053-1061, 2005.

Peer D., Karp J. M., Hong S., FaroKhazad O. C., Margalit R., and Langer R., Nanocarriers As An Emerging Platform For Cancer Therapy: *Nature Nanotechnology*, 2, 751-760, 2007.

Pinaud F., Michalet X., Bentolila L. A., Tsay J. M., Doose S, Li JJ, Iyer G., Weiss S., Advances In Fluorescence Imaging With Quantum Dot Bio-Probes, *Biomaterials*, 27, 1679–87, 2006.

Raab R. M. and Stephanopoulos G., Dynamics of Gene Silencing by RNA Interference, *Biotechnol. Bioeng.*, 88, 121–32, 2004.

Ranade V. V. and Holinger M. A., *Drug Delivery Systems*, CRC Press, USA, 2004.

Rossetti R., Nakahara S., Brus L.E., Quantum Size Effects in The Redox Potentials, Resonance Raman-Spectra And Electronic-Spectra of CdS Crystallites In Aqueous-Solution, *J. Chem. Phys.* 79, 1086 -1088, 1983.

Sahoo S. K., and Labhasetwar V., Nanotech Approaches in Drug Delivery and Imaging, *Drug Discovery Today*, 8 (24), 1112-1120, 2003.

Schroeder J. E., Shweky I., Shmeeda H., Banin U., Gabizon A., Folate-mediated Tumor Cell Uptake of Quantum Dots Entrapped in Lipid Nanoparticles, *J Control Release*, 124-2, 28-34, 2007.

Sengupta, S., Eavarone, D., Capila, I., Zhao, G., Watson, N., Kiziltepe, T., Sasisekharan, R., Temporal Targeting of Tumour Cells and Neovasculature with a Nanoscale Delivery System, *Nature*, 436- 7050, 568-572, 2005.

Sheridan M. H., Shea L. D., Peters M.C., Mooney D.J., Bioabsorbable Polymer Scaffolds For Tissue Engineering Capable Of Sustained Growth Factor Delivery, *J Control. Release*, 64, 91-102, 2000.

Smith A. M., Duan H., Mohs A. M., Nie S., Bioconjugated Quantum Dots For *In Vivo* Molecular and Cellular Imaging, *Advanced Drug Delivery Reviews*, 60-11, 1226-1240, 2008.

Soloman R. and Gabizon A. A., Clinical Pharmacology of Liposomal Anthracyclines: Focus on Pegylated Liposomal Doxorubicin, *Clin. Lymphoma Myeloma*, 8-1, 21-32, 2008.

Storm G., Belliot S. O., Daemen T., and Lasic D. D., Surface Modification Of Nanoparticles To Oppose Uptake By The Mononuclear Phagocyte System, *Advanced Drug Delivery Reviews*, 17, 31-48, 1995.

Taurin S., Nehoff H., Greish K., Anticancer Nanomedicine And Tumor Vascular Permeability; Where Is The Missing Link? *J. Control Release*, 164-3, 265-75, 2012.

Torchilin V., Drug Targeting, *European Journal of Pharmaceutical Sciences*, 11-Supplement 2, S81-S91, 2000.

Torchilin, V., and Weissig V., *Liposomes - A Practical Approach*, Oxford University Press, USA, 2003.

Torchilin V., *Multifunctional Pharmaceutical Nanocarriers*, Springer, USA, 2008.

Uekama K., Hirayama F., Irie T., Cyclodextrin Drug Carrier Systems, *Chem. Rev.* 98, 2045-2076, 1998.

Visani G. and Isidori A., Doxorubicin Variants for Hematological Malignancies, *Nanomedicine*, 6- 2, 303-306, 2011.

Walling M. A., Novak J. A., and Shepard J. R. E., Quantum Dots for Live Cell and *In Vivo* Imaging, *Int J Mol Sci.* 10-2, 441-491, 2009.

Wang B., Siahaan T. and Soltero R. A., *Drug Delivery Principles and Applications*, John Wiley & Sons, Inc. Publication, Canada, 2005.

Xu Y., PhD Thesis, Virginia Polytechnic Institute and State University, Virginia, USA, 2005.

Yang C., Ding N., Xu Y., Qu X., Zhang J., Zhao C., Hong L., Lu Y., Xiang G., Folate Receptor-Targeted Quantum Dot Liposomes as Fluorescence Probes, *J Drug Targeting*, 17-7, 502-511, 2009.

Yu W. W., Qu L., Guo W., and Peng X., Experimental Determination of the Extinction Coefficient of CdTe, CdSe, and CdS Nanocrystals, *Chem. Mater.*, 15-14, 2854–2860, 2003.

Yun Y. H., Goetz D. J., Yellen P., Chen W., Hyaluronan Microspheres For Sustained Gene Delivery And Site-Specific Targeting, *Biomaterials*, 25-1, 147-157, 2004.

Zelphati O., Nguyen C., Ferrari M., Felgner J., Tsai Y., Felgner P.L., Stable and Monodisperse Lipoplex Formulations for Gene Delivery. *Gene Ther.*, 5-9, 1272-1282, 1998.

APPENDICES

A. Saos2 MTS/PES Calibration Curve

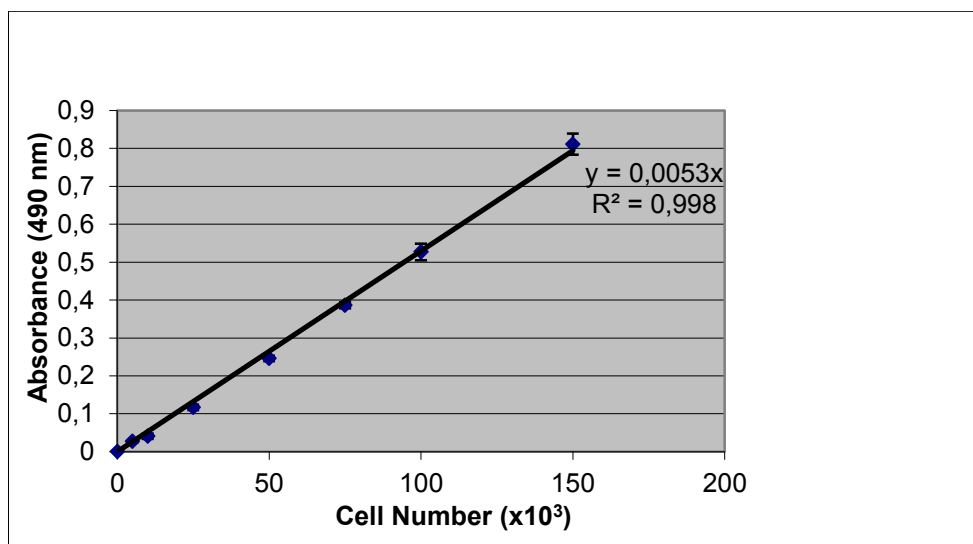


Figure 79. Saos2 MTS/PES Calibration Curve

B. HUVEC Alamar Blue Calibration Curve

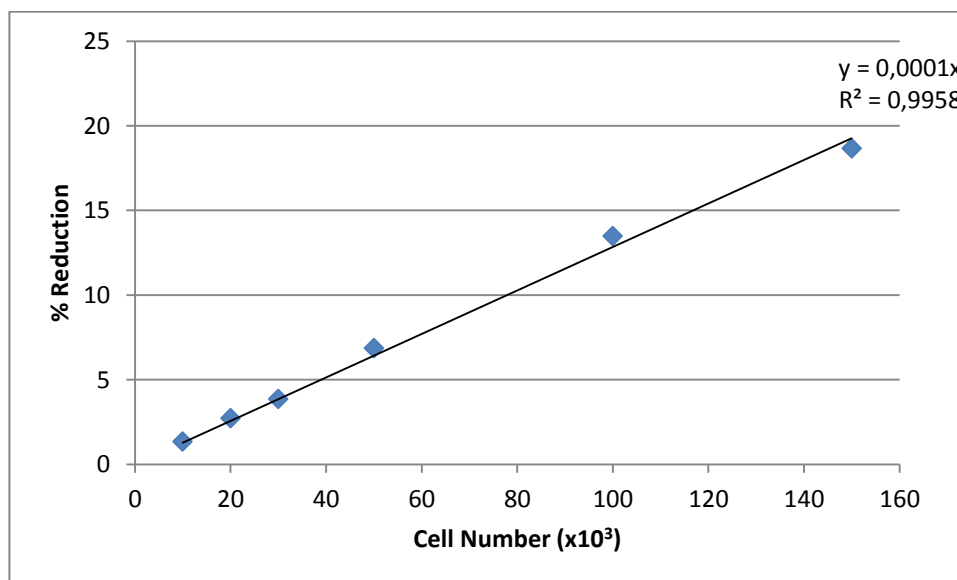


Figure 80. HUVEC Alamar Blue Calibration Curve

CURRICULUM VITAE

PERSONAL INFORMATION

Surname, Name: Büyüksungur, Arda

Nationality: Turkish (T.C.)

Date and Place of Birth: 06 July 1979, Ankara, Turkey

Marital Status: Single

E-mail: ardasungur@gmail.com

EDUCATION

Degree	Institution	Year of Graduation
MS	METU, Dept. of Biotechnology	2006
BS	Ankara University, Dept. of Biology	2002

ACADEMIC EXPERIENCE

Year	Place	Enrollment
2007-2013	METU, BIOMATEN	Full time Researcher
2009	Paul-Scherer Institute, Department of Nano-Micro Technology, Switzerland	Visiting Researcher
2003-2006	METU, Chemical Engineering Dept., Industrial Biotechnology and Metabolic Engineering Research Lab	Full time Researcher

Awards:

- TUBİTAK National Scholarship Programme for PhD Students-2211
- Rudolf Cimdins Scholarships 2011- 24th European Conference on Biomaterials

PUBLICATIONS

- G. Bahcecioglu, **A. Buyuksungur**, A. Kiziltay, N. Hasirci and V. Hasirci, Construction and *in vitro* testing of a multilayered tissue engineered meniscus, J of Bioactive and Compatible Polymers, Submitted.

- B. Demirbag, P. Y. Huri, G. T. Kose, **A. Buyuksungur** and V. Hasirci, Advanced cell therapies with and without scaffolds, *Biotechnology Journal*, 6(12), 1437-1453, DOI: 10.1002/biot.201100261, 2011.

Book chapters

- B. Demirbag, S. Kardesler, **A. Buyuksungur**, A. Kucukturhan, G. Eke, N. Hasirci, and V. Hasirci, *Nanotechnology in Biomaterials: Nanoparticulates as Drug Delivery Systems*, *Bionanotechnology II: Global Prospects*, Taylor & Francis Inc, 2011

Proceedings

- **A. Buyuksungur**, P. Calik, Extracellular benzaldehyde lyase production by *Pichia pastoris*, *Journal of Biotechnology*, Volume 131 (2), 175-176, 2007.
- H. Levent, **A. Buyuksungur**, P. Calik, Fed-batch operation for benzaldehyde lyase production by recombinant *Escherichia coli*, *Journal of Biotechnology*, Volume 131 (2), 225-226, 2007.

Refereed International Conference Papers

- **Buyuksungur**, P. Yilgor Huri, N. Hasirci and V. Hasirci, Bioplotting Scaffolds for Bone Tissue Engineering, Bruker MicroCT User Meeting 2013, Hasselt, Belgium, April 16-18 2013. (Oral Presentation- Presented by AB)
- G. Bahcecioglu, **A. Buyuksungur**, N. Hasirci and V. Hasirci, Poly(L-Lactic Acid) -Based Meniscus Tissue Engineering, SkyScan User Meeting 2012, Brussels, Belgium, April 02-05 2012. (Oral Presentation- Presented by AB)
- **A. Buyuksungur**, E. Mutlugun, H. V. Demir, V. Hasirci, Liposomes and Cytotoxicity of Quantum Dots, 16th International Biomedical Science and Technology Symposium. Istanbul, Turkey. September 28- October 2, 2010.
- **A. Buyuksungur**, C. Padeste, V. Hasirci, Entrapment in Liposome Prevents Toxicity of Quantum Dots, International Symposium on Biotechnology: Developments and Trends. 27-30 September, 2009. Middle East Technical University, Ankara, Turkey.
- **A. Buyuksungur**, V. Hasirci, Bioactive Agent Carrying Quantum Dot Labeled Liposomes, 15th International Biomedical Science and Technology Symposium. Güzelyurt, TRNC. August 16-19, 2009.
- E. Aydin, **A. Buyuksungur**, I. Tekeli, V. Hasirci, Characterization of Cell Behavior on a Range of Nanopatterned Polyester Films, 15th International Biomedical Science and Technology Symposium. Güzelyurt, TRNC. August 16-19, 2009.

- **A. Buyuksungur**, H.Kaya, P.Calık, Comparison of Benzaldehyde Lyase Production Capacity of Recombinant *Escherichia coli*, *Bacillus subtilis* and *Pichia pastoris* , Somer Symposium Series I, 14-15/05/2007.
- H. Kaya, **A. Buyuksungur**, P. Calık, T. H. Ozdamar, Recombinant microorganism development and medium design for extracellular benzaldehyde lyase production, ESBES 6th European Symposium on Biochemical Engineering Science, Abstract Book p148, Salzburg, Austria, 27-30/08/2006.
- H. Kaya, **A. Buyuksungur**, P. Calık, T.H. Ozdamar, Recombinant *Bacillus sp.* development for extracellular benzaldehyde lyase production. 14th National Biotechnology Congress, Abstract Book p90, 2005. (Oral Presentation)

Memberships

- Biomaterials and Tissue Engineering Society (2009-)
- Controlled Release Society Turkey (2008-)
- Turkish Biotechnology Association (2006-)